

~~LEVEL II~~

(12)

NOSC

NOSC TD 431

NOSC TD 431

Technical Document 431

TRANSEQUATORIAL PROPAGATION OF VERY LOW FREQUENCY RADIOWAVES

AD A 1 0 0 3 7 3



F. Perry Snyder

15 April 1981

Final Report

Prepared for
U.S. Coast Guard

Approved for public release; distribution unlimited

file copy
DMC

NAVAL OCEAN SYSTEMS CENTER
SAN DIEGO, CALIFORNIA 92152

81 6 17 039



NAVAL OCEAN SYSTEMS CENTER, SAN DIEGO, CA 92152

AN ACTIVITY OF THE NAVAL MATERIAL COMMAND

SL GUILLE, CAPT, USN

Commander

HL BLOOD

Technical Director

ADMINISTRATIVE INFORMATION

Analysis for this report was completed over the last two years. Funding was provided by the U.S. Coast Guard under task area 532-MP01.

Reviewed by

J. H. Richter, Head
EM Propagation Division

Under authority of

J. D. Hightower, Head
Environmental Sciences
Department

UNCLASSIFIED

SECURITY CLASSIFICATION OF THIS PAGE (When Data Entered)

REPORT DOCUMENTATION PAGE		READ INSTRUCTIONS BEFORE COMPLETING FORM
1. REPORT NUMBER NOSC Technical Document 431 (TD 431)	2. GOVT ACCESSION NO. <i>AD-A100 373</i>	3. RECIPIENT'S CATALOG NUMBER
4. TITLE (and Subtitle) TRANSEQUATORIAL PROPAGATION OF VERY LOW FREQUENCY RADIOWAVES	5. TYPE OF REPORT & PERIOD COVERED Final Report	
7. AUTHOR(s) F. Perry Snyder	6. PERFORMING ORG. REPORT NUMBER	
9. PERFORMING ORGANIZATION NAME AND ADDRESS Naval Ocean Systems Center San Diego, CA 92152	10. PROGRAM ELEMENT, PROJECT, TASK AREA & WORK UNIT NUMBERS EGOV USCG 0 532-MPU	
11. CONTROLLING OFFICE NAME AND ADDRESS United States Coast Guard	12. REPORT DATE 15 April 1981	
14. MONITORING AGENCY NAME & ADDRESS (if different from Controlling Office)	13. NUMBER OF PAGES 107	
16. DISTRIBUTION STATEMENT (of this Report) Approved for public release; distribution unlimited.	15. SECURITY CLASS. (of this report) Unclassified	
17. DISTRIBUTION STATEMENT (of the abstract entered in Block 20, if different from Report)		
18. SUPPLEMENTARY NOTES		
19. KEY WORDS (Continue on reverse side if necessary and identify by block number) VLF radiowaves Transequatorial propagation Geomagnetics Equatorial anomalies		
20. ABSTRACT (Continue on reverse side if necessary and identify by block number) This study reports on observations of dawn/dusk transition fading of very low frequency radiowaves on a long, transequatorial northeasterly propagation path. A mode conversion model is developed and numerical modeling results are presented for transition fading on long transequatorial paths, both northeasterly and southwesterly. From these results the following general conclusions are drawn: (a) Anomalous transequatorial transition fading is not observed for the northeasterly propagation path. The transition fading data support completely the mode conversion model of transition fading developed by Crombie.		

UNCLASSIFIED

SECURITY CLASSIFICATION OF THIS PAGE (When Data Entered)

20. ABSTRACT (Continued)

(b) The transequatorial sunrise transition reported in the literature as anomalous is completely explained by correctly allowing for variations of the geomagnetic field along the path. The geomagnetic field influences the nighttime modal parameters to such an extent for the southwesterly path considered that the approximate WKB method of mode summation cannot be employed.

(c) Careful application of model techniques appears to be capable of describing all LF and VLF propagation in the earth-ionosphere waveguide, provided the effect of the earth's magnetic field is properly included at night. However, an improved model of the ionosphere at altitudes below 100 km is desired.

UNCLASSIFIED

SECURITY CLASSIFICATION OF THIS PAGE (When Data Entered)

SUMMARY

This study reports on observations of dawn/dusk transition fading of very low frequency radio waves on a long, transequatorial northeasterly propagation path. A mode conversion model is developed and numerical modeling results are presented for transition fading on long transequatorial paths, both northeasterly and southwesterly. From these results the following general conclusions are drawn:

- a. Anomalous transequatorial transition fading is not observed for the northeasterly propagation path. The transition fading data support completely the mode conversion model of transition fading developed by Crombie.
- b. The transequatorial sunrise transition reported in the literature as anomalous is completely explained by correctly allowing for variations of the geomagnetic field along the path. The geomagnetic field influences the night-time modal parameters to such an extent for the southwesterly path considered that the approximate WKM method of mode summation cannot be employed.
- c. Careful application of modal techniques appears to be capable of describing all LF and VLF propagation in the earth-ionosphere waveguide, provided the effect of the earth's magnetic field is properly included at night. However, an improved model of the ionosphere at altitudes below 100 km is desired.

Accession For	
NTIS GRA&I <input checked="" type="checkbox"/>	
DTIC TAB <input type="checkbox"/>	
Unannounced <input type="checkbox"/>	
Justification _____	
By _____	
Distribution/	
Availability Codes	
Dist	Avail and/or
	Special
A	

CONTENTS

	Page
I. INTRODUCTION	1
A. VLF Radiowave Propagation to Great Distances	2
1. Theoretical Development	2
2. Observed Propagation Variations	10
3. The Equatorial Anomaly	13
B. Description of Research	16
II. THEORY	18
A. Horizontally Homogeneous Guides	18
1. Coordinate Transformation	18
2. The Mode Equation	21
3. Point Sources and Line Sources	22
4. Modal Excitation Factors and Polarization Coupling	24
5. Determination of Reflection Coefficients	29
B. Horizontally Inhomogeneous Guides	33
1. The Operator Equations	35
2. Mode Conversion	37
III. EXPERIMENTAL RESULTS	46
A. Equipment Used	46
B. The Terminator and the Propagation Path	48
C. Transition Fading Data	49
1. Time of Signal Minima	49
2. Terminator Position at Maximum Signal Fade	50
IV. NUMERICAL MODELING RESULTS	52
A. Review of VLF Propagation Environment	52
B. Sample Calculation Comparisons	55
C. Modeling Results	56
1. NWC to San Diego	57
a. Nighttime	57
b. Sunrise/Sunset Transition	58
2. NLK to Brisbane	60
a. Nighttime	60
b. Sunrise/Sunset Transition	62
V. CONCLUSIONS	63
REFERENCES	64

LIST OF FIGURES

Figure	Page
1. Ionospheric Sunrise/Sunset Model with Plan View of Propagation Path Intersection with Transition Region.....	69
2. Model of Propagation Path Intersection with Transition Region.....	70
3. Periods of Night, Day and Transition Versus Date for NWC to San Diego Propagation Path.....	71
4. Times of Signal Minima for Night to Day Transition - Sunrise (no average).....	72
5. Times of Signal Minima for Night to Day Transition - Sunrise (15 day average).....	73
6. Times of Signal Minima for Day to Night Transition - Sunset (no average).....	74
7. Times of Signal Minima for Day to Night Transition - Sunset (15 day average).....	75
8. Transmitter/Terminator Distance ($\chi = 96^\circ$) at Times of Signal Minima for Night to Day Transition - Sunrise (no average).....	76
9. Distance Moved by Terminator ($\chi = 96^\circ$) Between Signal Minima for Night to Day Transition - Sunrise (no average).....	77
10. Transmitter/Terminator Distance ($\chi = 96^\circ$) at Times of Signal Minima for Day to Night Transition - Sunset (no average).....	78
11. Ratio of Measured Propagation Path Length in Transition Region to the Minimum Possible Path Length.....	79
12. Signal Amplitude - NWC; 22.3 kHz Received at San Diego - June 1, 2, 3, 1975.....	80
13. Comparison of Computed (IRI-78) with Measured (NPM to Ontario, CA) Amplitude Night - 23.4 kHz.....	81
14. Comparison of Computed (IRI-78) with Measured (Hawaii Sounder to San Diego) Amplitude Day - 21.8 kHz.....	82
15. Height Gains for $\beta = .5 \text{ km}^{-1}$; $h' = 70 \text{ km}$; 18.6 khz.....	83
16. Height Gains for $\beta = .3 \text{ km}^{-1}$; $h' = 70 \text{ km}$; 18.6 kHz.....	84
17. Geomagnetic Field Variation Along the Propagation Path.....	85
18. Complex Eigenangles vs. Distance for NWC to San Diego.....	86

19. Polarization Mixing Ratio for NWC to San Diego.....	87
20. Normalized Phase Velocities for NWC to San Diego.....	88
21. Attenuation Rates for NWC to San Diego.....	89
22. Excitation Factors for NWC to San Diego.....	90
23. Mode Sums for NWC to San Diego.....	91
24. a. Computed Transition Fading - NWC to San Diego Night to Day ($h' = 86$ km to $h' = 74$ km).....	92
b. Computed Transition Fading - NWC to San Diego Day to Night ($h' = 74$ km to $h' = 86$ km).....	93
25. Computed Transition Fading - Variable Receiver Locations on NWC to San Diego Path Day to Night ($h' = 74$ km to $h' = 86$ km).....	94
26. Computed Transition Fading - Variable Receiver Locations on NWC to San Diego Path Night to Day ($h' = 86$ km to $h' = 74$ km).....	95
27. Complex Eigenangles vs. Distance for NLK to Brisbane.....	96
28. Polarization Mixing Ratios for NLK to Brisbane.....	97
29. Normalized Phase Velocities for NLK to Brisbane.....	98
30. Attenuation Rates for NLK to Brisbane.....	99
31. Mode Sums for NLK to Brisbane.....	100
32. Computed Transition Fading - Variable Receiver Locations on NLK to Brisbane Path Day to Night ($h' = 74$ km to $h' = 86$ km).....	101
33. Computed Transition Fading - Variable Receiver Locations on NLK to Brisbane Path Night to Day ($h' = 86$ km to $h' = 74$ km).....	102

LIST OF TABLES

Table 1.....	56
--------------	----

I. INTRODUCTION

The propagation of low and very low frequency (LF and VLF) radio waves has been of interest since the beginning days of radio. The epoch-marking experiments at the beginning of this century by Marconi were made using what is now called the LF band. These experiments gave impetus to the development of LF and VLF radio communications and to studies of their propagation characteristics, particularly to the variation of signal strength with distance from the transmitter.

There are many practical disadvantages to using these frequency bands (Watt, 1967). These include the very high atmospheric noise level, which necessitates high power transmissions, the limited bandwidth available and the high cost and low efficiency of transmitting antennas. These disadvantages did not exist at shorter wavelengths and the development of shortwave radio in the 1920s led to the near demise of interest in the longer wavelengths.

For a variety of reasons, interest in VLF radiowave propagation was revived and has greatly increased during the last two decades. Near the earth's surface, the structure of the VLF electromagnetic field depends on the properties not only of the earth but also of the lower regions of the ionosphere between 50 to 100 km, the D-region and lower E-region. VLF signals are not greatly affected by most ionospheric disturbances, apart from polar cap events (Al'pert and Fligel, 1970), and the use of this frequency band affords a very useful tool for studying the upper regions of the ionosphere, out to several earth radii. This use stems from the fact that VLF signals, either man-made or natural, from electric storms for example, propagate through the lower regions of the ionosphere and are guided by ducts aligned along the geomagnetic field lines (the so-called whistler mode) whereupon they enter the earth's other hemisphere. Thus analysis of such signals can yield information about the near earth plasma and in fact provided the first evidence for the existence of a plasmasphere above the F-region. Furthermore, VLF has been found to be perhaps the most sensitive terrestrial means of detecting ionospheric disturbances produced by the entry of solar particles into the ionosphere (Potemra and Rosenberg, 1973).

Practical application of VLF, particularly from 10 to 30 kHz has also stimulated interest in this frequency band - VLF signals exhibit low attenuation (on the order of a few dB per 1000 km), and this frequency band is widely used in low data rate, global communication systems. The phase of VLF transmission is highly stable and undergoes nearly reproducible diurnal variations. It has been found, for example (Belrose, 1968), that the stability of VLF transmissions is sufficient to permit frequency comparisons to within a few parts in 10^{12} which is a few powers of ten better than is possible at high frequencies. This phase stability leads to applications in navigational systems, frequency comparisons and clock synchronization or timing systems.

The ability to determine, through VLF propagation theory, the variations of VLF radiowaves as a function of distance is of importance to the navigation or communications engineer, who must design his system for optimum performance in his total operational environment, which includes the propagation environment. Such theoretical calculations require an adequate description of the propagation environment. A comparison of calculated propagation parameters with those measured experimentally enables information to be obtained regarding the parameters of the propagation medium. A knowledge of these parameters is important for the study of physical processes which occur in the propagation medium.

A. VLF Radiowave Propagation to Great Distances

1. Theoretical Developments

This study is concerned with some aspects of the propagation of VLF radiowaves to great distances, i.e., with their amplitude, polarization and phase variations. VLF propagation to great distances has been considered in a large number of theoretical papers, using a variety of formulations. We will not attempt to review this massive literature but will concentrate on some general ideas that have been incorporated into the various formulations.

One of the major formulations for consideration of VLF propagation to great distances, the VLF wave-hop theory, has been presented by Berry and Chrisman (1965). In this formulation, the solution for propagation of VLF waves between a spherical earth and a concentric ionosphere is developed in a rigorous complex integral representation and the integrand is then expanded in

terms of a geometrical-type series. With the order of summation and integration exchanged, evaluation of the complex integrals using saddle point approximations leads to the identification of the series as the ray-hop series of geometric optics. The complex integrals are thus called wave-hops. For distances near or beyond the caustic, numerical integration or application of residue theory must be employed to evaluate the integrals. The wave-hop formulation requires both azimuthal and longitudinal invariance of the earth and ionosphere, a situation which exists only for short ranges.

Johler (1970) has presented a theory for radiowave propagation from VLF to MF in terms of spherical wave functions. As with the wave-hop formulation, the spherical wave formulation is not applicable to consideration of variations of the earth or ionosphere in either the longitudinal or azimuthal directions. The spherical wave function formulation has not been widely used because of its complexity and difficulty of numerical implementation.

VLF propagation to great distances can be conveniently represented in terms of waveguide mode propagation, where the finitely conducting curved earth and the anisotropic, imperfectly conducting curved ionosphere with dipping magnetic field form the boundaries of a waveguide. The basic idea that the earth and lower ionosphere form a waveguide actually goes back to the work of Watson (1918, 1919), who postulated that the Kennelly-Heaviside layer could be represented as a conducting shell concentric with the spherical conducting earth. Watson developed an exact slowly convergent, harmonic series-type solution to the F propagation problem and further devised a transformation of the series to a highly convergent form. The transformation, which involves distortion of the contour of integration in the complex wave number plane, is now identified with Watson's name, although the transformed series is often "rediscovered" by subsequent workers. Although "waveguides" were not really "discovered" until the 1930s, the terms in Watson's transformed series were simply waveguide modes.

The theory of VLF waveguide mode propagation has been presented in the literature in two different formulations. One formulation, based on the pioneering work of Watson (1919) and more recently in the theory given by Schumann (1952, 1954) and developed extensively by Wait (1962), treats the problem in spherical coordinates wherein the fields are expanded in terms of

azimuthal, longitudinal and radial functions. In a sequence of simplifying approximations, including the assumption of azimuthal and longitudinal independence of both ground and ionospheric properties, Wait (1962) develops a modal (eigenvalue) equation in terms of Airy functions. The Airy functions come about as a result of a third-order approximation to spherical wave functions (Watson, 1944). The solution of the eigenvalue equation yields the propagation characteristics of the VLF modes in the earth-ionosphere waveguide and consideration of orthogonality properties of the radial (Airy) functions yields excitation factors of the modes. The excitation factor is a quantity giving the amplitude of the wave excited in a given mode by a given source. Another simplifying approximation often made involves the replacement of the inhomogeneous ionosphere with an impedance boundary, placed at a height where the bulk of the VLF energy is assumed to be reflected. A similar impedance boundary replacement is also made for the earth. The impedance boundary formulation permits the specification of the ratio of an electric field component to a magnetic field component at the boundary without further consideration of the region beyond the boundary. Analytically, formulation in terms of impedance boundaries is equivalent to assumption of "homogeneous boundary conditions" (Friedman, 1959; Morse and Feshbach, 1953). The replacement of an inhomogeneous, isotropic ionosphere by an "equivalent" impedance boundary is a straightforward procedure. Such a replacement for an anisotropic ionosphere is greatly complicated by the coupling of transverse magnetic and transverse electric polarizations. Boundary conditions must then be formulated in terms of an impedance matrix. Unfortunately, the complication is sufficient to render many of Wait's results inapplicable to the highly anisotropic nighttime ionosphere and to limit their application to the daytime ionosphere, for which the effect of anisotropy is slight. The theory has been significantly modified and extended to anisotropic ionospheres by Galejs (1972).

Another formulation of the earth-ionosphere waveguide problem has been presented by Budden (1961a). It is Budden's formulation that forms the basis for this study and will be discussed in more detail in following sections. In this formulation, a modal equation is developed in terms of reflection coefficients of the ionosphere and the earth. The formulation in terms of reflec-

tion coefficients permits determination of propagation characteristics of waveguide modes for essentially any ionospheric or ground conditions, limited only by the ability to compute reflection coefficients for the environment considered. Budden's formulation is essentially planar, although he does point out how to include earth curvature in the direction of propagation in an approximate way by modifying the refractive index in the space between the earth and the ionosphere (Budden, 1962). A more rigorous technique was introduced by Richter (1966) and has been employed in VLF propagation studies by Pappert (1968) and Abbas et al. (1975). This technique, which is employed in this study and will be discussed more fully in following sections, is to assume cylindrical stratification and effect a conformal transformation from cylindrical to Cartesian coordinates. Modal excitation values are determined in Budden's formulation by application of residue theory rather than using the modal orthogonality properties of conventional waveguide theory employed by Wait.

Whichever formulation is used at the outset, the use of waveguide mode theory leads to specification of the VLF field as a summation of terms called modes. Because most VLF transmitters in common use radiate a vertically polarized field, only the radial or vertical component of the electric field is usually considered. For a time harmonic source, the VLF mode sum for the vertical electric field may be written as

$$E_v(d) = \frac{K(P,f)}{\sqrt{\sin d/a}} \sum_n A_n G_n^T G_n^R e^{-ik_0 S_n d}, \quad (1)$$

where $K(P,f)$ is a complex constant dependent on transmitted power (P) and frequency (f); d is the distance from the transmitter on a homogeneous, smooth earth of radius a ; A_n is the excitation factor for mode n , normalized to unity for flat earth, perfectly conducting boundaries; k_0 is the free space wave number; S_n is the propagation factor; and $G_n^{T,R}$ represents height-gain functions for mode n , normalized to unity at the ground. One height-gain function is needed for the transmitter (T) and one for the receiver (R). Generally, both A_n and S_n are complex. The real part of S_n determines the distance dependence of the phase for a mode while the imaginary part of S_n determines the attenuation rate. Thus

$$\begin{aligned}\alpha_n &= -k_0 \operatorname{Im}(S_n) \\ v_n/c &= 1/\operatorname{Re}(S_n)\end{aligned}\quad (2)$$

where α_n is the modal attenuation rate, v_n is the phase velocity and c is the speed of light in free space.

Numerous assumptions and approximations, some of which will be removed in following sections, are implicit in equation (1). It is assumed that the propagation environment is homogeneous in all but the vertical direction. Thus, the propagation factor S_n is independent of position. The influence of the curvature of the earth transverse to the propagation direction is approximately accounted for in the $(\sin d/a)$ term. The energy flux for a wave traveling outwards with cylindrical symmetry on a flat earth without attenuation is proportional to $1/r$. For a spherically curved earth this energy flux would be proportional to $1/\sin(r/a)$. Thus the usual $r^{-1/2}$ term for a cylindrical wave is replaced by the $(\sin(r/a))^{-1/2}$ term. A careful derivation of the mode equation in spherical coordinates, such as that presented by Wait (1962) and discussed previously, yields the $\sin(d/a)$ term as a consequence of an asymptotic approximation to a Legendre function. The mode sum in equation (1) further assumes that "round-the-world" signals are absent, an approximation not valid when receiver locations are near the antipode of the transmitter; multi-path focusing then occurs.

Extensive results of numerical calculations of VLF waveguide mode constants have been presented in the literature. Early results given by Wait and Spies (1964) show some general properties of VLF modes for typical daytime and nighttime ionospheres with various ground conductivities and for propagation in the east to west or west to east directions at the magnetic equator or when the earth's magnetic field is ignored. In general, the attenuation rate of the lowest order mode is less at night than during day, and is less for west to east propagation than for east to west. The attenuation rate increases as ground conductivity decreases and does so rapidly at low conductivities such as occur for the polar icecaps. Each successive mode order suffers a larger attenuation rate than the previous order mode for both day and night.

Typically, daytime attenuation rates for the first order mode range from 2 to 4 dB/1000 km over the VLF band for sea water ground conditions (essen-

tially equivalent to a perfect conductor at VLF). The nighttime attenuation rates range from about 0.5 to 2 dB/1000 km over the VLF band for the same ground conductivities.

The results of Wait and Spies show that the modal phase velocities for the curved earth can be less than the free space speed of light at intermediate to higher VLF frequencies but increase markedly at lower frequencies. Moreover, phase velocities increase at low ionosphere heights (daytime) compared to higher heights (night) and a decrease in ground conductivity produces a decrease in phase velocity. An increase in phase velocity with mode number is also indicated.

The modal excitation factors and height gains given by Wait and Spies show little dependence on the terrestrial magnetic field. At higher frequencies for isotropic conditions, the excitation factor for the first mode is significantly reduced in comparison with that for a flat earth case. The second mode exhibits a much smaller reduction at higher frequencies. Generally, lower ground conductivities produce an increase in excitation factor. The excitation factor for the second order mode is significantly higher than that for the first order mode, especially at higher frequencies and at night. At night the second order mode may be dominant at the ground to distances of several thousand km. For the first mode the effect of height-gain is to cause the dominance of the second mode to be greatly diminished or even reversed. This height-gain increase with height for the first order mode has been called the whispering gallery effect by Budden and Martin (1962) or the earth-detached mode by Wait and Spies (1963). It involves successive reflections from the ionosphere with essentially no intermediate bounce at the ground.

The modal constants characteristics presented above become considerably more complicated with full consideration of the geomagnetic field. From earliest days of VLF, experimental investigation provided evidence of an apparent violation of the reciprocity principle. Pound (1925), for example, found that VLF radiowaves apparently suffered significantly larger attenuation for propagation in a generally easterly direction than in the reverse direction. Some very early results presented by Wait (1961) for sharply bounded model ionospheres suggested that simple harmonic functions may adequately

describe the azimuthal dependence of mode constants under daytime conditions. Further, a numerical modeling study by Ferguson (1968) showed that, for daytime conditions, only the horizontal component of the geomagnetic field which is transverse to the direction of propagation is important. This component of the magnetic field is the source of nonreciprocity, and the remaining components were commonly assumed only to alter the propagation characteristics somewhat (Makorov et al., 1970). The most severe geomagnetic field effects were thus expected in the equatorial region for propagation across the magnetic meridians.

Perhaps the first indications of extreme complexity in modal behavior due to the geomagnetic field are found in the numerical modeling results of Snyder (1968a,b) and Pappert (1968). Snyder (1968a) addressed the problem of mode numbering for typical nighttime ionospheres as a function of azimuthal variation for a horizontal magnetic field. Results indicated that a mode with lowest phase velocity in the west to east direction evolved as a result of continuous variation in magnetic azimuth into a mode in the reverse direction with only second lowest phase velocity. Thus, numbering modes in terms of increasing phase velocity, as is commonly done, results in the first order mode in the west to east direction evolving into the second order mode in the opposite direction and vice versa. Further analysis (Snyder, 1968b) indicated that, for a certain inclination of a dipping geomagnetic field, and at a specific azimuth (near the north-south direction), the two modes considered above became degenerate, forming a single mode. For inclinations more nearly horizontal than the degenerate conditions, mode numbering inconsistencies resulted but, for more nearly vertical inclinations, inconsistencies in mode numbering vanished. Pappert (1968) presented the results of numerical modeling for easterly propagation at midlatitudes. Assuming a vertical dipole exciter, Pappert found that, at the high frequency end of the VLF band (only near 30 kHz), modes which are principally transverse electric (TE) may be of importance in a mode sum. Note that a TE mode can be excited by a vertical dipole only because of the presence of the geomagnetic field.

Snyder and Pappert (1969) extended the analysis to consider both easterly and westerly midlatitude nighttime propagation throughout the VLF band as well as to include azimuthal dependencies of mode parameters for a central VLF fre-

quency at both midlatitudes and equatorial latitudes. It was found that the importance of principally TE modes is much more pronounced for westerly propagation at midlatitudes than for easterly, and that the influence of the principally TE modes on the mode sum can be significant at frequencies at least as low as 20 kHz for the case of westerly propagation. Azimuthal anomalies included drastic polarization changes in going from easterly to westerly paths. In the case of transverse propagation at the magnetic equator, it was shown that modes which are pure transverse magnetic (TM) for propagation to the east may be pure TE for propagation to the west. This is tantamount to the statement that modes which have dominant excitation for easterly propagation may have vanishingly small excitation for westerly propagation. Azimuthal dependencies are characterized by rapid variation of the mode constants in the neighborhood of north-south or south-north propagation both for equatorial and midlatitudes. These variations manifest themselves in marked differences in mode sums for azimuthal changes at least as small as 10°. Further, it was shown that the maximum total signal attenuation occurs for north-south propagation rather than for east-west propagation.

Although Snyder and Pappert (1969) used hypothetical ionospheres, their results have been further substantiated by Foley et al. (1973) using "realistic models of the ionosphere." Foley et al. (1973) essentially duplicated the analysis of Synder and Pappert but used ionospheric models presented in the literature by Deeks (1966) and Smith et al. (1968). Foley et al. concluded that mode characteristics are dependent on the ionosphere model assumed. For example, results with the Smith profile were similar to the results of Snyder and Pappert while under certain circumstances results with the Deeks profile differed. For propagation in the north-south direction with the Deeks profile anomalies were found in the behavior of modes 1 and 2. It would appear that between 16 and 20 kHz, modes 1 and 2 interchange their identity. Although unknown to Foley et al., this identity interchange would seem to be just another manifestation of the modal degeneration reported by Snyder (1968b).

2. Observed Propagation Variations

It is well known that many propagating modes may be supported in metallic waveguides of sufficiently large cross section compared to a wavelength. In such a guide each mode has a different phase velocity, producing interference phenomena as the various modes go in and out of phase at varying distances along the guide. Furthermore, changes in the cross section of the guide are known to produce higher order modes which result in a modified modal interference pattern.

The earth-ionosphere waveguide is four to six wavelengths in height at typical VLF wavelengths. Higher order modes can be excited in the VLF waveguide with greater amplitude than the lowest order mode even though the lowest order mode suffers less attenuation. Thus modal interference as a function of distance from a VLF transmitter is to be expected just as for a metallic guide. Such is indeed the case. For example, VLF field amplitudes were recorded by Rhoads and Garner (1967) aboard an airplane flying between Hawaii and the west coast of the United States. Comparison of their daytime measured amplitudes with results computed using the daytime mode constants of Wait and Spies (1964) showed almost ideal agreement. Rhoads and Garner (1967) showed that under day conditions the effect of the earth's magnetic field on the VLF modal constants can be ignored, at least for distances less than 4000 km. They also confirmed that at distances up to at least 3000 km higher order modes must be considered. The good agreement obtained for daytime data could not be obtained for night data.

Early investigations of VLF propagation to great distances were confined to amplitude measurements. Because of the distances involved, the ground wave could not be used as a reference, and oscillators then available were not sufficiently stable to be used as local reference. In consequence, it was not possible to study the phase of the VLF signals. With the development of atomic frequency standards in the 1960s, investigation of the phase variability of VLF signals became possible. The availability of such stable oscillators, combined with the growing interest in the use of the phase of VLF signals for navigation, prompted several investigations of long distance propagation of VLF radiowaves.

Recall that one of the characteristics of modal excitation and attenuation is the possible change in modal dominance at some distance from a transmitter. At the point where mode dominance changes, the two modes are of equal amplitude. If at this point the two modes are in phase opposition, then the resultant mode interference will result in a deep amplitude minimum accompanied by local instability in the dependence of phase on distance. For example, a minor change in conditions, such as a small change in height of the ionosphere, results in a stepwise change in phase by as much as 2π . Observations of VLF signal phase during daytime at 16 kHz were made by Burgess (1967) aboard an inflight aircraft. A significant result of the measurements was the detection of an abrupt (with respect to distance) change in phase at about 3000 km from the transmitter, which is in good agreement with results using the modal constants from Wait and Spies (1964) for a daytime ionosphere.

Another manifestation of multimode propagation is found in the phenomena of sunrise and sunset fading. This fading is characterized by periodic and repeatable variations in amplitude and phase as the dawn/dusk terminator moves along a VLF propagation path. This fading, typically most pronounced at sunrise on easterly paths and at higher frequencies, was first studied by Yokoyama and Tanimura (1933) who attempted, without success, to explain their observations in terms of a ray-optical propagation model. Another attempt, also not successful, to explain the fading using ray-optical concepts was presented by Rieker (1963). It remained for Crombie (1964) to explain the phenomena using waveguide mode concepts. Of all possible combinations of conditions - sunrise and sunset, position of terminator on propagation path, relative positions of transmitter and receiver, etc. - only two fundamental situations occur within the confines of Crombie's explanation.

The first case depicts the field incident on the terminator from the transmitter as determined by two modes and the field at the receiver determined by only one mode. This situation would be characteristic of a transmitter on the night side of the terminator and the receiver on the day side sufficiently removed to avoid multimode propagation. The received signal then depends on the amplitude and phase relationships of the modes incident on the terminator and on the efficiency with which these modes are converted by the terminator to the single mode which reaches the receiver. Because the modal

relationships are determined by the distance of the terminator from the transmitter, as the terminator moves along the propagation path periodic variations will occur in the received signal. The periods will be determined by the difference in the phase velocities of the two modes entering the terminator, and the variations must occur simultaneously for all points in the portion of the propagation path beyond the terminator region. The fading would be most intense when the two entering modes have the most pronounced interference, which is usually when the terminator is near the transmitter.

The second case depicts the incident field as a single mode. The presence of the terminator leads to multimode generation in the region past the terminator which in turn leads to modal interference. In this case, the interference pattern would appear to be attached to the terminator and to move synchronously with it. Signal minima are then to be expected at fixed distances from the terminator, and the distance between fades will be determined by the difference between the phase velocities of the two modes leaving the terminator region. The deepest signal fades would be expected as the terminator approaches the receiver. This case corresponds to propagation from the sunlit side of the terminator into the night side. Note that in both cases, the fade spacing would be determined by the differences between the phase velocities of two nighttime modes.

A thorough experimental examination of the Crombie model was conducted by Walker (1965) who recorded 18 kHz transmissions from NBA, Balboa, Panama while making repeated shipboard crossings of the Atlantic in the equatorial region. During sunrise (propagation from night to day) signal fades were observed simultaneously at all points in the day portion of the path - in agreement with the first case discussed above. Walker determined the change in terminator position between successive fades and from this calculated the required differences in the phase velocities of the two interfering modes. These results were in good agreement with theoretical results for nighttime ionospheres - further substantiating the Crombie model. Observations were also made during sunset (propagation from day to night) and results were in excellent agreement with the Crombie model.

3. The Equatorial Anomaly

The observations just discussed were, for the most part, made at middle or low latitudes. As the previous discussion indicates, such observations have been adequately explained using quite simple VLF waveguide mode theory. However, some observations made of VLF transmissions over long transequatorial paths have apparently indicated an anomalous effect associated with nighttime or transitional transequatorial VLF propagation.

One of the earliest reports on transequatorial VLF propagation to show an apparent anomaly was by Chilton et al. (1964). They made simultaneous observations of NBA transmissions (Canal Zone, Panama) at 18 kHz for paths to both the northern and southern hemispheres. Both paths were of similar length but the southern hemisphere path crossed the magnetic equator. Although they did not look at transition fading, they did observe an anomalous difference in the diurnal changes of signal amplitude and phase. Chilton et al., suggested their observations resulted from a difference in ionization profile due to latitudinal dependence of cosmic rays. More recently, Chilton and Crary (1971) have suggested that the latitude-dependent ionization source might arise from the recently discovered x-ray stars.

Araki et al. (1969) recorded dual frequency (15.5 and 22.3 kHz) VLF signals in Japan from station NWC in Australia. They reported sunrise fading on 22.3 kHz but not on 15.5 kHz and further noticed that during fading at 22.3 kHz the first phase change was an increase followed by a phase decrease. The nighttime field strength was somewhat less at 15.5 kHz and somewhat higher at 22.3 kHz than during the day. Araki et al. (1969) concluded that their results suggest the existence of a frequency-dependent anomaly of the nighttime field relative to the daytime field along their transequatorial propagation path.

Bickel et al. (1970) conducted an experiment to investigate the apparently anomalous results of Snyder and Pappert (1969), who predicted maximum signal attenuation in a southerly rather than westerly direction. Measurements of 23.4 kHz signals from station NPM (Luaualei, Hawaii) were made aboard an airplane, flying radials along the propagation paths to Seattle, Ontario (California), Samoa, and Wake Island. Bickel et al., confirmed the Snyder and

Pappert (1969) results and concluded the increased southerly attenuation is an effect of the geomagnetic field. An unexplained effect, however, was observed. For the radial to Samoa, rapid signal amplitude variations with distance were observed in the vicinity of the geomagnetic equator. Although equipment problems may be suspected, simultaneous recordings of other Hawaii-based transmissions, made using completely separate equipments, displayed similar results (Bickel, private communication, 1970).

The first report of an equatorial anomaly associated with transition fading was made by Lynn (1967). He reported on VLF transmissions from NLK (Jim Creek, Washington) at 18.6 kHz to Smithfield, South Australia. This propagation path is approximately 13,500 km long and the receiver to geomagnetic equator distance along the path is approximately 5700 km. The direction of propagation is essentially southwesterly. The interference distance reported by Lynn for sunrise transition fading is approximately 2000 km for the terminator located in midlatitudes, that is, in excess of $\pm 20^\circ$ from the geomagnetic equator. Whenever sunrise transition fading was observed while the terminator was within $\pm 20^\circ$ of the geomagnetic equator, the interference distance increased to as much as 3700 km, and when averaged over the anomaly had a value of 2900 km. Lynn (1967) concluded from his observations that the change in interference distance resulted from a change in the difference of phase velocity for two modes as well as from a change in the relative phases of the appropriate mode conversion coefficients. The question of a possible cause for these changes was left unanswered by Lynn. It is interesting to note that Lynn's conclusions are dependent on his selection of a VLF propagation model as well as his selection of a mode conversion model. Lynn (1967) assumed an isotropic propagation model wherein any changes in propagation parameters necessitates changes in ionospheric conditions.

Kaiser (1968) has examined VLF signals from NLK at 18.6 and 24 kHz and WWVL at 20 kHz received at Lower Hutt, New Zealand. These propagation paths are similar to the path considered by Lynn (1967) and Kaiser's results are much the same as Lynn's. An anomalously large interference distance (in excess of 3000 km) was observed for sunrise transition fading when the terminator was within about $\pm 20^\circ$ of the magnetic equator. Kaiser also examined transition fading data previously published elsewhere and concluded that

anomalously large values of the sunrise interference distance is characteristic of generally east to west VLF propagation below about 30° magnetic latitude. A further conclusion by Kaiser (1968) is that any anomaly in sunset transition fading for such paths is relatively minor. Kaiser suggests that a possible cause of the anomaly might be a larger and sharper day-night waveguide transition near the geomagnetic equator as compared to higher latitudes. He does not however suggest a possible cause for the latitudinal dependence of the day-night waveguide transition.

Additional observations of this transition fading anomaly have been reported by Lynn (1969, 1970). These observations further substantiate the general characteristics of the anomaly. A theoretical interpretation of the transequatorial anomaly was presented by Lynn (1970). His interpretation is based only on assumed latitudinal variations in modal phase velocities and relative phases of the mode conversion coefficients. He does not suggest a possible cause for the variations.

Meara (1973) has extended Lynn's (1970) analysis to include determination of the changes in phase velocities within the equatorial anomaly region. He concludes that the phase velocity of the first mode is essentially unaltered when propagating through the equatorial region, whereas that of the second mode is reduced. It should be noted that Meara's results are entirely dependent on the assumed propagation and mode conversion models. Once again, no explanation of a possible cause for the variations in phase velocities is given.

A further application of Lynn's (1970) analysis to explain some anomalous diurnal changes in transequatorial VLF propagation has been made by Araki (1973). The analysis follows essentially that previously discussed. Araki does go a step further than Lynn (1970) and Meara (1973) however, in that he claims the validity of the isotropic propagation model and asserts that any change in propagation parameters results from a modification of the nighttime equatorial ionosphere. Lynn (1978) has pointed out that the propagation paths of Chilton et al. (1964) and Araki (1973) have a west-east component rather than an east-west component, as do the other paths discussed here. He further claims that only a minor azimuthal variation in relative phase velocities of interfering nighttime modes can account for the observations of Chilton et al.

(1964) and Araki (1973). Lynn (1978) thus concludes that the observations of Chilton and Crary (1971) cannot be seen as direct evidence for the control of night VLF reflection heights by stellar x-ray sources. However, Svennesson and Westerlund (1979), using waveguide mode theory combined with nighttime profiles given by ionospheric theory, claim results that support the reports of x-ray star effects on VLF radio signals.

B. Description of Research

This research is concerned with a theoretical and observational characterization of VLF radiowave propagation in equatorial latitudes. It is necessary to be able to model purely propagational effects for this region in order to interpret observational results in terms of changes in the geophysical environment. Examples of some specific questions to be addressed are:

Can the anomalously large interference distance observed for generally east to west transequatorial paths be explained by extending conventional VLF propagation models? For example, can the anomaly be explained simply by including geomagnetic field effects on VLF waveguide mode parameters (as suggested by Lynn)? Can the equatorial magnetic field per se cause enhanced mode conversion, or must a modified terminator (as suggested by Kaiser) or a modified nighttime ionosphere (as suggested by Araki) be employed near the geomagnetic equator? If a modified equatorial terminator or nighttime ionosphere is necessary, what causes the modification? If geomagnetic field effects on the modal constants is the answer, what is the cause for the effect?

Trans-terminator propagation of VLF radiowaves in equatorial latitudes for generally east to west paths is characterized by the anomaly in interference distance. In order to address the question of a cause for this anomaly (e.g., geomagnetic field effects on waveguide modal parameters vs. a modified equatorial terminator), data are needed for additional propagation directions. If the anomaly is caused by a modified equatorial terminator, it seems reasonable to expect a similar effect on a propagation path essentially reciprocal to the paths already discussed. If it is caused by strictly geomagnetic field effects, a reciprocal path should exhibit dissimilar results or perhaps no anomaly at all.

A VLF propagation path nearly reciprocal to those employed by Lynn and Kaiser is available. We shall analyze VLF signals recorded in San Diego from station NWC, Australia. This provides the needed information for a reciprocal path.

Relevant theoretical modeling of VLF radiowave propagation will be performed. This will include consideration of inhomogeneities both in the vertical direction as well as along the propagation path. Anisotropic effects due to the geomagnetic field will be considered.

II. Theory

A. Horizontally Homogeneous Guides

1. Coordinate Transformation

Formulation of waveguide mode theory for VLF propagation in the earth-ionosphere waveguide, homogeneous in and transverse to the direction of propagation, is presented in this section. The earth-ionosphere guide is modeled as cylindrical, with effects of curvature transverse to the direction of propagation accounted for through use of an appropriate "spreading term" as described in Chapter I. Also as mentioned in Chapter I, the formulation employed in this study is based on the pioneering work of Budden (1961, 1962). Because Budden's formulation is essentially planar, a coordinate transformation is employed to convert between cylindrical geometry and planar geometry. The transformation, introduced by Richter (1966) with respect to earth flattening techniques, and used by Pappert (1968) and Abbas et al. (1975) in VLF propagation studies is briefly outlined.

Application of the conformal coordinate transformation of the form $\rho = ae^{z/a}$; $\phi = x/a$ results in circles ($\rho = \text{constant}$) in the ρ, ϕ plane becoming straight lines ($z = \text{constant}$) in the x, z plane. If a represents the radius of the earth, the transformation maps the surface of the earth ($\rho = a$) to the line $z = 0$. The transformation further maps radii ($\phi = \text{constant}$) from the ρ, ϕ plane to lines $x = \text{constant}$ in the x, z plane. A full circular arc ($\phi = 2\pi$) at $\rho=0$ is mapped so that the length of x is the circumference of the earth.

The transformation used here differs from that employed by Richter (1966), Pappert (1968) and Abbas et al. (1975) in that they maintained some selected altitude (H) as invariant in both coordinate frames. However, the two transformations differ only in quantities of second order in smallness. As the invariant altitude (H) approaches zero, the two transformations become identical.

Maxwell's curl equations with time variation of the form $e^{i\omega t}$ for a medium characterized by a dielectric tensor may be written as

$$\begin{aligned}\nabla \times \tilde{\mathbf{E}} &= -ik_o \tilde{\mathbf{H}} \\ \nabla \times \tilde{\mathbf{H}} &= ik_o \tilde{\epsilon} \cdot \tilde{\mathbf{E}}\end{aligned}\quad (1)$$

where k_o is the wave number of free space ($k_o = \omega/c$) and $\tilde{\epsilon}$ is the dielectric tensor. In equations (1), the variable $\tilde{\mathbf{H}}$ is actually the magnetic intensity multiplied by the free space impedance. Assuming $\partial/\partial y = 0$, equation (1) in cylindrical coordinates may be written

$$\begin{aligned}\frac{1}{\rho} \frac{\partial \mathbf{E}_Y}{\partial \phi} &= -ik_o H_\rho; \quad \frac{1}{\rho} \frac{\partial H_Y}{\partial \phi} = ik_o (\tilde{\epsilon} \cdot \tilde{\mathbf{E}})_\rho \\ \frac{\partial \mathbf{E}_Y}{\partial \rho} &= ik_o H_\phi; \quad \frac{\partial H_Y}{\partial \rho} = -ik_o (\tilde{\epsilon} \cdot \tilde{\mathbf{E}})_\phi \\ \frac{1}{\rho} \frac{\partial}{\partial \rho} (\rho \mathbf{E}_\phi) - \frac{1}{\rho} \frac{\partial \mathbf{E}_\rho}{\partial \phi} &= -ik_o H_Y; \quad \frac{1}{\rho} \frac{\partial}{\partial \rho} (\rho H_\phi) - \frac{1}{\rho} \frac{\partial}{\partial \rho} H_\rho = ik_o (\tilde{\epsilon} \cdot \tilde{\mathbf{E}})_Y.\end{aligned}\quad (2)$$

Applying the coordinate transformation to equation (2) yields

$$\frac{\partial \mathbf{E}_Y}{\partial x} = -ik_{oa} \frac{\rho}{a} H_\rho; \quad \frac{\partial H_Y}{\partial x} = ik_{oa} \frac{\rho}{a} (\tilde{\epsilon} \cdot \tilde{\mathbf{E}})_\rho \quad (3a)$$

$$\frac{\partial \mathbf{E}_Y}{\partial z} = ik_{oa} \frac{\rho}{a} H_\phi; \quad \frac{\partial H_Y}{\partial z} = -ik_{oa} \frac{\rho}{a} (\tilde{\epsilon} \cdot \tilde{\mathbf{E}})_\phi \quad (3b)$$

$$\frac{\partial}{\partial z} \left(\frac{\rho}{a} H_\phi \right) - \frac{\partial}{\partial x} \left(\frac{\rho}{a} H_\rho \right) = ik_o \frac{\rho^2}{a^2} (\tilde{\epsilon} \cdot \tilde{\mathbf{E}})_Y; \quad (3c)$$

$$\frac{\partial}{\partial z} \left(\frac{\rho}{a} \mathbf{E}_\phi \right) - \frac{\partial}{\partial x} \left(\frac{\rho}{a} \mathbf{E}_\rho \right) = -ik_o \frac{\rho^2}{a^2} \mathbf{H}_Y. \quad (3d)$$

By making the identifications

$$\begin{aligned} E_x &= \rho/a E_\phi; & E_y &= E_y; & E_z &= \rho/a E_\rho; \\ H_x &= \rho/a H_\phi; & H_y &= H_y; & H_z &= \rho/a H_\rho; \end{aligned} \quad (4)$$

equations (3) become identical to what would be obtained in a rectangular coordinate frame for a medium characterized by permeability tensor and dielectric tensor of the form

$$\underline{\mu} = \begin{pmatrix} 1 & 0 & 0 \\ 0 & e^{2z/a} & 0 \\ 0 & 0 & 1 \end{pmatrix} \quad (5)$$

$$\underline{\epsilon} = \begin{pmatrix} \epsilon_{\phi\phi} & e^{z/a} \epsilon_{y\phi} & e_{\rho\phi} \\ e^{z/a} \epsilon_{\phi y} & e^{2z/a} \epsilon_{yy} & e^{z/a} \epsilon_{\rho y} \\ \epsilon_{\phi\rho} & e^{z/a} \epsilon_{y\rho} & \epsilon_{\rho\rho} \end{pmatrix}. \quad (6)$$

Some additional insight is obtained by considering the transformed equations in the free space region between the earth and ionosphere. Making the usual substitutions into equations (3c) and (3d) from equations (3a) and (3b), along with the free space assumption, yields

$$\left(\frac{\partial^2}{\partial z^2} + \frac{\partial^2}{\partial x^2} \right) E_y = -k_o^2 e^{2z/a} E_y \quad (7a)$$

$$\left(\frac{\partial^2}{\partial z^2} + \frac{\partial^2}{\partial x^2} \right) H_y = -k_o^2 e^{2z/a} H_y. \quad (7b)$$

Thus, the effect of the transformation is to replace the original cylindrical free space region with a planar region filled with a medium which has refractive index equal to $e^{z/a}$ for TE polarized waves or which has permeability equal to $e^{2z/a}$ for TM polarized waves.

2. The Mode Equation

The prototype waveguide model considered here consists of two plates of infinite extent, parallel to the x-y plane and located at $z = 0$ and $z = h$. The interior of the guide is assumed to be free space. This prototype waveguide corresponds to the "fictitious free space region" to be later discussed in Section 4 where it will be used to determine modal excitation factors and polarization coupling. The electromagnetic field is assumed to be independent of the y-coordinate and propagation is assumed to be in the x-direction. Any given waveguide mode will be considered as composed of two crossing plane waves, upgoing and downgoing, with wave normals at the angles $\pm\theta$ to the x-axis.

The nature of the boundary planes will be specified in terms of reflection coefficients. These coefficients are defined in terms of the ratios of specific components of the upgoing and downgoing waves and are therefore dependent on the polarization of the waves. A convenient way of describing the polarization is in terms of the linear components of the complex electric vector which are perpendicular and parallel to the plane of incidence (the x-z plane). The notation $\parallel(1)$ will indicate that the electric vector is parallel (perpendicular) to the plane of incidence.

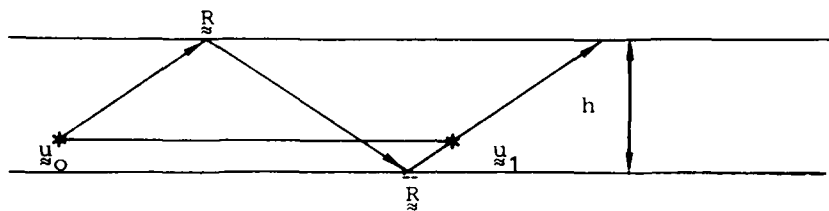
In general, the upper boundary must be considered anisotropic. Thus, there can be a change in polarization upon reflection. The reflecting properties of the upper boundary are given by reflection coefficients having the matrix form

$$\underline{\underline{R}} = \begin{pmatrix} R_{\parallel\parallel} & R_{\perp\parallel} \\ R_{\parallel\perp} & R_{\perp\perp} \end{pmatrix}, \quad (8)$$

where the first subscript describes the polarization of the incident (upgoing) wave and the second subscript denotes the polarization of the reflected wave. The properties of the lower boundary are assumed isotropic and specified by a diagonal reflection matrix of the form

$$\bar{\bar{R}} = \begin{pmatrix} \bar{R}_{\parallel} & 0 \\ 0 & \bar{R}_{\perp} \end{pmatrix}. \quad (9)$$

By considering the upgoing wave as the primary or incident wave, the downgoing wave can be considered as resulting from reflection at the upper boundary. This wave will in turn be reflected at the lower boundary giving rise to another upgoing wave. The requirement that the second upgoing wave be the same as the original yields the mode condition. This process is shown in the diagram below.



The primary wave is represented by the column matrix \bar{u}_0 . The second upgoing wave (\bar{u}_1) is therefore given by

$$\bar{u}_1 = \bar{\bar{R}} \bar{R} \bar{u}_0 \exp[-2ikhsin\theta]$$

where the exponential term accounts for phase change in the double passage across the guide. The self-consistency requirement for the waveguide mode is thus

$$\det [\bar{\bar{R}} \bar{R} \exp(-2ikhsin\theta) - \mathbb{I}] = 0 \quad (10)$$

where \mathbb{I} is the unit diagonal matrix.

3. Point Sources and Line Sources

The source is assumed to be a vertical Hertzian dipole. Budden (1961, 1962) has shown that a vertical dipole is equivalent to an infinite set of line quadrupoles, where the line quadrupoles are located parallel to the x-y plane and inclined at (complex) angles to the y-axis. This is easily seen by considering the Hertz vector for a dipole at the origin. If the dipole is

parallel to the z-axis, the Hertz vector has only a z-component and is proportional to $\exp(-ikr)/r$. For a dipole of unit strength, the Hertz vector is given by (Budden, 1962)

$$\frac{e^{-ikr}}{4\pi r} = -\frac{k}{8\pi} \int_{-\pi/2-i\infty}^{\pi/2+i\infty} \cos(\alpha) H_1^{(2)}(ks) d\omega , \quad (11)$$

where

$$\begin{aligned} \alpha &= \arctan [z/(x \cos(\omega) + y \sin(\omega))] \\ s &= [(x \cos(\omega) + y \sin(\omega))^2 + z^2]^{1/2}. \end{aligned} \quad (12)$$

Thus s is the distance from a point (x, y, z) to a line in the x-y plane passing through the origin at an angle ω to the y-axis and α is the angle between the x-y plane and the line along s . $H_1^{(2)}$ is a Hankel function of the second kind of order one. The term $\cos(\alpha)H_1^{(2)}(ks)$ would result from a line quadrupole source in the x-y plane at an angle ω to the y-axis. Consider a line quadrupole source as composed of two line dipole sources at $x = \frac{1}{2}\delta x$ and $x = -\frac{1}{2}\delta x$ in the x-y plane. The line dipoles consist of closely spaced dipoles oriented parallel or antiparallel to the z-axis and distributed parallel to the y-axis. The Hertz vector for the line dipoles is proportional to $H_0^{(2)}(kp)$ where $p = (x^2 + z^2)^{1/2}$. Letting δx tend to zero and letting the strengths $(M, -M)$ of the line dipoles increase in such a way that the product $M\delta x$ remains finite will result in a term proportional to $\partial H_0^{(2)}(kp)/\partial x$, which reduces to a term of the form $\cos(\theta)H_1^{(2)}(kp)$, where $\cos\theta=x/p$. From the definitions of s and α in (12), it is clear that the integral in (11) results from an infinite set of line quadrupoles in the x-y plane, each at a different angle ω to the y-axis. Because the path of integration in (11) is not unique, there is an infinite number of ways in which the angles ω may be chosen.

Consider a guide bounded by perfectly conducting plates with a line source parallel to the y-axis. This source generates waveguide modes and each consists of crossing plane waves with normals in the x-y plane at angles $\pm\theta_m$ to the x-axis. For a line source at an angle ω to the y-axis, the component plane wave has the form $\exp[-ik([x \cos(\omega) + y \sin(\omega)] C_m + z S_m)]$ where $C_m =$

$\cos(\theta_m)$ and $S_m = \sin(\theta_m)$. A point source within the guide is now represented by an infinite set of line sources such that the total field of the component wave is proportional to

$$\int_{-\pi/2-i\infty}^{\pi/2+i\infty} \exp[-ik([x \cos(\omega) + y \sin(\omega)]C_m + zS_m)] d\omega. \quad (13)$$

Making the substitutions $\rho = (x^2 + y^2)^{1/2}$ and $\cos(u) = x/\rho$ in (13) gives

$$\int_{-\pi/2-i\infty}^{\pi/2+i\infty} \exp[-ik\rho C_m \cos(\omega-u)] \exp(-ikzS_m) d\omega. \quad (14)$$

The integration in (14) yields a Hankel function of the second kind of order zero (Sommerfeld, 1949). Thus, the total field of the component wave is proportional to

$$H_0^{(2)}(k\rho C_m) \exp(-ikzS_m).$$

The appropriate Hankel function exchange for the exponential term when using a line source is therefore

$$\exp(-ikxC_m) + H_0^{(2)}(k\rho C_m). \quad (15)$$

4. Modal Excitation Factors and Polarization Coupling

The excitation of waveguide modes is conveniently treated in terms of line sources. The technique consists of selecting one of the possible line sources for the integrand in (11), finding the mode excitation for this line source and then effecting a change from an exponential term to the appropriate Hankel function. Following the method of Budden (1961, 1962), the source is a line of quadrupoles at height d (near the ground) parallel to the y -axis. A fictitious free space region is introduced extending from $z = 1$ to $z = u$ such

that $l < d < u$ (the line source is assumed within the free space region). The region above $z = u$ is characterized by the reflection coefficient matrix \bar{R}_u while the region below $z = l$ is characterized by a reflection coefficient matrix \bar{R}_1 . Assuming that the line source has unit strength, the y -component of the magnetic field in infinite free space can be written

$$H_y = \frac{k_0^3}{4\pi\epsilon_0} \int_{0-i\infty}^{\pi+i\infty} \exp[ik_0(xC + |z-d|S)] C^2 d\theta, \quad (16)$$

where $C = \cos(\theta)$, $S = \sin(\theta)$ and the limits of integration are selected to ensure convergence for all x (Sommerfeld, 1949). The primary field integrand in equation (16) represents a plane wave which undergoes reflections at $z=u$ and $z=1$, and these reflected waves must be added to the primary field to obtain the total field. Four combinations are possible, two from waves initially upgoing or downgoing at the source and two from waves reaching the reception point upgoing or downgoing.

An initially upgoing wave is converted to a downgoing wave by the reflection process denoted by the operator $(\bar{R}_u \bar{R}_1)^N \bar{R}_u$ and to an upgoing wave by the operator $(\bar{R}_1 \bar{R}_u)^N$. An initially downgoing wave is converted to an upgoing wave by the operator $(\bar{R}_1 \bar{R}_u)^N \bar{R}_1$ and to a downgoing by the operator $(\bar{R}_u \bar{R}_1)^N$. The N denotes N reflection processes of the type described by the bracketed term. Phase terms must also be associated with each reflection process to account for the transversals to-and-fro between $z=1$ and $z=u$. The subscripts u and 1 denote reflection coefficients evaluated at $z=u$ and $z=1$, respectively.

The total field is obtained by combining the primary and all reflected fields and letting the dimensions of the free space region tend to zero. This requires taking the limits $l \rightarrow u$ and $z \rightarrow d$ in such a way that $l < d < u$ is maintained. The total field may be written as

$$\begin{aligned}
 H_Y &= \frac{k_o^3}{4\pi\epsilon_o} \sum_{N=0}^{\infty} \int e^{-ik_o x c} (\bar{R} \bar{R})^N \bar{p} c^2 d\theta \\
 &+ \frac{k_o^3}{4\pi\epsilon_o} \sum_{N=0}^{\infty} \int e^{-ik_o x c} (\bar{R} \bar{R})^N \bar{R} \bar{p} c^2 d\theta \\
 &+ \frac{k_o^3}{4\pi\epsilon_o} \sum_{N=1}^{\infty} \int e^{-ik_o x c} (\bar{R} \bar{R})^N \bar{p} c^2 d\theta \\
 &+ \frac{k_o^3}{4\pi\epsilon_o} \sum_{N=1}^{\infty} \int e^{-ik_o x c} (\bar{R} \bar{R})^N \bar{R} \bar{p} c^2 d\theta . \tag{17}
 \end{aligned}$$

The reflection coefficients are evaluated at $z=d$ and the subscripts l,u are no longer needed. In equation (17), the first summation starts with $N=0$ in order to include the primary, nonreflected wave, and \bar{p} is a column matrix whose second element is zero corresponding to a vertical electric dipole source.

The order of summation and integration is now reversed so that each integrand will contain a geometric series. It can be shown (Budden, 1961, 1962) that the series converges for certain simplified cases, and convergence is assumed here. Summation of the geometrical series gives

$$\sum_{N=0}^{\infty} (\bar{R} \bar{R})^N = [1 - \bar{R} \bar{R}]^{-1} \tag{18}$$

$$\begin{aligned}
 \sum_{N=1}^{\infty} (\bar{R} \bar{R})^N &= (\bar{R} \bar{R}) [1 - \bar{R} \bar{R}]^{-1} \\
 &= \bar{R} [1 - \bar{R} \bar{R}]^{-1} \bar{R}
 \end{aligned} \tag{19}$$

$$\begin{aligned}
 \sum_{N=1}^{\infty} (\bar{R} \bar{R})^N \bar{R} &= \bar{R}^{-1} \sum_{N=1}^{\infty} (\bar{R} \bar{R})^N \\
 &= \bar{R} [1 - \bar{R} \bar{R}]^{-1} .
 \end{aligned} \tag{20}$$

Consequently the result of summing the series in equation (17) is

$$H_y = \frac{k_o^3}{4\pi\epsilon_o} \int_{0-i\infty}^{\pi+i\infty} e^{-ik_o x C_n} (1 + \frac{R}{a}) [1 - \frac{R}{a} \frac{R}{a}]^{-1} (1 + \frac{R}{a}) \frac{R}{a} C^2 d\theta . \quad (21)$$

If the sign of θ is reversed, the role of incident and reflected wave is exchanged and each reflection element is replaced by its inverse. The integrand simply changes sign upon reversal of the sign of θ . The integral may be evaluated using the theory of residues by deforming the contour to run from $\pi/2 + i\infty$ to $-\pi/2 - i\infty$ symmetrically through the origin. Because the integrand is antisymmetric about $\theta = 0$, the integral along the new contour is zero. In changing the contour, however, singularities are crossed, the most important of which are poles of the factor $[1 - \frac{R}{a} \frac{R}{a}]^{-1}$. The residue contribution of a simple pole at θ_n is

$$H_{yn} = \frac{ik_o^3}{2\epsilon_o} e^{-ik_o x C_n} \frac{(1 + \frac{R}{a})_n X_n (1 + \frac{R}{a})_n \frac{R}{a} C_n^2}{(\frac{\partial F}{\partial \theta})_{\theta_n}} , \quad (22)$$

where

$$F = \det [1 - \frac{R}{a} \frac{R}{a}] \quad (23)$$

$$X_n = \lim_{\theta \rightarrow \theta_n} \{F[1 - \frac{R}{a} \frac{R}{a}]^{-1}\}$$

and the subscript, n , signifies that the quantities are evaluated at $\theta = \theta_n$. The pole condition $F = 0$ is identical to the waveguide mode equation (10) in the limit $h \rightarrow 0$. Thus, the solution of the pole condition yields the waveguide modes and the residues at the poles give the excitation factors. Performing the matrix multiplications in equation (22), using the Hankel function substitution (equation (15)) and employing the geometrical spreading factor yields

$$H_{yn} = \frac{-k_o^{5/2} C_n^{3/2} e^{i\frac{\pi}{4}}}{2\epsilon_o \sqrt{2\pi a \sin(\rho/a)}} \frac{(1 + \frac{R}{a})^2 (1 - \frac{R_{11} R_1}{R_{11} R_1})}{\frac{R_{11}}{R_{11}} (\frac{\partial F}{\partial \theta})_{\theta_n}} e^{-ik_o \rho C_n} . \quad (24)$$

To be compatible with the mode sum of Chapter I (equation (1)) it is necessary to change the reference direction for θ from the x -axis to the z -axis. Doing so simply requires the interchange of $\sin\theta$ and $\cos\theta$.

Equation (24) requires the source and reception point to be at the same height, which is also the height at which the reflection elements are to be determined. If the dependence of H_{yn} on height z is given by the function $G_n(z)$, then an obvious extension of equation (24) to include arbitrary source and reception height involves multiplication by the function

$$\frac{G_n(z_T)}{G_n(d)} \frac{G_n(z_R)}{G_n(d)},$$

where z_T is the transmitter height, z_R is the receiver height and d is the evaluation height for the reflection elements, assumed to be below the ionosphere.

Whenever the ionosphere is assumed to be isotropic (no geomagnetic field) the field components can be divided into two sets. These are the well known TE ($H_y = 0$) and TM ($E_y = 0$) modes. When anisotropy is included, however, a given mode in general involves both H_y and E_y . To determine the coupling between the TM and TE components of the eigenfunctions again we introduce a thin, fictitious region of free space within the transformed planar waveguide. The region is assumed to be centered at some altitude $z=d$ which is below the ionosphere so that the region $z < d$ can be considered isotropic. Within this region, the fields of the TM and TE components can be considered in terms of upgoing and downgoing plane waves. Furthermore, the eigenfunctions satisfy the condition that a particular component, say the upgoing, must be returned to its original value after being reflected from the two boundaries of the thin free space region. Thus, for the upgoing component e_1^u (the component perpendicular to the plane of propagation), the requirement is

$$e_1^u = l_{1R}^{-} l_{1R}^{+} e_1^u + l_{1R}^{-} R_{1R} l_{1R}^{+} e_{||}^u$$

or,

$$\frac{e_{\parallel}^u}{e_{\perp}^u} = \frac{1 - \frac{\perp R_{\perp}}{\parallel R_{\parallel}} \frac{\perp R_{\perp}}{\parallel R_{\parallel}}}{\frac{\perp R_{\perp}}{\parallel R_{\parallel}} \frac{\parallel R_{\parallel}}{\perp R_{\perp}}} . \quad (25)$$

In the free space region

$$e_{\parallel}^u = \cos(\theta) e_x^u - \sin(\theta) e_z^u \equiv h_y^u$$

$$e_{\perp}^u = e_y^u ,$$

where h_y^u is the upgoing component of H_y and e_y^u is the upgoing component of E_y . The total H_y and E_y fields within the free space gap at $z=d$ are therefore

$$E_y = e^{-ik_o Cd} \left(1 + \frac{1}{\frac{\perp R_{\perp}}{\parallel R_{\parallel}}} \right)$$

$$H_y = \left(\frac{1 - \frac{\perp R_{\perp}}{\parallel R_{\parallel}} \frac{\perp R_{\perp}}{\parallel R_{\parallel}}}{\frac{\perp R_{\perp}}{\parallel R_{\parallel}} \frac{\parallel R_{\parallel}}{\perp R_{\perp}}} \right) \left(1 + \frac{1}{\frac{\perp R_{\perp}}{\parallel R_{\parallel}}} \right) e^{-ik_o Cd}$$

and their ratio is

$$\frac{E_y(d)}{H_y(d)} = \frac{\parallel R_{\parallel} \frac{\perp R_{\perp}}{\parallel R_{\parallel}} \left(1 + \frac{\perp R_{\perp}}{\parallel R_{\parallel}} \right)}{\left(1 - \frac{\perp R_{\perp}}{\parallel R_{\parallel}} \frac{\perp R_{\perp}}{\parallel R_{\parallel}} \right) \left(1 + \frac{\perp R_{\perp}}{\parallel R_{\parallel}} \right)} \equiv \gamma(d) . \quad (26)$$

In equation (26) the reflection coefficients are evaluated at $z=d$.

5. Determination of Reflection Coefficients

Two basic methods have been employed for the numerical calculation of ionospheric reflection coefficients for horizontally stratified anisotropic media. One involves the numerical integration of a set of differential equations describing the EM fields directly, such as the equations of Clemmow and Heading (1954). Use of the equations of Clemmow and Heading implies consider-

ation of the ionosphere as a cold magnetoplasma. Instability problems are encountered if the field equations are directly integrated. This may be avoided by introducing a new variable for integration, which does not have such instabilities.

Thus, Budden (1955) considered integration of the linear Clemmow and Heading equations, pointing out the numerical instabilities, and then introducing a non-linear differential equation for the reflection coefficients. It can be easily shown that the differential equation for the reflection coefficient is of the Riccati type for many simple ionospheric models. As pointed out by Ralston and Wilf (1967), the Riccati equation exhibits excellent stability for numerical integration. Budden (1955) pointed out that the new integration not only did not have numerical instabilities but also required less computer time and core than integration of the wavefields directly. Barron and Budden (1959) introduced a different variable, the admittance matrix, which they claimed required less computer time and core than the reflection matrix. However, use of the admittance matrix sometimes leads to numerical difficulties. A disadvantage of using either the reflection or admittance matrix is that it is difficult to obtain the wavefields directly from the functions employed in the integration.

Pitteway (1955) introduced a numerical way to overcome the instability. Pitteway's technique was to integrate the Clemmow-Heading field equations directly and to use Gram-Schmidt orthogonalization at various steps in the integration process. An advantage of this scheme is that wavefields within the ionosphere are made available. However, this is achieved at the price of large computer core requirements. Alternative schemes using Pitteway's basic idea have been developed. Walsh (1967) and Seliga (1966), for example, integrate a set of equations for what they term "vacuum modes" (Poeverlein, 1967), applying Gram-Schmidt orthogonalization to avoid numerical instability.

The other basic method involves dividing the inhomogeneous ionosphere into thin homogeneous layers. For example, Johler and Harper (1962) devised a matrix of large dimension to describe a multislab ionosphere, and Price (1964) simplified the matrix to a series of 4x4 matrices. The problem of numerical instability was not addressed. Wieder (1968) attempted to solve the numerical instability problem with the Price 4x4 matrix by performing the iterative multiplication from the bottom of the ionosphere upward, stopping where

reflection coefficients seemed to stabilize. Although usually effective, this scheme is also subject to numerical problems. Nagano et al. (1975) solved the numerical swamping problem using Gram-Schmidt orthogonalization with the iterative matrix multiplication applied to a layered ionosphere.

The original reflection coefficient matrix integration (Budden, 1955), using standard fourth order Runge-Kutta techniques (Ralston and Wilf, 1967), has been adopted for this study. The integration is started at some height above which negligible reflection occurs. Error control and adjustment of the integration step size is determined by comparing second-order Runge-Kutta results with fourth-order results.

Analytic expressions are obtained for the ground reflection coefficients. Consider looking downward at some height (d) below the ionosphere in the transformed planar guide of Section 1. In order to be compatible with the assumptions of Sections 2 and 4, the region above d is assumed to be free space, whereas the region below d is filled with the "equivalent" permeability or dielectric medium as described in Section 1. The fields in the region between $z=d$ and $z=0$ satisfy equations (7a,b) while the fields above d and within the earth have simple exponential forms.

Recognizing that all altitudes of interest are small compared to the radius of the earth (a), the exponential term in equation (7) is expanded to first order in z/a . A variation in the x -direction of the form $e^{-ik_0 Sx}$ is assumed. Note that later the variable S will be identified as $\sin(\theta)$ where the angle θ is referenced to the vertical rather than the horizontal as in previous sections. With the above assumptions, equation (7b) for TM waves becomes

$$\frac{H''}{Y} + k_0^2 (C^2 + \alpha z) \frac{H}{Y} = 0, \quad (27)$$

where $C^2 = 1 - S^2$, $\alpha = 2/a$ and the double prime denotes second differentiation with respect to z .

With the change of variable

$$t = \left(\frac{k_0}{\alpha}\right)^{2/3} (C^2 + \alpha z), \quad (28)$$

the equation becomes

$$\frac{H''}{y} + t \frac{H}{y} = 0, \quad (29)$$

where now the double prime denotes differentiation with respect to t . Equation (29) is Stokes' equation. Thus, H_y is linearly expressible in terms of solutions to Stokes' equation. In this study, we shall use the modified Hankel functions of order one third (h_1, h_2), as defined by the Computation Laboratory at Cambridge, Massachusetts (1945). Using a similar procedure for TE polarization, we shall arrive at similar results except that the transformed planar guide will contain a medium with refractive index given by $e^{z/a}$.

The waves in the three regions are given by

$$H_y = e^{ik_o Cz} + \bar{R}_{\parallel} e^{-ik_o Cz}$$

Region I:

$$z > d \quad E_x = -C \left(e^{ik_o Cz} - \bar{R}_{\parallel} e^{-ik_o Cz} \right)$$

$$H_y = a_1 h_1(t) + a_2 h_2(t)$$

Region II:

$$0 < z < d \quad E_x = i \left(\frac{\alpha}{k_o} \right)^{1/3} (a_1 h'_1(t) + a_2 h'_2(t))$$

$$H_y = e^{ik_o \tau z}$$

Region III:

$$z < 0 \quad E_x = -\frac{\tau}{N^2} e^{ik_o \tau z},$$

where \bar{R}_{\parallel} is the TM reflection coefficient being sought, h_1 and h_2 are modified Hankel functions of order one third, N is the refractive index of the ground and $\tau = (N^2 - s^2)^{1/2}$, taken with negative imaginary part. Continuity requirements between the regions leads to the results

$$\bar{R}_{\parallel} = \frac{C f_{\parallel}(d) + i \left(\frac{\alpha}{k_o} \right)^{1/3} f'_{\parallel}(d)}{C f_{\parallel}(d) - i \left(\frac{\alpha}{k_o} \right)^{1/3} f'_{\parallel}(d)},$$

where

$$\begin{aligned}
 f_{\parallel}(z) &= H_2(t_0) h_1(t) - H_1(t_0) h_2(t) \\
 H_j(t) &= h_j'(t) - i \left(\frac{\alpha}{k_0}\right)^{1/3} \frac{\tau}{N^2} h_j(t) \\
 t &= \left(\frac{\alpha}{k_0}\right)^{2/3} (c^2 + \alpha z) \\
 t_d &= \left(\frac{\alpha}{k_0}\right)^{2/3} (c^2 + \alpha d) .
 \end{aligned} \tag{30}$$

Following a similar procedure, results for the TE polarization are given by

$$\bar{R}_\perp = \frac{c f_\perp(d) + i \left(\frac{\alpha}{k_0}\right)^{1/3} f'_\perp(d)}{c f_\perp(d) - i \left(\frac{\alpha}{k_0}\right)^{1/3} f'_\perp(d)} ,$$

where

$$\begin{aligned}
 f_\perp(z) &= F_2(t_0) h_1(t) - F_1(t_0) h_2(t) \\
 F_j(t) &= h_j'(t) - i \left(\frac{\alpha}{k_0}\right)^{1/3} \tau h_j(t) .
 \end{aligned} \tag{31}$$

B. Horizontally Inhomogeneous Guides

If significant variations occur along the direction of propagation, which is often the case in the earth-ionosphere waveguide, then homogeneous guide formulations require modification. For such cases, there are two techniques for mode summation that are commonly used at VLF. One employs a WKB approach and the other uses mode conversion.

In the WKB technique, an eigenmode is assumed to be uniquely and independently identifiable anywhere along a propagation path. Furthermore, each mode is assumed to depend only on the local characteristics of the waveguide and to propagate independently of the existence of any other modes. The WKB formulation generalizes the expression for the mode summation in equation (1), Chapter I, to the form

$$E_v(d) = \frac{K(P, f)}{\sqrt{\sin d/a}} \sum_n \frac{T_n R^{1/2}}{(\Lambda_n \Lambda_n)} G_n G_n e^{-ik_0 \int_0^d S_n(x) dx} . \tag{32}$$

Note that the only differences arise from the use of the geometric mean of the excitation factors at transmitter (Λ_n^T) and from receiver (Λ_n^R) locations and from the integration of the complex propagation factor along the path. The WKB formulation was apparently introduced simply as an "obvious extension" of the homogeneous mode sum by Wait (1964), who further noted that the form is similar to what would be expected if a WKB formulation were applied, although no actual derivation was presented. The use of the name WKB mode sum has persisted.

In the mode conversion method, eigenmodes are assumed to be uniquely and independently identified only in a local sense. Even though the eigen characteristics of a mode depends only on local characteristics of the waveguide, the propagation of each mode depends not only on the existence of other modes but also on the past and future propagation history of itself and the other modes.

The approach using mode conversion does not lend itself conveniently to consideration of transition fading on very long VLF propagation paths. The WKB method, although easily applied, is unable to handle the rapid change in guide characteristics that occur at the terminator (Pappert and Snyder, 1972). A difficulty encountered when using mode conversion arises from the necessity of knowing the future propagation history of each mode. Making appropriate assumptions to relieve this requirement can lead to some simplification, but the resulting formulation is still not convenient for very long paths. A further difficulty is that conventional mode conversion techniques require a knowledge of all the vector components of the electromagnetic field throughout all space.

Numerous methods have been presented for circumventing this latter problem. Wait (1968a,b) for example, formulated mode conversion using isotropic impedance boundary conditions with the result that fields were required only for the region between the upper (ionospheric) impedance boundary and the lower (ground) impedance boundary. Such boundary conditions are certainly not appropriate for the nighttime ionosphere and thus not for consideration of transitions from night to day. Smith (1974) extended Wait's (1968a,b) results to include boundary anisotropy by using impedance matrix boundary conditions. His analysis however, was for a planar, empty waveguide and was directed

towards considering ground effects. For the ionosphere Smith (1974) assumed the quasi-longitudinal approximation (given by Budden, 1961) for a homogeneous cold plasma, and this is not suitable for the study at hand.

Galejs (1971) presented a modified mode conversion formulation for an abrupt change between daytime and nighttime anisotropic ionospheres. Conventional mode conversion theory usually represents the EM field as an expansion in terms of a suitably chosen complete set of orthogonal functions. The Galejs formulation employs an incomplete set of non-orthogonal functions. The formulation now to be employed is similar to that of Galejs (1971).

1. The Operator Equations

The operator equations presented in this section are based on Maxwell's equations in two (rectangular) dimensions and are patterned after the formulations of Pappert and Smith (1972). Furthermore, material media are assumed to be characterized by constitutive parameters (permittivity and permeability) that can be inhomogeneous in one dimension. This is quite compatible with the usual procedure for handling the earth-ionosphere waveguide by describing the electromagnetic properties of the ionosphere with the aid of a vertically inhomogeneous dielectric tensor.

We start with equation (3), use the substitutions in equation (4), and eliminate the E_x and H_x components. This leads to the differential operator equation

$$\underline{L} \underline{e} = - \frac{1}{ik_0} \frac{\partial \underline{e}}{\partial x}, \quad (33)$$

where \underline{e} is a four element column vector given by

$$\underline{e} = \begin{pmatrix} E_y \\ E_z \\ H_y \\ H_z \end{pmatrix} \quad (34)$$

and \underline{L} is a 4×4 matrix differential operator. Equation (33) is cast as an eigenvalue equation by using the functional form $\exp(-ik_0 s_n x)$, so that $\underline{L} \underline{e}_n = s_n \underline{e}_n$. These \underline{e}_n form the set of expansion functions used in conventional mode conversion theory.

To find an operator adjoint to \tilde{L} a procedure discussed by Pappert and Smith (1972) is used. First, let the inner product be defined by

$$\langle \tilde{a}, \tilde{b} \rangle = \int_{-\infty}^{\infty} \tilde{a}^* \cdot \tilde{b} dz \quad (35)$$

where the tilde over a denotes transpose and the asterisk denotes conjugation. Next, the operator adjoint to \tilde{L} is defined by the relationship

$$\langle \tilde{L}^+ \tilde{w}, \tilde{e} \rangle \equiv \langle \tilde{w}, \tilde{L} e \rangle \quad (36)$$

which is just a prescription for integration by parts to find the form of \tilde{L}^+ as well as the necessary boundary conditions on the adjoint functions (w) in order that the integrated contributions vanish. Pappert and Smith (1972) showed that the adjoint functions can be obtained from direct functions by considering a second waveguide which is related to the original one in a simple way. In the original guide, the z -axis is taken as vertical, and propagation is assumed in the xz -plane. The x -direction-cosine of the geomagnetic field is 1 in the original guide. The adjoint guide is obtained by replacing 1 with -1. By examining symmetry properties of the elements of the ionospheric permittivity tensor, Pappert and Smith (1972) showed that the adjoint eigenfunctions are given in terms of eigenfunctions of the adjoint waveguide according to the relationship

$$\tilde{w}_n^* = \begin{pmatrix} w_{1n}^* \\ w_{2n}^* \\ w_{3n}^* \\ w_{4n}^* \end{pmatrix} = \begin{pmatrix} H_{zn}(-1) \\ -H_{yn}(-1) \\ -E_{zn}(-1) \\ E_{yn}(-1) \end{pmatrix}. \quad (37)$$

Further, from the definition of adjoint given by equation (36) the usual biorthogonality relations hold. Thus

$$\begin{aligned} \langle \tilde{L}^+ \tilde{w}_n, \tilde{e}_m \rangle &= \lambda_n^* \langle \tilde{w}_n, \tilde{e}_m \rangle \\ &= \langle \tilde{w}_n, \tilde{L} \tilde{e}_m \rangle \\ &= S_m \langle \tilde{w}_n, \tilde{e}_m \rangle \end{aligned}$$

which shows that $\langle \tilde{w}_n, \tilde{e}_m \rangle = 0$ as well as $\lambda_n = S_n^*$, for nondegenerate eigenfunctions.

2. Mode Conversion

Fundamental to the mode conversion formulation employed here is the notion that any variation in the VLF propagation conditions along a path can be modeled as a series of discrete changes between homogeneous sections along the path. With this in mind, it is seen that the fundamental analytical requirement is the determination of mode conversion coefficients due to a single abrupt change in waveguide characteristics.

Following classical procedures, consider a mode of unit amplitude incident on such a discontinuity in a waveguide. This mode is described in terms of its height-gain function $\vec{e}_j^I(z)$, where the superscript I denotes the incident region, the subscript j denotes the jth mode, the overarrow indicates a forward propagating mode, and the underrbrace indicates a vector quantity. Note that the terms height-gain function and eigenfunction are used here interchangeably even though more traditional usage limits the term height-gain to individual components of the vector eigenfunction. The discontinuity in the guide generates both reflected, or backward propagating, modes within the incident region (I) and transmitted, or forward propagating, modes within the transmission region (II). Backward propagating modes might also exist in region II due to another discontinuity; these will therefore be included. The continuity requirements lead to the equation

$$\vec{e}_j^I(z) + \sum_m r_{mj} \vec{e}_m^I(z) = \sum_n T_{nj} \vec{e}_n^{II}(z) + \sum_l R_{lj} \vec{e}_l^{II}(z) \quad (38)$$

which is independent of the position of the discontinuity between regions I and II. In equation (38), the coefficient r_{mj} is a coefficient describing the conversion of the incident mode (j) into a backward traveling mode (m) in region I ($\vec{e}_m^I(z)$), and T_{nj} is a coefficient describing conversion of the incident mode (j) into the forward traveling mode (n) of region II ($\vec{e}_n^{II}(z)$). The R_{lj} are the coefficients appropriate to possible backward traveling modes in region II ($\vec{e}_l^{II}(z)$).

Recall that a major problem with implementation of mode conversion concepts arises from the need to know the future propagation history. In terms of equation (38), this concept is represented by the coefficients R_{lj} . By making the assumption that appreciable reflection does not occur, so that there can be no backward traveling modes, the R_{lj} may be set equal to zero. The r_{mj} are then also all zero and equation (38) reduces to

$$\tilde{e}_j^I(z) = \sum_n T_{nj} \tilde{e}_n^{II}(z). \quad (39)$$

The assumption of negligible reflection is not unique to this study. It is commonly made and has been demonstrated to be adequate in numerous cases (Wait, 1968a,b; Galejs, 1971; Pappert and Snyder, 1972; Smith, 1974). In equation (39), there are assumed to be N modes in region II so that there are N conversion coefficients.

Conventional mode conversion techniques require multiplication of equation (39) by the transpose conjugate of the adjoint function for the m th forward traveling mode in region II, followed by integration over all space. Doing so, and recalling the biorthogonality relationships, we obtain the well-known result

$$\int_{-\infty}^{\infty} \tilde{w}_m^* \cdot \tilde{e}_j^I dz = T_{mj} \int_{-\infty}^{\infty} \tilde{w}_m^* \cdot \tilde{e}_m^{II} dz,$$

more conveniently written as

$$I_{m,j}^{II,I} = T_{mj} I_{m,m}^{II,II} \quad (m = 1, N). \quad (40)$$

Solving for the conversion coefficient yields the apparently simple result

$$T_{mj} = I_{m,j}^{II,I} / I_{m,m}^{II,II}. \quad (41)$$

The simplicity of equation (40) depends on knowing the height-gain functions throughout all space. Such a requirement is the main limitation to the

application of mode conversion techniques to very long VLF paths. Relaxing the integration limits to some finite value prevents use of the biorthogonality relationships and yields, instead of equation (40), the result

$$I_{m,j}^{II,I} = \sum_n T_{nj} I_{m,n}^{II,II} \quad (m = 1, N), \quad (42)$$

where there are N equations and N unknowns so that the system can be solved for the T_{nj} . In equation (42)

$$\begin{aligned} I_{m,j}^{II,I} &= \int_0^h \tilde{w}_m^{*II} \cdot \tilde{e}_j^I dz \\ I_{m,n}^{II,II} &= \int_0^h \tilde{w}_m^{*II} \cdot \tilde{e}_n^{II} dz \end{aligned} \quad (43)$$

where the overarrow notation is dropped because only forward propagating modes are considered.

For application to the VLF earth-ionosphere problem, the above procedure may be justified as follows. First, the various eigenvalues and eigenfunctions are determined using the complete geometry, $(-\infty < z < +\infty)$. Second, the eigenfunctions can be expected to decay rapidly within the earth and within the ionosphere. Below the ionosphere but within the waveguide, the vector eigenfunctions degenerate into the isotropic TM and TE components with a prescribed coupling between the two for a given mode. By taking the upper limit $\cdot i$ the integral to be within the guide and below the ionosphere it is possible to write the various $I_{n,k}$ in terms of known functions; namely the modified Hankel functions discussed in Section A.5. The procedure used here is actually expansion in terms of "non-orthogonal" functions and is certainly better than assuming orthogonality and "throwing away" the contributions to the integrals from the ionosphere.

The j th vector eigenfunction for either region is defined to be (from equation (34))

$$\tilde{e}_j = \begin{pmatrix} e_y j \\ e_z j \\ h_y j \\ h_z j \end{pmatrix}. \quad (44)$$

Because the upper limit on the integrals in equation (43) is to be taken below the ionosphere, equation (44) can be written as

$$\mathbf{e}_j = \begin{pmatrix} e_{yj} \\ -s_j h_{yj} \\ h_{yj} \\ s_j e_{yj} \end{pmatrix}.$$

The adjoint vector eigenfunction is given by equation (37) as

$$\mathbf{w}_m = \begin{pmatrix} h_{zm}^*(-1) \\ -h_{ym}^*(-1) \\ -e_{zm}^*(-1) \\ e_{ym}^*(-1) \end{pmatrix} = \begin{pmatrix} s_m^* e_{ym}^*(-1) \\ -h_{ym}^*(-1) \\ s_m^* h_{ym}^*(-1) \\ e_{ym}^*(-1) \end{pmatrix}$$

where the notation indicates that elements of the adjoint eigenfunction are obtained by reversing the x-axis direction-cosine of the earth's biasing magnetic field. The first integral in equation (43) thus becomes

$$I_{m,j}^{II,I} = (s_m^{II} + s_j^I) \int_0^h (e_{ym}^{II}(-1) e_{yj}^I + h_{ym}^{II}(-1) h_{yj}^I) dz. \quad (45)$$

From Section A.4 and A.5 it is seen that $h_{ym}(-1) = h_{ym}$ but that $e_{ym}(-1) \neq e_{ym}$. However, from equation (36) of Section A.4

$$\begin{aligned} \frac{e_y(-1)}{e_y} &= \frac{\gamma(d, -1)}{\gamma(d)} \\ &= \frac{\|R_\perp(-1)(1 - \bar{R}_\perp R_\perp)\}}{\|R_\perp(1 - \bar{R}_\perp R_\perp(-1))\}}. \end{aligned} \quad (46)$$

Because $\bar{R}_\perp(-1) = \bar{R}_\perp$ and $\|R_\perp(-1) = \|R_\perp$ (Budden, 1955, 1961b), equation (46) becomes

$$\frac{e_y(-1)}{e_y} = \frac{\|R_\parallel(1)}{\|R_\perp(1)}. \quad (47)$$

Denoting this ratio as A_m , equation (45) becomes

$$I_{m,j}^{II,I} = (S_m^{II} + S_j^I) \int_0^h (A_m \frac{e^{II}}{y^m} \frac{e^I}{y^j} + h^{II} \frac{h^I}{y^m} \frac{h^I}{y^j}) dz. \quad (48)$$

The integrals in equation (48) are now easily evaluated by using the conventional "multiply and subtract" method. Using the method with equation (27) for modes of index m and n , which may be in the same region or differing regions, leads to the result

$$h_{ym} \frac{d^2 h_{yn}}{dz^2} - h_{yn} \frac{d^2 h_{ym}}{dz^2} - k_o^2 (c_m^2 - c_n^2) h_{ym} h_{yn} = 0$$

or

$$\frac{dh}{dz} (h_{ym} \frac{dh_{yn}}{dz} - h_{yn} \frac{dh_{ym}}{dz}) = k_o^2 (c_m^2 - c_n^2) h_{ym} h_{yn}.$$

The second integral in equation (48) thus becomes

$$\begin{aligned} \int_0^h h_{ym}^{II} h_{yj}^I dz &= \frac{\left(h_{ym}^{II} \frac{dh_{yj}^I}{dz} - h_{yj}^I \frac{dh_{ym}^{II}}{dz} \right)_0^h}{k_o^2 (c_m^{II2} - c_j^{I2})} \\ &= \frac{-i(h_{ym}^{II} e_{xj}^I - h_{yj}^I e_{xm}^{II})_0^h}{k_o^2 (c_m^{II2} - c_j^{I2})} \end{aligned} \quad (49)$$

while the first integral in equation (48) is

$$\int_0^h e_{ym}^{II} e_{yj}^I dz = \frac{i(e_{ym}^{II} h_{xj}^I - e_{yj}^I h_{xm}^{II})_0^h}{k_o^2 (c_m^{II2} - c_j^{I2})}. \quad (50)$$

In equations (49) and (50), it is assumed that $C_m^{II} \neq C_j^I$ for all m and j . Evaluation of the second integral in equation (43) proceeds in the same manner. The only difference is the fact that all field components in this case pertain to region II of the waveguide. In this case however, the situation $m=j$ results in division by zero in equations (49) and (50) and special treatment is required. For the case $m=j$ in region II, the use of L'Hospital's rule yields

$$\int_0^h h_{yj}^2 dz = \frac{1}{\alpha} [(C_j^2 + \alpha z) h_{yj}^2 - e_{xj}^2]_0^h \quad (51)$$

$$\int_0^h e_{yj}^2 dz = \frac{1}{\alpha} [(C_j^2 + \alpha z) e_{yj}^2 - h_{xj}^2]_0^h, \quad (52)$$

where the superscript "II" is omitted.

The individual height gains can be written from equations (30), (31) and (26) as

$$h_y(z) = f_{\parallel}(z)/f_{\parallel}(0)$$

$$e_x(z) = i(\frac{\alpha}{k_0})^{1/3} \frac{df_{\parallel}}{dt}/f_{\parallel}(0)$$

$$e_y(z) = \gamma(d) \frac{f_{\parallel}(d) f_{\perp}(z)}{f_{\parallel}(0) f_{\perp}(d)}$$

$$h_x(z) = -i (\frac{\alpha}{k_0})^{1/3} \frac{\rho(d) f_{\parallel}(d)}{f_{\parallel}(0) f_{\perp}(d)} \frac{df_{\perp}}{dt}. \quad (53)$$

Once the conversion coefficients are obtained, it is necessary to sum over all the incident modes. This requires evaluation of the amplitudes of the incident modes. This can be done by starting at the transmitter, where the modal excitation factors give the mode amplitudes, and using the assumption that the regions between the discontinuities are homogeneous.

Notationally this can be written as

$$\tilde{A}^I = \tilde{P}^I \tilde{a}^I$$

where

$$\tilde{a}^I = \begin{pmatrix} a_1^I \\ \vdots \\ a_j^I \\ \vdots \\ a_n^I \end{pmatrix} \quad (54)$$

represents the amplitudes of the incident modes (a_j^I) at the end of the region I and

$$\tilde{a}^I = \begin{pmatrix} a_1^I \\ \vdots \\ a_j^I \\ \vdots \\ a_n^I \end{pmatrix}$$

represents the amplitudes of the modes at the start of region I. The factor \tilde{P}^I is a diagonal matrix with the nth diagonal element given by

$$P_n = e^{-ik_o S_n^I (\Delta\rho)^I} . \quad (55)$$

Note that P_n represents the propagation factor appropriate to a homogeneous section of length $(\Delta\rho)^I$, assumed to be the length of region I. Note that the amplitudes of the modes in region II just after conversion can be conveniently written as

$$\tilde{a}^{II} = T \tilde{a}^I = T \tilde{P}^I \tilde{a}^I \quad (56)$$

where T is a rectangular matrix of the conversion coefficients from region I into region II.

A mode conversion formulation has been presented by Pappert and Shockley (1974), but important differences exist between their treatment and that employed here. This occurs not only in the numerical procedures employed but also in the definition of the conversion coefficients. In the present formulation the conversion coefficient is computed at each slab interface independently of any previous conditions. In the Pappert formulation, the conversion coefficients are defined and computed in such a way that the effect of the propagation factor (equation (55)) is included. Both definitions of conversion coefficients are reasonable, although their numerical values can be quite different. For example, first consider the case of an isolated terminator

specified as an abrupt transition. The two formulations will give the same results for the conversion coefficients. Next suppose that the terminator has a substantial extent. The conversion coefficients then differ for each slab interface after the first because the Pappert formulation includes the accumulated effects of propagation through the transition region, whereas the current formulation does not.

The Pappert definition of conversion coefficients is useful for studying a horizontal inhomogeneity existing over a small distance, such as the dawn-dusk terminator. A similar conversion coefficient can be derived from the mode constants and the mode conversion coefficients presented in this study. What is required is the complex amplitude of a mode at the end of such a confined inhomogeneity resulting from a single mode of unit amplitude at the start of the inhomogeneity.

Denote by region 1 the region prior to the start of the inhomogeneity. The complex amplitudes of the modes in the first region of inhomogeneity (called region 2) due to a mode of unit amplitude and number k in region 1 are given by the conversion coefficients $T_{m,k}^{2,1}$ (see equation (42)). The complex amplitudes of the modes at the end of region 2 are $A_{m,k}^2$ where

$$A_{m,k}^2 = p_m^2 T_{m,k}^{2,1}$$

and p_m^2 is the propagation factor for mode m in region 2 (see equation (55)). The complex amplitude of mode n at the start of the next region (region 3) due to a mode of unit amplitude in region 2 is $T_{n,m}^{3,2}$, so that the actual complex amplitude of the mode n in region 3 is given by the product of $T_{n,m}^{3,2}$ and $A_{m,k}^2$. Summation over all the modes of region 2 gives the total complex amplitude of mode n . Thus

$$a_{n,k}^3 = \sum_m A_{m,k}^2 T_{n,m}^{3,2} p_m^2 T_{m,k}^{2,1}. \quad (57)$$

This result can be generalized to any inhomogeneity along the path. We obtain

$$a_{m,k}^p = \sum_n T_{m,n}^{p,p-1} p_n^{p-1} a_{n,k}^{p-1} \quad p > 3. \quad (58)$$

The formulations presented in this Chapter have been implemented in a computer program written in FORTRAN. Before discussing some computed results, however, we shall discuss observations of signals received in San Diego from station NWC in Australia.

III. EXPERIMENTAL RESULTS

The majority of the experimental results relating to the transequatorial anomaly discussed previously in Chapter I pertain to propagation paths which are essentially southwesterly. Further, some theoretical results presented in Chapter I suggested a marked difference between the transequatorial propagation to the southwest as compared to the northeast. Transequatorial, transterminator propagation in a northeasterly direction is thus expected to be different from that for a southwesterly direction. In order to determine the validity of this expectation, experimental results are needed.

A seemingly ideal situation exists for obtaining such results. A VLF communications station is located at the North West Cape, Australia. This station is currently broadcasting a phase stable signal at 22.3 kHz, a frequency sufficiently high to insure the occurrence of mode conversion at the ionospheric terminator. A receiving site located at San Diego, California further presents an ideal situation in that the propagation path from North West Cape to San Diego is nearly reciprocal to the paths employed by Lynn (1969). NWC transmissions recorded in San Diego during 1975 are discussed in this chapter.

A. Equipment Used

The NWC transmissions were received at San Diego using essentially "off the shelf" items, commercially available. In particular, one receiver was an EECO Model 880 VLF Receiver and two were TRACOR Model 599 VLF Tracking Receivers, factory modified to provide amplitude. Integration time-constants for all receivers were from one to three minutes, with three minutes most often used. All receivers obtained phase reference from a cesium clock standard.

One of the receivers, the EECO, was connected most of the time to a commercially available loop antenna and part of the time to a whip antenna. One of the TRACORS (no. 2) was always connected to a whip antenna and the other TRACOR (no. 1) was connected to a Textron Model 611 Cardioid Unit. The cardioid unit was used to "null out" any possible long path signal from the NWC transmitter.

Signal levels, in dB above an arbitrary reference, were recorded on Easterline Angus Recorders (Model S6015) running at .75 inches per hour, resulting in a time resolution of about two minutes. The signal phase from the EECO was recorded using a Rustrak Model 88 Recorder whereas Easterline Angus Recorders were used with the Tracors. Two receivers were always tuned to NWC, TRACOR no. 1 and either the EECO or the other TRACOR. The redundancy of receivers tuned to NWC was to provide a "back-up" in case of failure in one of the receivers, a not infrequent occurrence.

The receivers were calibrated by feeding a rf signal through a Hewlett Packard Model 355D Attenuator into the receiver antenna input from an EECO Model 883 Coherent Frequency Synthesizer. The chart unit deflections for a given input voltage were recorded and converted to an equivalent dB level. All signal levels are thus known on a relative but not an absolute scale.

An additional calibration procedure was followed occasionally. All receivers were tuned to the same frequency, usually 22.3 kHz for NWC, for at least one full diurnal period. Any differences were noted in order to ascertain if the various antenna systems used were influenced differently by changing local factors. Such differences were never found to be significant except during rainy days when the whip antenna apparently became flooded.

Conversion of data from analog to digital form was accomplished through use of a Talos graphics tablet. This tablet is an electromagnetic sensing probe and plate with approximately a 2 ft by 2 ft surface. Changes in analog data to within ± 0.005 inches can be digitized with the graphics tablet. A "reading" line was inscribed on the analog tracings of the EA recorders. Because the more than 60 dB dynamic variation in received signal amplitude exceeded the full scale deflection capabilities of the recorders, the amplitudes of deep signal fades were often lost. The time of occurrence of the minima, however, could be accurately determined.

The digitized data were processed by computer to determine times of signal minima. Signal amplitudes were also processed, but they have not been used in this study due to the frequent loss of minima data. For preliminary processing a data point was considered to correspond to a signal minimum if it was more than 0.25 dB below both the three previous and three following data points. Further examination of the preliminary data was then made in order to eliminate any erroneous data. Data obtained during periods when only one

receiver was operating properly were examined with particular care. Before discussing the final processed data some properties of the propagation paths and the ionospheric sunrise/sunset terminator are discussed.

B. The Terminator and the Propagation Path

The ionospheric sunrise/sunset model used in this study is the one commonly employed in VLF propagation analysis. Shown in figure 1a* is a pictorial representation of the terminator model. The model depicts an ozone layer of thickness h_{03} which is assumed to be a perfect absorber of relevant solar radiation. The terminator model shows that ionospheric sunrise and sunset are given in terms of solar zenith angles according to the expression

$$\sin x_j = \frac{a + h_{03}}{a + h_j} \quad j = \text{day or night},$$

where a is the radius of the earth and h_j is usually assumed to be 70 km for day and 90 km for night. Assuming a nominal 50 km ozone layer leads to the results $x_D \approx 94^\circ$, $x_N \approx 96^\circ$. Typically, only the value x_N is used.

Another important property of the transition region model is shown in figure 1b. In that figure is a plan view of the transition region, with an intersecting propagation path. Note that the length of the propagation path within the transition is given essentially as

$$L = L_{\min}/\cos\beta$$

where planar geometry is assumed to be adequate for the distances involved. If the above values of x_D and x_N are used, a value of about 200 km is obtained for L_{\min} . Even though the value of L_{\min} depends on a choice of solar zenith angles for the day and night sides of the transition region, note that the ratio L/L_{\min} depends only on β . A pictorial representation of the intersection of the propagation path with the transition region is shown in figure 2.

*Figures appear at the end of the document.

The period during which a particular propagation path is in total day, total night or transition depends on a number of factors, including path orientation and location, time of year, etc. Periods of night, day and transition for the NWC to San Diego path are shown in figure 3 using an ionospheric terminator corresponding to a solar zenith angle of 96°. Note that the propagation path is predominantly transitional over any 24 hour period throughout the entire year. Maximum sunrise transition period is during the northern hemisphere summer while for sunset it is during the winter.

C. Transition Fading Data

1. Time of Signal Minima

The times of minimum signal strength are shown in figure 4 for NWC transmissions at 22.3 kHz as received at San Diego, California during night to day transition (sunrise). The relative terminator movement between transmitter and receiver is depicted in the upper right insert. In this case the terminator moves from receiver location to transmitter location so that the first fade (in time) occurs with maximum night length to the path. The last fade occurs with minimum night length to the path. Seven signal minima are observed. The data of figure 4 indicate the variability of the times of signal minima throughout the year. Maximum length of sunrise fading occurs near midyear, consistent with the data of figure 3. Daily variability is also shown by figure 4. The times of signal minima fluctuate by as much as 5 to 10 min from day to day. The effect of averaging the times of the minima over a 15 day period are shown in figure 5.

Times for sunset signal minima are shown in figure 6. Also shown is the relative terminator movement between transmitter and receiver. In this case, the first fade occurs with maximum day length to the path. Seven signal minima are indicated for the sunset transition as for the sunrise. The variability of fading times throughout the year again are consistent with the data of figure 3. The day to day variability of the sunset data is noticeably larger than for the sunrise data. Times of sunset signal strength minima averaged over 15 days are shown in figure 7.

2. Terminator Position at Maximum Signal Fade

Associated with the times of occurrence of minima is the location of the terminator at those times. The location of the terminator is here defined to be the point along the propagation path where the solar zenith angle is 96°. A more precise definition would be the point on the propagation path where the angle from the sub-solar point is 96°. The transmitter/terminator distance at times of signal minima for night-to-day transition (sunrise) were computed from the data of figure 4 and are shown in figure 8. The fade numbering scheme, based on time, is shown at the right. Also shown in the figure are the relative positions of the geomagnetic equator and 20° magnetic latitude (north and south). Signal minima 4 and 5 are well within the equatorial region and minima 3 and 6 are marginally so. Thus, if the equatorial spacing anomaly in transition fading is to occur for this path, the data should clearly so indicate.

The distances moved by the sunrise terminator between signal minima, shown in figure 9, are nearly constant throughout the year, with the possible exception of the minima 1 and 2. The changes in these minima could possibly be due to the proximity of the transition region to the receiver location, resulting in interference effects from additional modes. Even without any smoothing or averaging, the data contain no anomalies due to the presence of the terminator in the equatorial region.

Transmitter/terminator distances for times of signal minima for day-to-night transition (sunset) are shown in figure 10. There are significant differences from the sunrise case. There is, first of all, an obvious seasonal dependence. This dependence does seem to be common to all the fades. A perusal of the original strip charts showed no indications of equipment failure. It seems, then, that there is a significant seasonal difference between the sunrise and sunset fading.

There is, however, an even more significant difference between the sunrise and sunset fades. This is indicated in fades numbered 4, 5, 6 and 7. During early midyear, there seems to be a change of as much as 1500 km in the location of the terminator for the fades 4, 5, 6 and 7. Note that these fades are essentially within the equatorial region, thus suggesting the possibility of an equatorial anomaly for the sunset transition case.

An explanation of the apparent anomaly may be found by considering the relative length of the transition region throughout the year as shown in figure 11. The ratio L/L_{\min} is computed as $1/\cos\beta$, where β is the angle depicted in figure 1b. Note from the lower figure (for sunset) that the effective length of the transition region increases rapidly, reaching a maximum near midyear. This increase in the effective length of the transition region has apparently reduced the mode conversion effects so greatly that the "fades" are little more than ripples in the amplitude data. This is seen in figure 12, which shows the amplitude during sunset for June 1, 2, and 3, 1975. In figure 12, at best, four transition fades can be identified.

The data presented here have demonstrated no geomagnetic field anomaly associated with the northeasterly propagation direction. Any apparent anomalies can be explained in terms of purely geometrical effects. There remains yet the unexplained differences in seasonal effects. It would seem reasonable to search for an explanation of the seasonal effects in terms of the seasonal behavior of the ionosphere, a subject not considered in this study.

IV. NUMERICAL MODELING RESULTS

Empirical observations discussed in Chapter I indicate an apparent anomaly in the nighttime VLF propagation across the geomagnetic equator for southwesterly paths. Limited theoretical results, also discussed in Chapter I, suggested such anomalies might not occur for northeasterly propagation across the geomagnetic equator. VLF propagation data taken during this study confirmed this latter point. Using the theoretical model discussed in Chapter II, numerical modeling results have been obtained for both northeasterly and southwesterly transequatorial VLF propagation. These results are discussed in this chapter.

A. Review of VLF Propagation Environment

A crucial input to the theoretical determination of VLF propagation is the environmental description. Long distance propagation of VLF radio waves is considered herein by mode theory in which the earth and the lower part of the ionosphere are considered to be the boundaries of a lossy waveguide. For this reason, a review of the VLF propagation medium requires a consideration of the electrical properties of the earth and the lower ionosphere.

The earth is usually considered to be a homogeneous isotropic conductor. For most of the surface, the effective ground conductivity ranges from about a millimho/m for typical soils to about 5 mho/m for sea water. For large areas covered with perma-frost or ice, such as the Greenland ice cap, the conductivity can be as low as 10^{-5} mho/m. For conductivity this low, the skin depth can be so large that consideration must be given to the lower substrata (Westerlund, 1974).

The detailed geometrical characteristics of the surface are not very important for VLF waves because the principal electric vector is largely perpendicular to the surface. However, if the electric vector has an appreciable horizontal component, these characteristics can be quite important (Galejs, 1972). Quite the opposite, however, is true concerning the conductivity (Westerlund, 1974).

The upper boundary of the VLF waveguide is considerably more complicated than the lower. The reflection of VLF waves from the upper boundary (the D-region and lower E-region) is generally accepted to be from about 70 km for

daytime and about 90 km for nighttime. The reflecting medium is a slightly ionized plasma, rendered anisotropic by the geomagnetic field. Because of the variable solar control, the variations in electro-chemical processes and the variations in thermal and mechanical influences, the medium is further rendered highly inhomogeneous.

The reflection process is quite a complicated process, of which all aspects have still not been fully explained. Both the density gradients and collision frequencies are known to play a major role (Budden, 1961). Reflection at VLF does not occur at the altitude where the operating frequency is suitably related to the plasma frequency, as in HF ionospheric propagation, but is controlled to a significant extent by the ratio of the plasma to the collision frequency. It can be said, however, that the upper boundary of the earth-ionosphere waveguide is controlled by the ionization at heights below about 100 km.

It would be nice to be able to report that the D- and lower E-regions are well understood. This is not, however, the case. It has been asserted, that many of the most interesting unsolved problems of the ionosphere are related to the D-region (Bowhill, 1975). In a recent review of the D-region, Thomas (1974) pointed out, that although there have been advances in theoretical models of the D-region in recent years, there has not been a significant improvement in our understanding of the aeronomical processes operating.

Ionization below 100 km is produced by electromagnetic and corpuscular radiation which bombards the earth from a variety of sources. The principal ionization sources for the quiet D-region are considered to be galactic cosmic rays, solar x-rays and solar H Ly α , both direct and scattered. An additional source only recently recognized and not yet universally accepted involves precipitation of energetic electrons.

The photoionization of nitric oxide by solar H Ly α constitutes the major source of ionization during the daytime between approximately 65 and 90 km altitude. Soft x-rays (31-100 Å) dominate above 90 km and galactic cosmic rays are most important below 65 km. At nighttime, ionization is usually assumed to be produced primarily by H Ly α in the nightglow. A drizzle of energetic particles is continually raining down onto the midlatitude atmosphere. According to Potemra and Zmuda (1970), these electrons are the dominant nighttime ionization source above about 80 km. Additional sources of

nighttime ionization have been proposed, including cosmic x-rays and solar UV ionization of metastable oxygen. These have, however, been discounted or demonstrated to be of only secondary importance.

The immediate effect of these ionization sources is the production of free electrons and positive ions of atomic or molecular size. The electrons can combine with neutral particles, forming negative ions. Positive ions and electrons, as well as positive and negative ions, can recombine forming neutrals. Balance equations describing these processes can be formulated and solved. However, the coefficients involved in such balance equations are usually quite uncertain. Additional chemical and physical processes, such as the presence of ions of larger size than single molecules, further complicate the balance, resulting in the frequent use of "nominal working models" of the ionosphere. Such models range from a homogeneous conductor sharply bounded at an assumed reflection height, to an "electron only" (positive ions assumed to be infinitely massive) exponentially varying ionosphere, to a "lumped parameter" model involving electrons together with positive and negative ions of a single mass.

Ionospheric profiles of the lumped parameter type were recently presented by Rawer et al. (1978) for electrons. These profiles, designated by the name IRI-78, are obtained from computer models that attempted to represent averages of measured ionospheric parameters. A set of exponentially varying electron density profiles were recently recommended for VLF propagation studies by Morfitt (1977). These profiles were obtained by fitting multifrequency long path VLF propagation data to theoretically computed data on a trial-and-error basis. An extensive comparison of the two sets of profiles was made in order to ascertain which to employ in this study. Typical comparative results are displayed in figures 13 and 14.

In figure 13, a mode sum computed using the IRI-78 nighttime profile and magnetic conditions corresponding to propagation from station NPM in Hawaii to Ontario, California, is presented along with VLF amplitude data recorded aboard an airplane flying on such a path. The computed mode sum differs significantly from the data. The corresponding "best fit" exponential electron density profile is given by Morfitt (1977) as one with reference height (h') of 85.5 km and gradient (β) of 0.5 km^{-1} . The β, h' notation is adopted from Wait and Spies (1964) who assumed that $w_p^{2/v} = 2.5 \times 10^5 \exp(\beta(z-h'))$,

where z is the height above ground in kilometers, ω_p is the angular plasma frequency, and v is the electron collision frequency, given by $v = 1.816 \times 10^{11} \exp [-.15z]$. Thus, a change in β or h' denotes a change in electron density only. In figure 14, similar results for a daytime case are presented. The mode sum computed using the IRI-78 is in better agreement in this case than for the nighttime case but is nonetheless still not in very good agreement. The "best fit" exponential profiles in the daytime case are $\beta = 0.3$, $h' = 75$ for 3 February. Based on numerous comparisons such as these, exponential electron density profiles are employed in this study. The nighttime profile selected has $\beta = 0.5 \text{ km}^{-1}$ and $h' = 86 \text{ km}$ while the daytime has $\beta = 0.3 \text{ km}^{-1}$ and $h' = 74 \text{ km}$.

B. Sample Calculation Comparisons

Height gains computed using the program based on the theory of Chapter II have been compared with those used in the work of Pappert and Snyder (1972). Three electron density profiles are considered: $\beta = 0.5 \text{ km}^{-1}$, $h = 86 \text{ km}$ and 70 km and $\beta = 0.3 \text{ km}^{-1}$, $h = 70 \text{ km}$. The geomagnetic field is taken to be horizontal, corresponding to the magnetic equator, and the propagation direction is taken to be directly west to east so that there is no coupling between the TM and TE eigenfunctions. Only the TM eigenfunctions are considered here. The earth is assumed to be sea water and a frequency of 18.6 kHz is used. These conditions correspond to those used by Pappert and Snyder (1972).

Shown in figure 15 are the magnitudes of three eigenfunctions for the $\beta = 0.5 \text{ km}^{-1}$; $h = 70 \text{ km}$ profile. The right hand part of the figure shows the h_y components whereas the left hand part shows the e_x component. The dashed curves for altitudes greater than about 65 km are derived from Pappert and Snyder (1972) and demonstrate the decay of the eigenfunctions within the ionosphere. Below 65 km there is complete agreement between the results obtained here and those of Pappert and Snyder, thereby verifying the results obtained in this study.

The profile here is relatively abrupt in that the region of the ionosphere from about 65 to 70 km is the most important. The region below 65 km is essentially free space whereas above 70 km the waves are largely evanescent

and decay by about two powers of ten from their nominal value within the guiding region.

Results for a less abrupt profile ($\beta = 0.3 \text{ km}^{-1}$, $h = 70 \text{ km}$) are shown in figure 16. From the results of Pappert and Snyder concerning phase velocity (their figures 3 and 4), it follows that the effective vertical width of the waveguide for this profile is about the same as for the $\beta = 0.5 \text{ km}^{-1}$ profile. However, as can be seen from figure 16, the guide is essentially free space only below about 55 or 60 km.

Mode conversion coefficients have been computed using the formulation discussed in Chapter II. For this purpose, region 1 was assumed to have the $\beta = 0.5 \text{ km}^{-1}$; $h = 86 \text{ km}$ profile and region 2 was assumed to have the $\beta = 0.3 \text{ km}^{-1}$; $h = 70 \text{ km}$ profile. This situation corresponds to one reported by Pappert and Snyder. The coefficients for converting incident modes 1 and 2 into transmitted mode 1 are given in table 1 using upper limits of integration from 55 to 70 km. The other conversion coefficients were insignificant, consistent with the results of Pappert and Snyder. Best agreement is obtained for an upper limit of integration equal to 60 km. The results computed here agree with the more exact results of Pappert and Snyder to within about 30% to 40%. The electromagnetic fields computed in region 2 by the methods presented here differ from those of Pappert and Snyder by only a few dB.

Table 1. Magnitude of the Mode Conversion Coefficients
Conversion from Incident M to Transmitted N

Mode Number		Integration Limit				Exact Results
N	M	70	65	60	55	
1	1	2.75	2.02	1.94	2.28	1.47
1	2	1.10	0.76	0.72	0.89	0.53

C. Modeling Results

The numerical modeling results will be presented in two parts. The first part addresses the northeasterly transequatorial path. The propagation path from station NWC (22.3 kHz), Australia to San Diego, California is used for this case. The second part addresses the southwesterly path from station NLK (18.6 kHz), Jim Creek, Washington to Brisbane, Australia. The variation of the geomagnetic field along the propagation paths are shown in figure 17. The individual data points on the plots denote locations at which modal constants

were computed. In both cases, the lower boundary is assumed to be sea water with a conductivity of 4.64 mho/m and a relative dielectric constant of 81.

1. NWC to San Diego

a. Nighttime

The propagation constants for the assumed night profile for the NWC path are shown in figure 18. Recall that the x-variation is assumed to be $\exp(-ik_0 S_n x)$, where the complex propagation factor S_n is equal to $\sin\theta_n'$, and θ_n' is the (complex) eigenangle. The eigenangle used here is referred to the altitude of $H = 50$ km in the "transformed" guide with refractive index $e^{z/a}$. From Snell's Law, $e^{H/a} \sin\theta_n' = \sin\theta_n$ where θ_n' is the eigenangle discussed further in this study. Figure 18a shows the real part of the eigenangles (θ_r), while figure 18b shows the imaginary part (θ_i), both plotted as a function of distance from the transmitter. The eigenangles appear to fall into two groups. One group, the odd numbered modes, is characterized by a nearly constant θ_r with perhaps a slight increase to a maximum at 6 megameters (the geomagnetic equator). The θ_i for these odd numbered modes diminishes in magnitude as the magnetic equator is approached. The even numbered modes have just the opposite behavior. Note that the mode numbering is arbitrary; it is chosen to increase monotonically with increasing θ_r at the transmitter.

There is a fundamental physical difference between the even and odd numbered modes for this case. This is seen by a consideration of the polarization mixing ratio, defined by Pappert (1968). This function is the magnitude of the reciprocal of equation (25) and is approximately equal to the ratio of the maximum magnitude of h_y to the maximum magnitude of e_y within the guide. Thus, a very large mixing ratio denotes a principally TM polarization whereas a very small ratio denotes principally TE polarization. The mixing ratios for this path are shown in figure 19. The even numbered modes are seen to be principally TE, dominantly so at the equator. The odd numbered modes are principally TM polarized.

The propagation characteristics of the two groups of modes are distinctly different. Mode constants are plotted in figures 20, 21 and 22. For the various modes, figure 20 shows the phase velocities and figure 21 the attenuation rates. Note that the phase velocities and attenuation rates can also be grouped into sets, even modes and odd modes. The even (TE) modes exhibit a maximum in both phase velocity and attenuation rate at the equator while the

odd (TM) modes do just the opposite. The increase in even mode phase velocity indicates a decrease in the effective ionospheric height. Decreasing the ionospheric height typically results in an increased attenuation rate, and this is what occurs. Recall from Chapter I that the modal excitation factor is conventionally defined for a vertical dipole source exciting a principally vertically polarized mode. Thus, from the polarization mixing ratio, the odd modes (TM) can be expected to increase in excitation efficiency at the equator and the even modes can be expected to decrease. This is indeed the case, as is indicated in figure 22.

It might be conjectured from the excitation factors that the mode sum for this case would exhibit a highly moded structure over the entire path length. However, examination of the attenuation rates shows that the highly excited odd modes also have high attenuation rates except close to the equator. Because mode 1 has a relatively small excitation, the dominant mode is mode 3. Mode 5 is second dominant to a distance of about 10 megameters, where mode 1 begins to increase in importance. The mode sums for this case are presented in figure 23. The WKB mode sum is presented along with the mode sum computed using the formulation of Chapter II. The two sums are very nearly identical, indicating essentially no mode coupling along the propagation path. This is a further indication of the correctness of the computer code used in this study.

b. Sunrise/Sunset Transition

Numerical modeling of transition fading requires an ionosphere model in the neighborhood of the terminator. The model used assumes a series of discrete steps approximating a linear variation in both β and h' . A preliminary investigation of transition fading was made by considering an approximate path with constant magnetic conditions and a variable terminator thickness. As a consequence of this approximation, the mode conversion coefficients for a given terminator thickness are independent of the location of the terminator along the path.

Computed amplitudes and phases of transition fading at San Diego (15,000 km from the transmitter) are shown in figure 24 for four different terminator dimensions. Figure 24a shows the sunrise results while figure 24b shows results for sunset. Note that the figures have the distance axes reversed so that time is modeled as progressing from left to right. For both sunrise and

sunset, the spacing between deep fades is approximately 2000 km for all values to the terminator thickness. The absolute position of each fade, however, does depend on the value of the terminator thickness. There is approximately a 400 km difference in the fade position among the various terminator thicknesses.

The fading results of figure 24, when compared with the mode sums of figure 23, point out an important result. The mode sum shows an interference spacing of approximately 1000 km over most of the path length. This might lead to a similar expectation for the transition fade spacing. However, the transition fade spacing depends primarily on the difference between the phase velocities of the modes that are most efficiently converted by the terminator, and not on all the modes that are involved in the pre-terminator mode sum. Examination of figure 23 reveals the existence of a dominant null spacing of 2000 km with a subdominant mode that is gradually decaying. Also, while the interference nulls for the mode sum are about 5 dB in depth, the transition fades are almost 10 dB in depth and often as much as 20 to 40 dB.

The change of phase during sunrise shows an increase over the first half of the sunrise transition and then a decrease over the second half. This implies that the phase velocity of the dominant mode was modified at midtransition, and this demonstrates that different modes were dominant in the early transition time and in the late transition time. The sunset phase follows a similar behavior except for the first fade with transition thickness of 750 km, where a phase reversal occurs.

Signal amplitudes as a function of terminator position along the NWC to San Diego propagation path, taking into account variations of the earth's magnetic field, have been computed for several distances from the transmitter and are shown in figures 25 and 26. The transition from $h' = 74$ km to $h' = 86$ km (sunset) is shown in figure 25, while the $h' = 86$ km to $h' = 74$ km (sunrise) case is shown in figure 26. The terminator width was taken as 500 km in both cases. The zero amplitude for each successive receiver position is offset 5 dB from that for the previous receiver in order to improve visual clarity. The figures support completely the simplified Crombie model of transition fading. In figure 25, the fades all occur when the receiver is a fixed distance from the terminator whereas in figure 26 all receiver positions experience a fade at the same time for an appropriate position of the termina-

tor. Variations from these patterns occur, of course, where higher order modes are important, such as for small transmitter/terminator distances for sunset and for large distances for sunrise.

The modeling results for the NWC to San Diego propagation path (magnetically northeasterly) support the experimental results of Chapter III in all essential details. There remains now to apply the model to the reverse magnetic conditions, that is, the path from NLK to Brisbane.

2. NLK to Brisbane

a. Nighttime

The propagation constants for the assumed night profile for the NLK path are presented in figure 27. Figure 27a shows the real part of the eigenangles (θ_r), the behavior of which is slightly more complicated than that for the NWC to San Diego path. The behavior of the imaginary part of the eigenangles (θ_i) in figure 27b is considerably more complicated than that for the northeasterly path. There does not appear to be a grouping in the θ_r . With the exception of modes 9 and 10, the odd numbered modes increase to a maximum in θ_r at the equator (7.5 megameters), while the even numbered decrease to a minimum. Mode 10 behaves as an odd mode while mode 9 behaves as an even mode. Recall that the mode numbering is established by ordering θ_r at the transmitter. If the θ_r were ordered for some other location, such as the end point of the path, the numbering of modes 9 and 10 would be reversed. The important feature is the grouping of the modes, not the numbering within the groups. Although not immediately obvious, the θ_i also fit into two groups. The even modes have less variation than the odd and are grouped together with small values, except in very close to the equator. The odd modes become most negative on each side of the equator, and then increase rapidly at the equator.

The variations of polarization with distance along the path are shown in figure 28. The behavior of this parameter is also markedly different from that for the northeasterly case. The modes begin at the transmitter in two groups. Modes 1, 4, 6, 8 and 9 are principally TE at the transmitter while the other modes are TM. All of the TM modes, except mode 3, become principally TE just prior to the equator, and even mode 3 increases its admixture of TE polarization. The TM admixture is then increased for all the modes through the equator and, except for mode 2, the modes attain a maximum of TM polariza-

tion just following the equator. Then the modal polarizations return essentially to the conditions at the transmitter. The behavior of the modal polarization exerts a strong influence on the mode conversion properties of the terminator.

Because the daytime ionosphere is only slightly anisotropic, the daytime modes are essentially purely TE or purely TM. Further, a purely TE mode does not convert to a purely TM mode. Thus, the conversion of the essentially TE nighttime modes at about 7 megameters from the transmitter to the TM daytime modes can be expected to be quite different from the conversion of the essentially TM nighttime modes at about 8 megameters.

The modal phase velocities and attenuation rates are shown in figures 29 and 30. The phase velocities (figure 29) exhibit the following characteristic. Not only do the phase velocities for modes 9 and 10 cross near the transmitter as might be expected from the θ_r plots, but there are also crossings near the equator for modes 4, 5 and 6, 7. A mode numbering scheme most commonly favored is to order modes according to phase velocity, smallest to largest. But this is unfeasible when the modal phase velocities cross at the equator.

Attenuation rates are shown in figure 30. Modes 1, 2, and 4 exhibit similar behavior with maximum attenuation rates at the equator. The remaining modes have maxima at pre-and post-equator locations, with minima at the equator. Mode 7 shows a slight recovery at the equator, as does mode 10, which has an attenuation rate larger than the maximum plotted scale. Clearly, the attenuation rate has no apparent correlation to the polarization. This behavior for the southwesterly direction is in complete contrast to that for the northeasterly direction.

Mode sums for our nighttime model of the ionosphere for this propagation path are shown in figure 31. Both the WKB and the mode conversion results are presented. In contrast to the behavior for the northeasterly path, the WKB and mode conversion results are not in agreement for path positions near and beyond the equator. For distances shorter than about 6 megameters, the two mode sums are in complete agreement and both indicate a dominant modal interference spacing of approximately 2 megameters. This spacing is not apparent however, for distances further removed from the transmitter.

b. Sunrise/Sunset Transition

Signal amplitudes as a function of terminator position along the NLK to Brisbane path, taking into account variations of the earth's magnetic field, have been completed for several distances from the transmitter using a terminator of 500 km width. Let us first consider a transition from $h' = 74$ to $h' = 86$. Because the path direction is reversed from the NWC to San Diego case, this transition corresponds to sunrise rather than sunset. Signal amplitudes as a function of terminator position along the path are presented in figure 32 for several receiver locations. The remarkable dissimilarity between these results and the northwesterly results (figure 25) is immediately apparent. A number of points should be noticed. Receiver distances 12 megameters or less have two clearly defined fading nulls, whereas receivers much further from the transmitter apparently exhibit three fading nulls. Further, the double null spacings are different for each receiver location. For terminator positions outside the equatorial region ($\pm 20^\circ$ latitude as shown), the last fade spacing for the triple fade cases is approximately 2 megameters while the fade spacing within the equatorial region is nearly 3.5 megameters. All of these observations are in complete agreement with the experimental results of Lynn (1969) on multiple observations of the equatorial anomaly. Thus, the transequatorial sunrise transition reported by Lynn as anomalous are completely explained by correctly allowing for variation of the geomagnetic field along the path.

The sunset results ($h' = 86$ km to $h' = 74$ km) are presented in figure 33. In this case, there are two, and possibly three, fades for the terminator on the transmitter side of the equatorial region. The fade spacing is approximately 2 megameters, in agreement with what is expected for midlatitude fading. Further, the fades are simultaneous at all receiver sites, also in agreement with what is expected for midlatitudes. When the terminator is in the equatorial region, a deep fade occurs at all receiver sites nearly simultaneously. This fade is at a distance of approximately 3.5 megameters of terminator movement from the previous very slight fade. These results, unfortunately, do not correspond with those of Lynn (1969), who reported no transition fading at all for the sunset case.

V. CONCLUSIONS

This study reports on observations of sunrise/sunset fading on a long, transequatorial northeasterly propagation path. A mode conversion model is developed and numerical modeling results are presented for transition fading on long transequatorial paths, both northeasterly and southwesterly.

From these results the following general conclusions are drawn:

- a. Anomalous transequatorial transition fading is not observed for the northeasterly propagation path. The transition fading data support completely the mode conversion model of transition fading developed by Crombie (1964).
- b. The procedures of terminating the integration limits on the orthogonalization integrals below the ionosphere at a height within the earth-ionosphere waveguide provides a considerable simplification for numerical modeling of mode conversion effects. Furthermore, the procedure provides acceptably accurate results for such modeling studies.
- c. The transequatorial sunrise transitions reported in the literature as anomalous are completely explained by correctly allowing for variations of the geomagnetic field along the path. The geomagnetic field influences the night-time modal parameters to such an extent for the southwesterly path considered that the approximate WKB method of mode summation cannot be employed.
- d. Careful application of model techniques appears to be capable of describing all LF and VLF propagation in the earth-ionosphere waveguide, provided the effect of the earth's magnetic field is properly included at night. However, an improved model of the ionosphere at altitudes below 100 km is much to be desired.

REFERENCES

- Abbas, M. M., Pidwell, D. W. and Walsh, E. J. (1971), Propagation of VLF waves below generally anisotropic ionospheres, Can. Jour. Phys., v. 49, 1040.
- Al'pert, Ya. L. and Fliegel, D. S. (1970), Propagation of ELF and VLF waves near the earth, Consultants Bureau, New York.
- Araki, T. (1973), Anomalous diurnal changes of transequatorial VLF radio waves, J. Atmos. Terr. Phys., v. 35, 693.
- Araki, T., Kitayama, S. and Susumu, K. (1969), Transequatorial reception of VLF radio waves from Australia, Radio Science, v. 4, no. 4, 367.
- Barren, D. W. and Budden, K. G. (1959), The numerical solution of differential equations governing the reflection of long radio waves from the ionosphere, Proc. Roy. Soc. London, A249, 387.
- Belrose, J. S. (1968), Low and very low frequency wave propagation, AGARD Lect. Ser. no. 29, Ch. 4.
- Berry, L. A. and Chrisman, M. E. (1965), The path integrals of LF/VLF wave hop theory, Radio Sci., 69D, no. 11, 1469.
- Bickel, J. E., Ferguson, J. A. and Stanley, G. V. (1970), Experimental observation of magnetic field effects on VLF propagation at night, Radio Sci., v. 5, no. 1, 19.
- Bowhill, S. A. (1975), Current and future trends in ionospheric research, Radio Sci., v. 10, no. 7, 693.
- Budden, K. G. (1955), The numerical solution of differential equations governing the reflection of long radio waves from the ionosphere, Proc. Roy. Soc. London, A249, 387.
- Budden, K. G. (1961a), The waveguide mode theory of wave propagation, Logos Press, London.
- Budden, K. G. (1961b), Radio waves in the ionosphere, Cambridge University Press, Cambridge.
- Budden, K. G. (1962), The influence of the earth's magnetic field on radio propagation by wave-guide modes, Proc. Roy. Soc. London, A, v. 265, 538.
- Budden, K. G. and Martin, H. G. (1962), The ionosphere as a whispering gallery, Proc. Roy. Soc. London, A265, 554-569.
- Burgess, B. (1967), An experimental determination of the phase delay of VLF radio waves propagating over great distances, Conf. on M.F., L.F., and V.L.F. Radio Propagation, IEEE Conf. Pub. 36, 159.

Chilton, C. J., Crary, J. H. (1971), VLF observations of nighttime D-region ionization enhancement by the Scorpius XR-1 x-ray source, Radio Sci., v. 6., no. 7, 699.

Chilton, C. J., Diede, A. H. and Radicella, S. M. (1964), Transequatorial reception of very-low-frequency transmission, J.G.R., v. 69, no. 7, 1319.

Clemmow, P. C. and Heading, J. (1954), Coupled forms of differential equations governing radio propagation in the ionosphere, Proc. Cambridge Phil. Soc., 50, 319.

Computation Laboratory Staff at Cambridge, Mass. (1945), Tables of the modified Hankel function of order one-third and of their derivatives, Harvard University Press, Cambridge, Mass.

Crombie, D. D. (1964), Periodic fading of VLF signals received over long paths during sunrise and sunset, Radio Sci. J. Res. NBS, 68D, no. 1, 27.

Deeks, D. G. (1966), D-region electron distributions in middle latitudes, Pro. Roy. Soc. London, A291, 413.

Ferguson, J. A. (1968), Effects of earth's magnetic field on VLF waveguide modes, Naval Electronics Laboratory Center Tech. Note 1398.

Foley, G., Wand, I. C., and Jones, T. B. (1973), Studies of the modal parameters of VLF radiowaves propagated below the night-time ionosphere, J. Atmos. Terr. Phys., v. 35, 2111.

Friedman, B. (1959), Principle and Techniques of Applied Mathematics, Wiley, New York.

Galejs, J. (1971), VLF propagation across discontinuous daytime to nighttime transitions in anisotropic terrestrial waveguide, IEEE Trans. Ant. Prop., AP-19(6), 756.

Galejs, J. (1972), Terrestrial propagation of long electromagnetic waves, Pergamon Press, Oxford.

Johler, J. R. (1970), Spherical wave theory for MF, LF and VLF propagation, Radio Sci., 5, no. 12, pp. 1425-1444.

Johler, J. R. and Harper, J. D. (1962), Reflection and transmission of radio waves at a continuously stratified plasma with arbitrary magnetic induction, J. Res. Nat. Bur. Standard. Sect. D., 66D, 81.

Kaiser, A. B. (1968), Latitude variation in VLF modal interference, Radio Sci., v. 3 (new series), no. 11, 1084.

Lynn, K. J. W. (1967), Anomalous sunrise effects observed on a long transequatorial VLF propagation path, Radio Sci., v. 2 (new series), no. 6, 521.

Lynn, K. J. W. (1969), Multisite observations of the VLF transequatorial propagation anomaly, Radio Sci., v. 4, no. 3, 203.

Lynn, K. J. W. (1970), The interpretation of transequatorial VLF sunrise observations, J. Atmos. Terr. Phys., v. 32, 57.

Lynn, K. J. W. (1978), Some differences in diurnal phase and amplitude variations for VLF signals, J. Atmos. Terr. Phys., v. 40, 145.

Makarov, G. I., Novikov, V. V. and Orlov, A. B. (1970), Modern state of investigations of the propagation of ultralong waves in the earth-ionosphere waveguide channel (review), Izv. Radiofizika, v. 13, no. 3, 321.

Meara, L. A. (1973), VLF modal interference effects observed on transequatorial paths, J. Atmos. Terr. Phys., v. 35, 305.

Morfitt, D. G. (1977), Effective electron density distributions describing VLF/LF propagation data, Naval Ocean Systems Center Technical Report 141.

Morse, P. M. and Feshbach, H. (1953), Methods of Theoretical Physics, McGraw-Hill, New York.

Nagano, I., Mambo, M. and Hutatsuishi, G. (1975), Numerical calculation of electromagnetic waves in an anisotropic multilayered medium, Radio Sci., v. 10, no. 6, 611.

Pappert, R. A. (1968), A numerical study of VLF mode structure and polarization below an anisotropic ionosphere, Radio Sci., v. 3, no. 3, 219.

Pappert, R. A. and Shockley, L. R. (1974), A simplified mode conversion program for VLF propagation in the earth-ionosphere waveguide, Defense Nuc. Agency Interim Report 751.

Pappert, R. A. and Smith, R. R. (1972), Orthogonality of height-gains in the earth-ionosphere waveguide, Radio Science, v. 7, 275.

Pappert, R. A. and Snyder, F. P. (1972), Some results of a mode-conversion program for VLF, Radio Sci., v. 7, no. 10, 913.

Pitteway, M. L. V. (1965), The numerical calculation of wavefields, reflection coefficients and polarizations for long waves in the lower ionosphere, Phil. Trans. Roy. Soc. London, A257, 219.

Poeverlein, H. (1967), Ionospheric wave theory using coupled vacuum modes, Radio Sci., v. 2, 905.

Potemra, T. A. and Zmuda, A. J. (1970), Precipitating energetic electrons as an ionization source in the midlatitude nighttime D-region, J. Geophys. Res., 75, 7161.

Potemra, T. A. and T. J. Rosenberg (1973), VLF propagation disturbances and electron precipitation at mid-latitudes, J. Geophys. Res., 78, 1572.

Price, G. H. (1964), Propagation of electromagnetic waves through a continuously varying stratified anisotropic medium, J. Res. Nat. Bur. Stand., D, 68D, 407.

Ralston, A. and Wilf, H. S. (1967), Mathematical methods for digital computers, v. II, Wiley, New York.

Rawer, K., Bilitza, D. and Ramakrishnan, S. (1978), Goals and status of the International Reference Ionosphere, Rev. Geo. and Space Phys., v. 16, no. 2, 177.

Rhoads, F. J. and Garner, W. E. (1967), An investigation of modal interference of VLF radiowaves, Radio Sci., 2, 539.

Richter, J. H. (1966), Applications of conformal mapping to earth-flattening procedures, Radio Sci., v. 1 (new series), no. 12, 1435.

Rieker, J. (1963), Sunset and sunrise in the ionosphere: effects on propagation of long waves, Radio Prop. (J. Res. NBS), 67D, 119.

Round, H. J., Eckersley, J. L., Tremellen, K. and Lunnon, F. C. (1925), Report on measurements made on signal strength at great distances during 1922 and 1923, J.E.E.E., 63, 933.

Schumann, W. O. (1952), On the radiation free self oscillations of a conducting sphere, which is surrounded by an air layer and an ionospheric shell (in German), Z. Naturforsch., 72, 149.

Schumann, W. O. (1954), Über die strahlung langer wellendes horizontalen dipols in dem lufthohlraum zwischen erde und ionosphare I, Zeitschrift für angewandte Physik, 6, 225.

Seliga, T. A. (1966), Numerical full wave solution techniques for the calculation of low frequency plasma wave fields in the ionosphere, J. Inst. Telecomm. Eng., 12, 198.

Smith, R. A., Coyne, T. N., Lock, R. G. and Bourne, I. A. (1968), Ground based radio wave propagation studies of the lower ionosphere, D.R.T.E., Ottawa, Canada, 335.

Smith, R. A. (1974), Approximate mode conversion coefficients in the earth-ionosphere waveguide for VLF propagation below an anisotropic ionosphere, J. Atmos. Terr. Phys., v. 36, 1683.

Snyder, F. P. (1968a), Mode numbering for an exponential anisotropic ionosphere, Naval Electronics Laboratory Center Tech. Note 1394.

Snyder, F. P. (1968b), Effect of magnetic dip-angle and azimuth-angle variations on mode numbering at VLF, Naval Electronics Laboratory Center R&D Report 1587.

Sommerfeld, A. (1949), Partial differential equations in physics, Academic Press, New York.

Svennesson, J. and Westerlund, S. (1979), Stellar x-ray effects on VLF radio-wave propagation, J. Atmos. Terr. Phys., v. 41, 361.

Thomas, L. (1974), Recent developments and outstanding problems in the theory of the D-region, Radio Sci., v. 9, no. 2, 121.

Wait, J. A. (1961), A new approach to the mode theory of VLF propagation, J. Res. NBS, 65D (Radio Prop.), no. 1, 37.

Wait, J. R. (1962), Electromagnetic waves in stratified media, Macmillan, New York.

Wait, J. R. (1964), Two-dimensional treatment of mode theory of the propagation of VLF radio waves, Radio Sci., v. 68D, no. 1, 81.

Wait, J. R. (1968a), Mode conversion and refraction effects in the earth-ionosphere waveguide for VLF radio waves, J. Geophys. Res., 73(11), 3537.

Wait, J. R. (1968b), On the theory of VLF propagation for a step model of the nonuniform earth-ionosphere waveguide, Can. J. Phys., 46(17), 1979.

Wait, J. R. and Spies, K. P. (1963), Height gain for VLF radiowaves, J. Res. NBS (Radio Prop.), 67D, 183-187.

Wait, J. R. and Spies, K. P. (1964), Characteristics of the earth-ionosphere waveguide for VLF radiowaves, NBS Tech. Note 300.

Walker, D. (1965), Phase steps and amplitude fading of VLF signals at dawn and dusk, Radio Sci., (J. Res. NBS), 69D, 1435.

Walsh, E. J. (1967), Full wave solutions in terms of coupled vacuum modes, Radio Sci., 2, 913.

Watson, G. N. (1918), The diffraction of radio waves by the earth, Proc. Roy. Soc. London, A95, 83-99.

Watson, G. N. (1919), The transmission of electric waves around the earth, Proc. Roy. Soc., A95, 546-563.

Watson, G. N. (1944), The theory of Bessel Functions, Cambridge University Press, Cambridge.

Watt, D. (1967), VLF radio engineering, Pergamon Press, Oxford.

Westerlund, S. (1974), The effect of ground conductivity on VLF propagation, J. Hottet (ed), ELF-VLF Radio Wave Propagation, D. Riedel Publ., 117-128.

Wieder, B. (1968), Rapid calculation of ionosphere reflection coefficients at low frequencies, paper presented at URSI Symposium on Electromagnetic Waves, Stresa, Italy, June.

Yokoyama, E. and Tanimura, I. (1933), Some long distance transmission phenomena of low frequency waves, Proc. IRE, 21, 263.

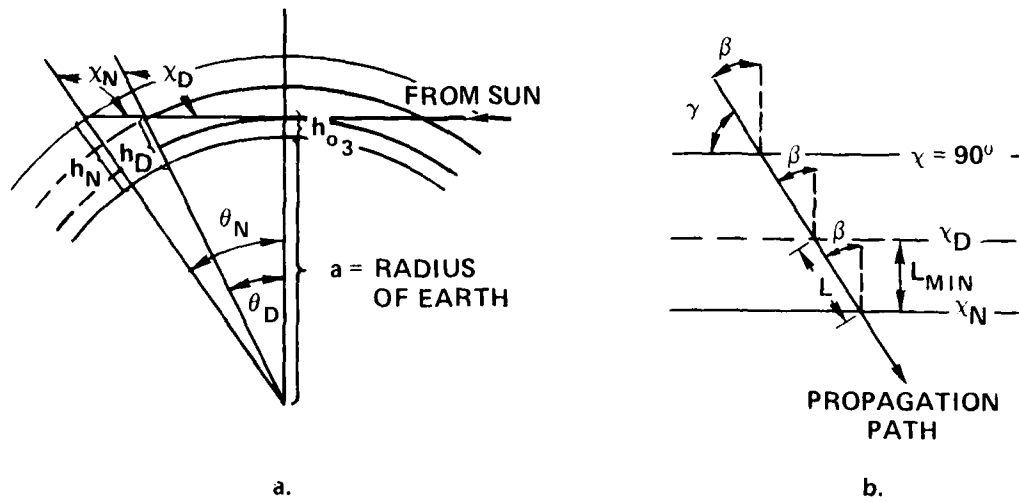


Figure 1. Ionospheric Sunrise/Sunset Model with Plan View of Propagation Path Intersection with Transition Region.

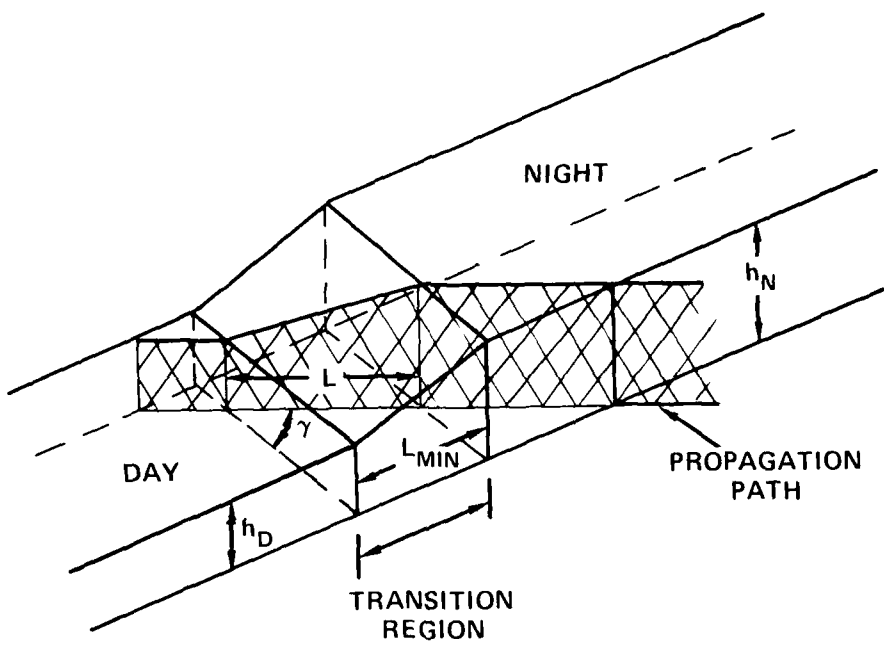


Figure 2. Model of Propagation Path Intersection with Transition Region.

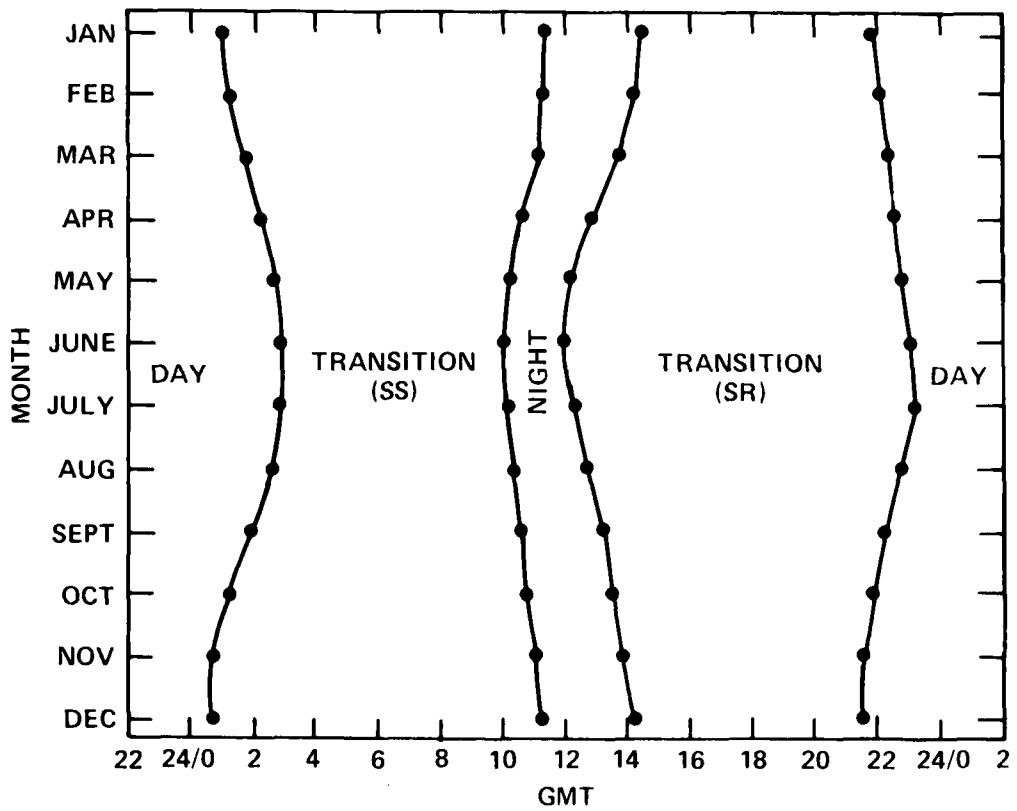


Figure 3. Periods of Night, Day and Transition Versus Date for NWC to San Diego Propagation Path

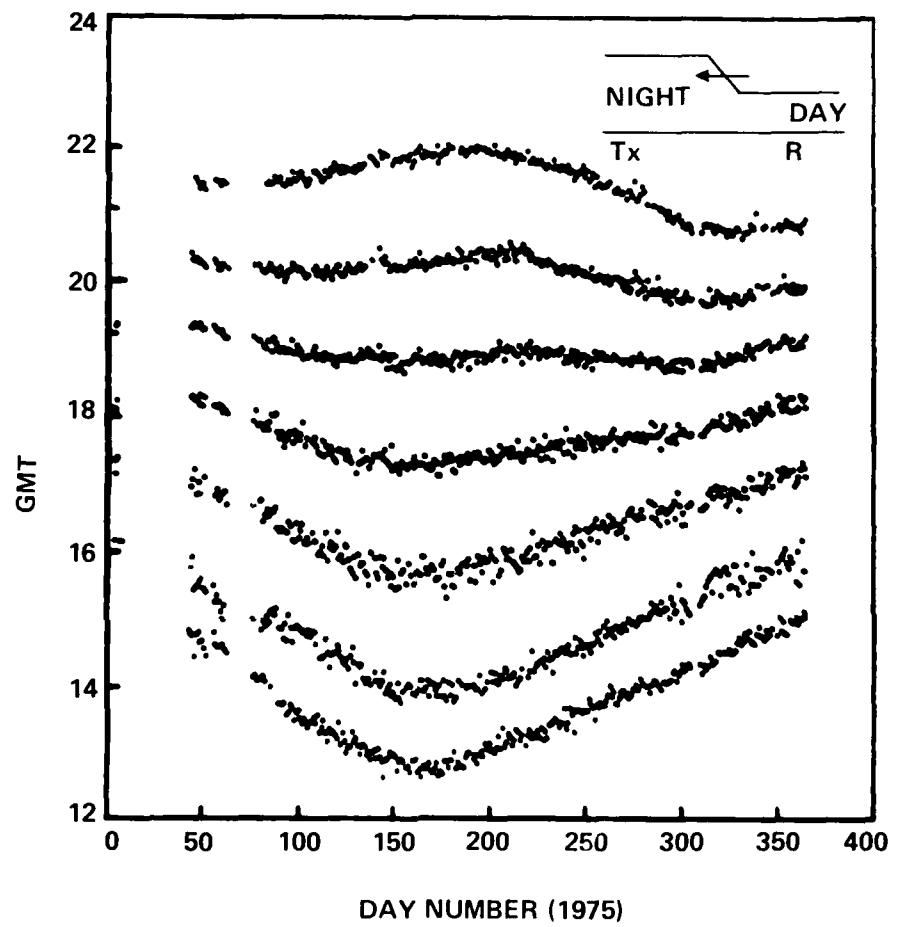


Figure 4. Times of Signal Minima for Night to Day Transition - Sunrise (No Average).

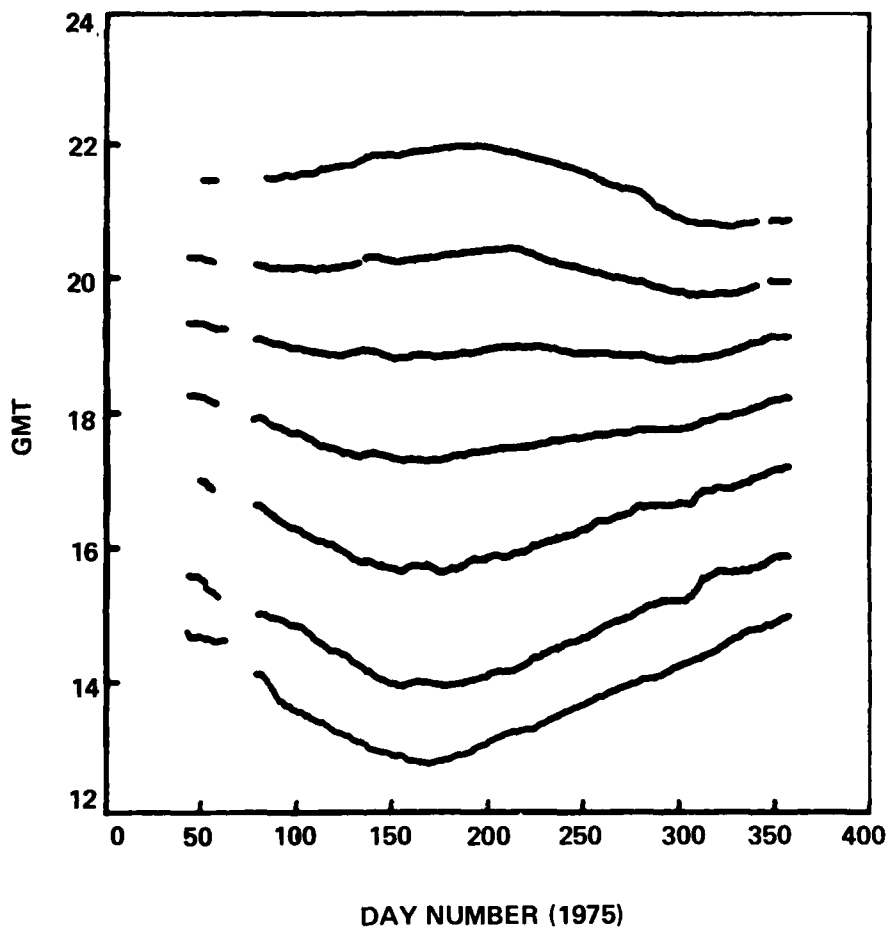


Figure 5. Times of Signal Minima for Night to Day Transition - Sunrise (15 Day Average).

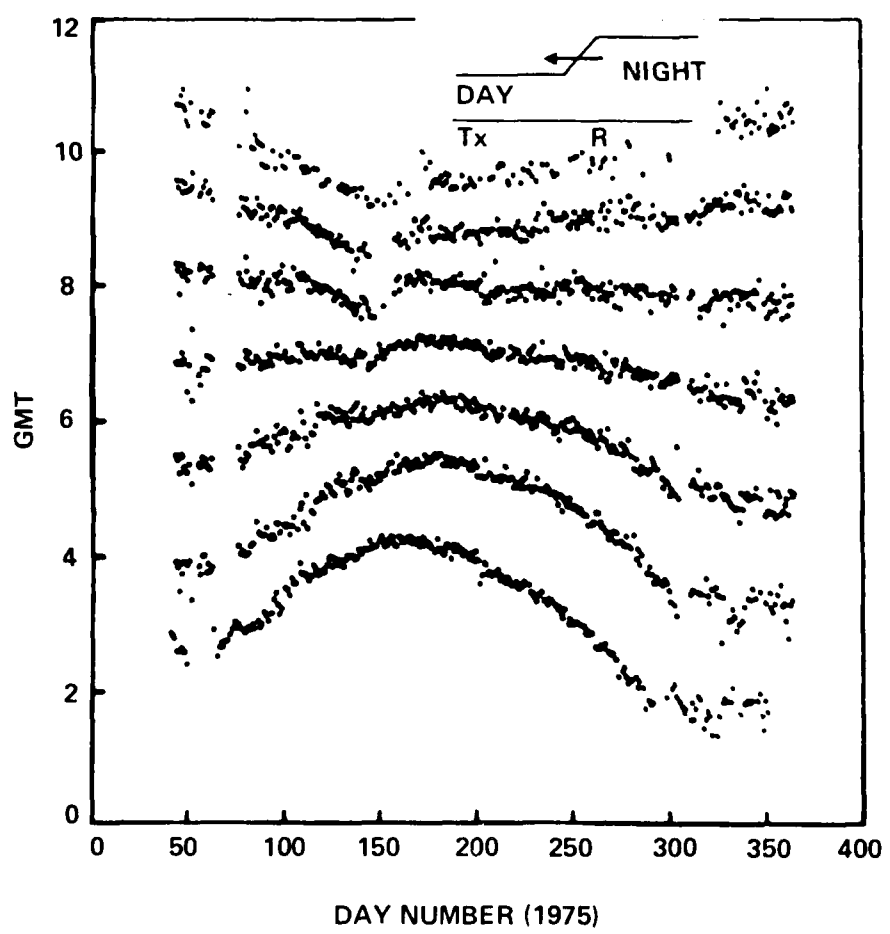


Figure 6. Times of Signal Minima for Day to Night Transition - Sunset (No Average).

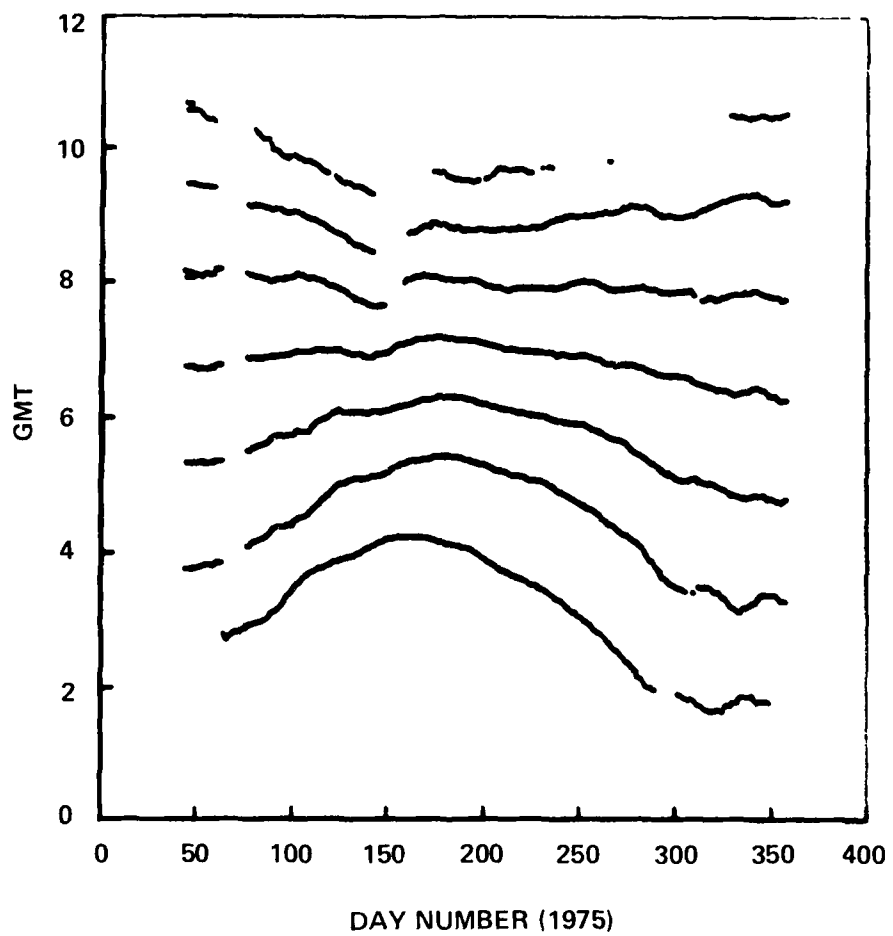


Figure 7. Times of Signal Minima for Day to Night Transition - Sunset (15 Day Average).

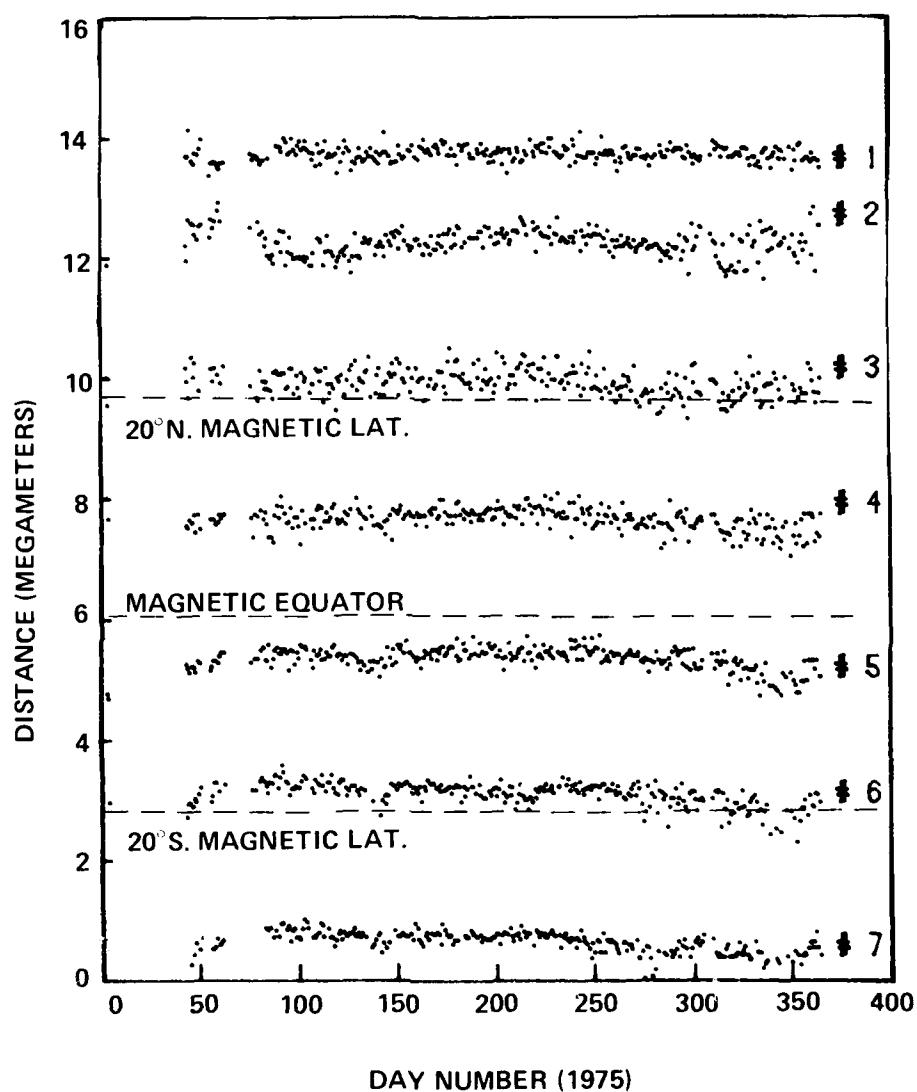


Figure 8. Transmitter/Terminator Distance ($\lambda = 96^\circ$) at Times of Signal Minima for Night to Day Transition - Sunrise (No Average).

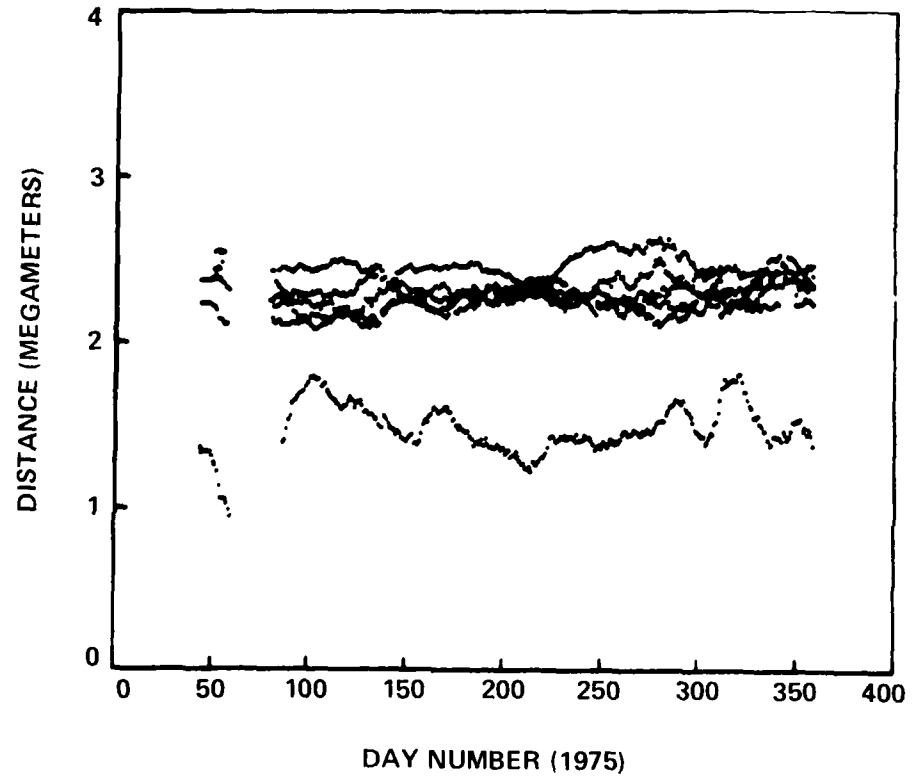


Figure 9. Distance Moved by Terminator ($\epsilon = 96^\circ$) Between Signal Minima for Night to Day Transition Sunrise (No Average).

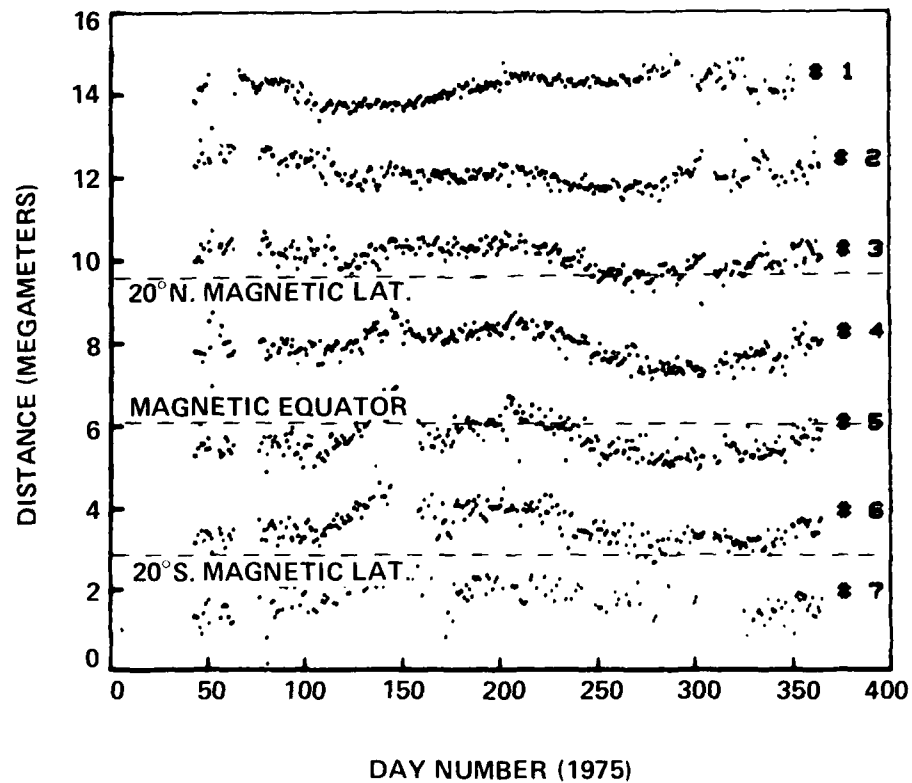


Figure 10. Transmitter Terminator Distance ($\pm 96^\circ$) at Times of Signal Minima for Day to Night Transition - Sunset (No Average).

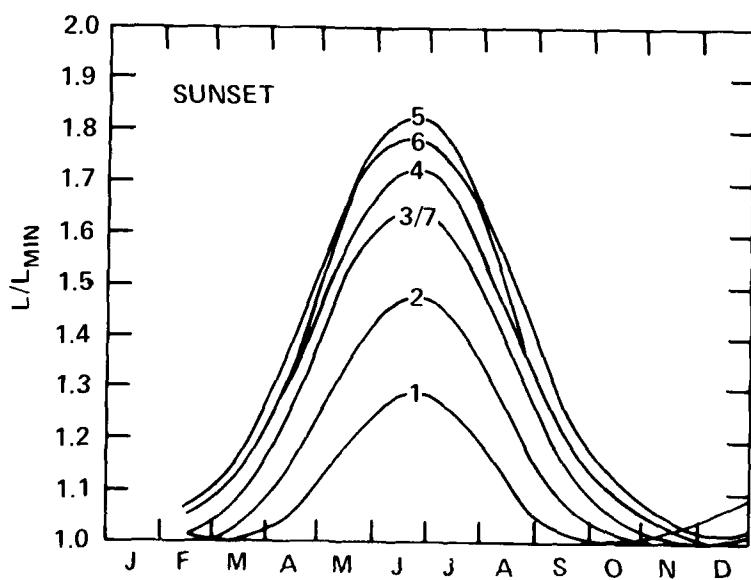
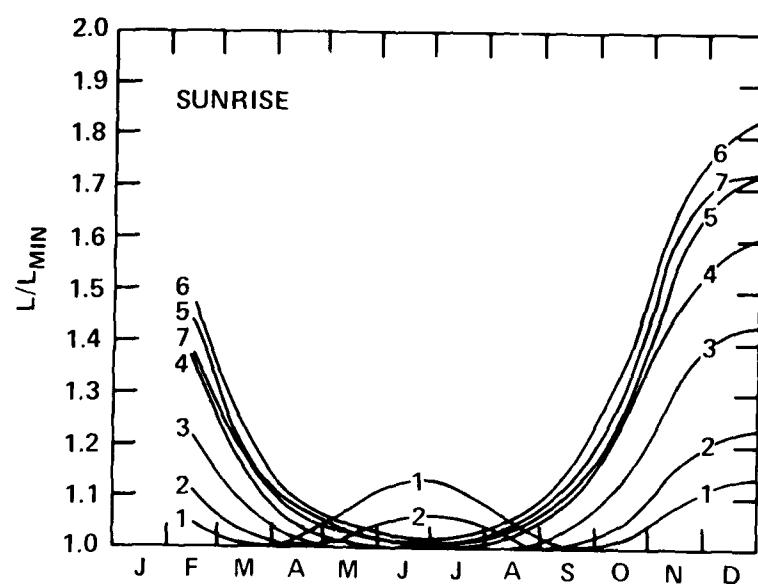


Figure 11 - Ratio of Measured Propagation Path Length in Transition Region to the Minimum Possible Path Length

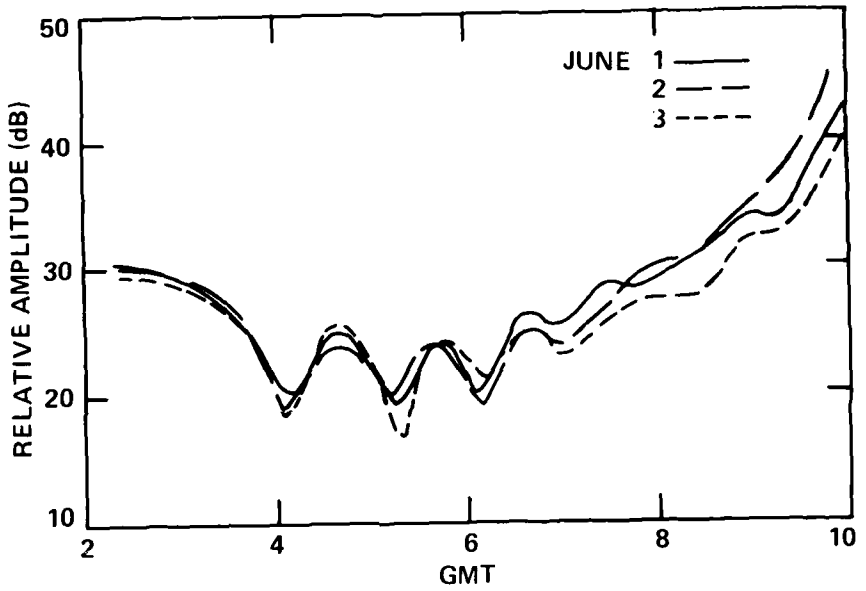


Figure 12. Signal Amplitude-NWC; 22.3 kHz Received at San Diego—June 1, 2, 3, 1975.

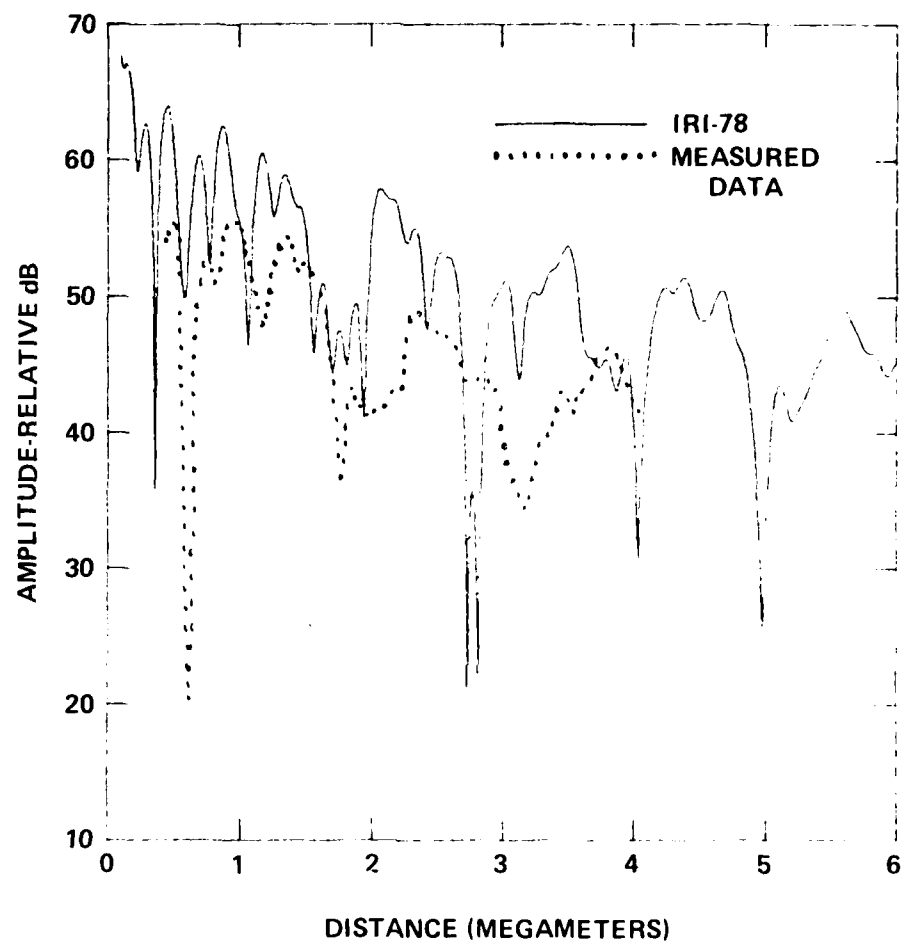


Figure 13. Comparison of Computed (IRI-78) with Measured (NPM to Ontario, Calif.) Amplitude
Night - 23.4 kHz.

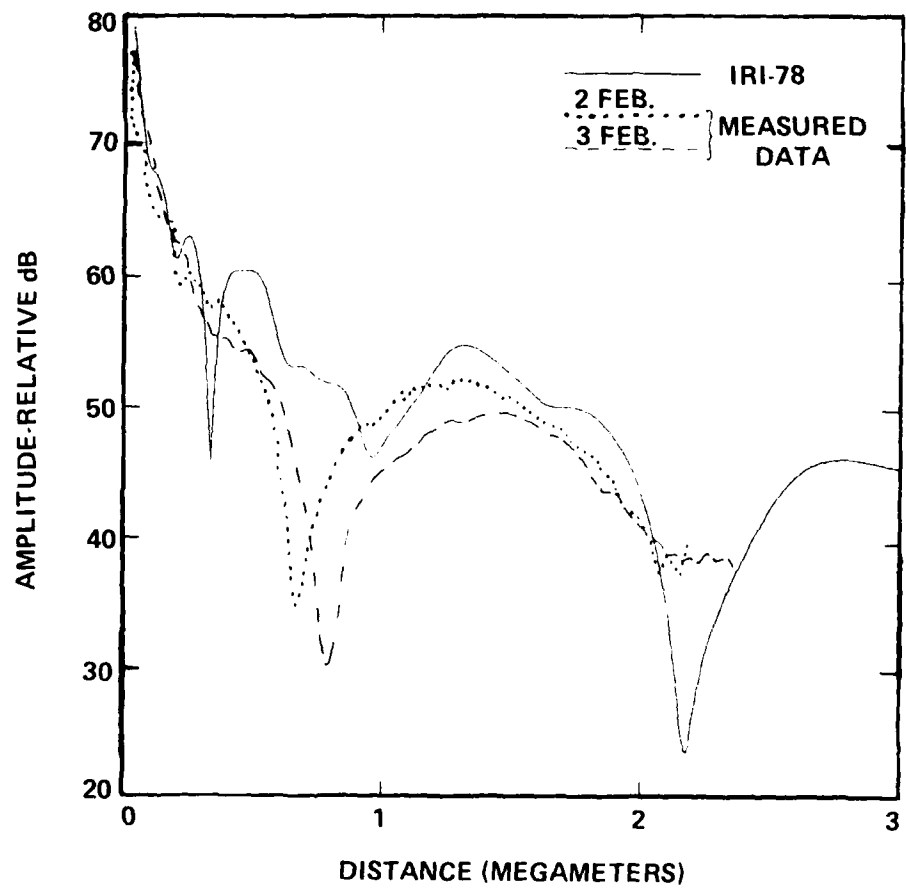


Figure 14. Comparison of Computed (IRI-78) with Measured (Hawai Sounder to San Diego) Amplitude
Day = 21.8 kHz.

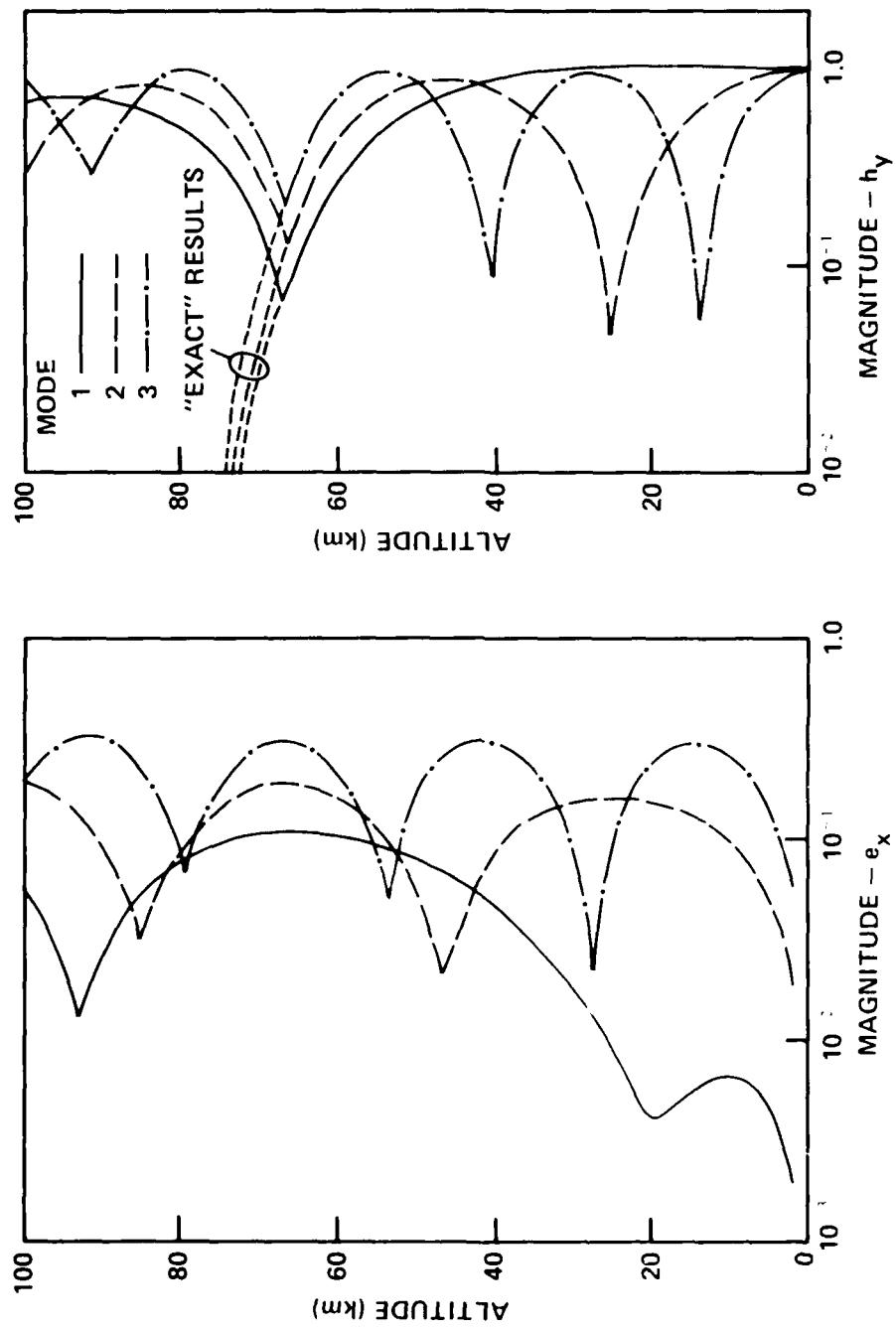


Figure 15. Electric fields for $\omega = 5 \text{ rad/sec}$, $E_0 = 10^4 \text{ volt/m}$.

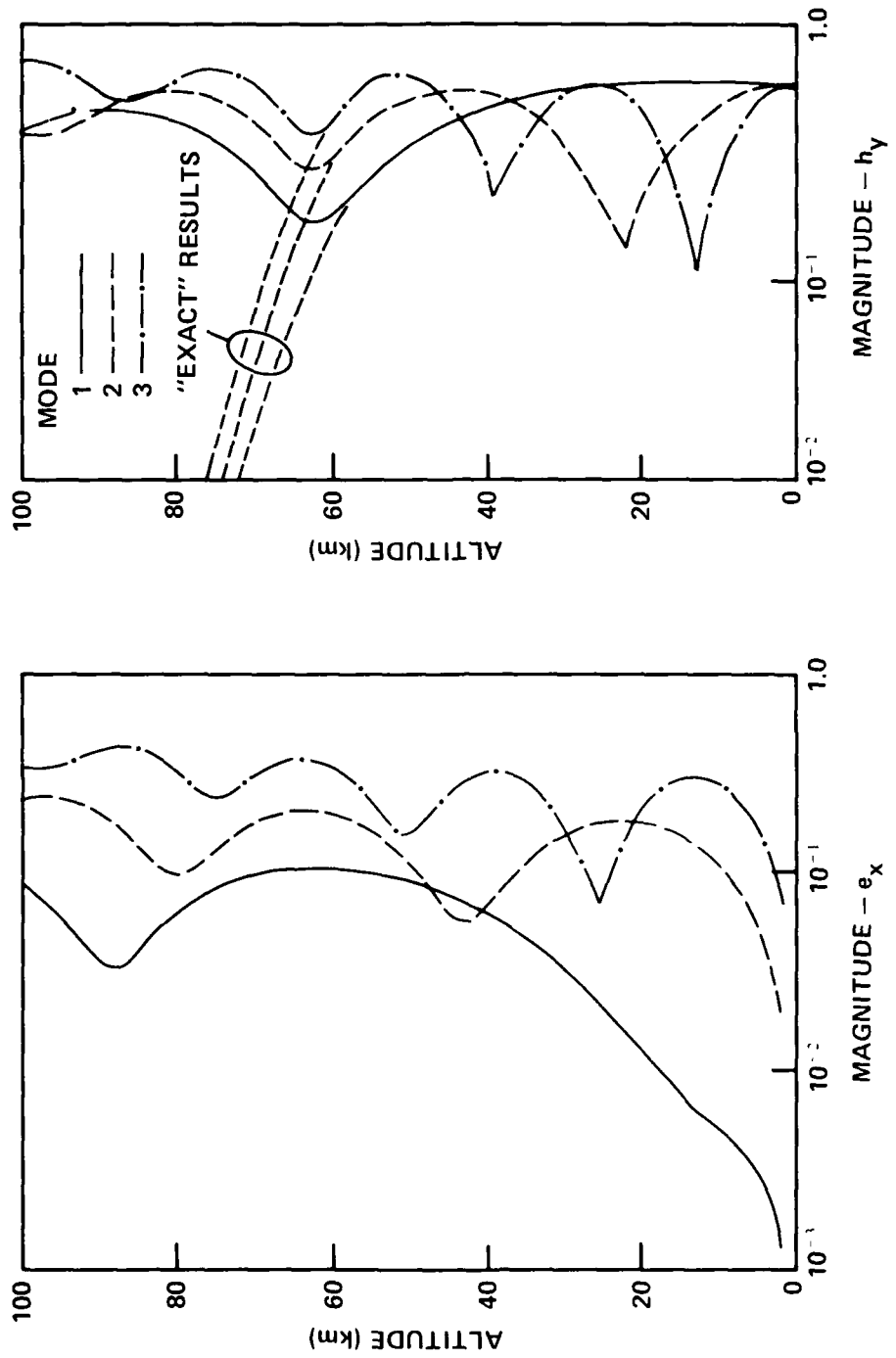


Figure 16. Height Gains for $\beta = .3 \text{ km}^{-1}$, $h' = 70 \text{ km}$, $f = 18.6 \text{ kHz}$.

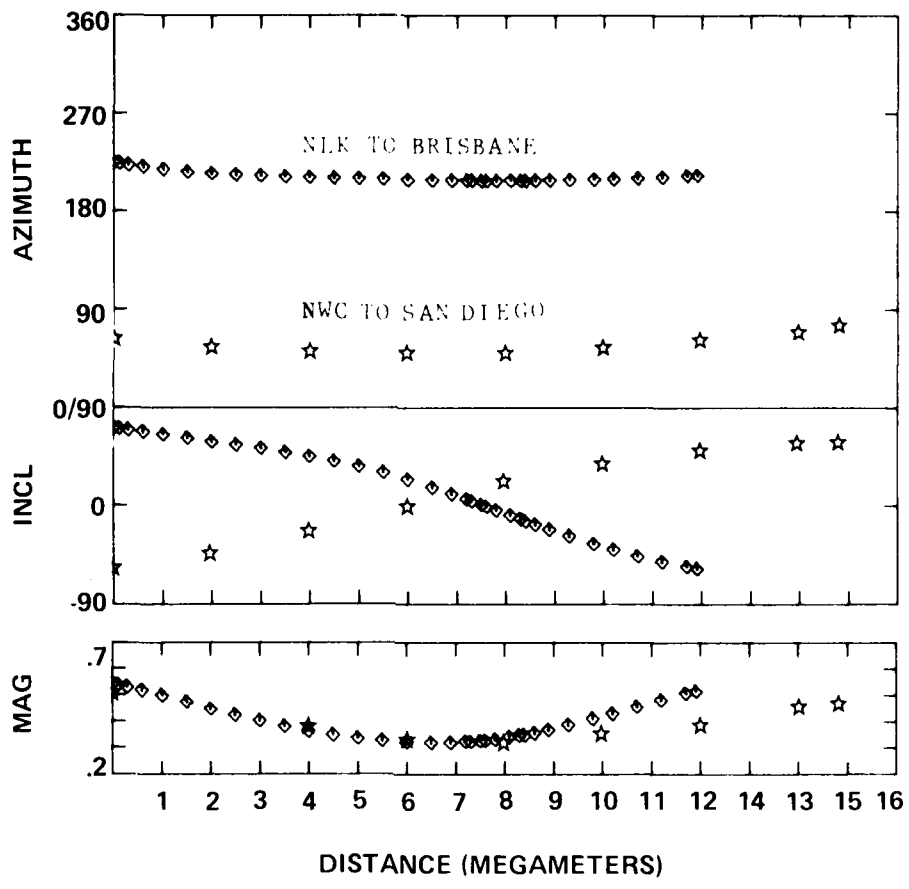
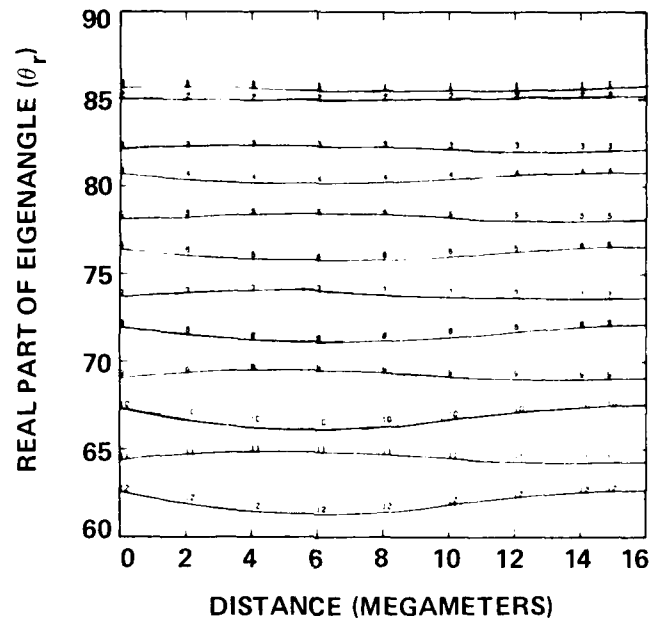
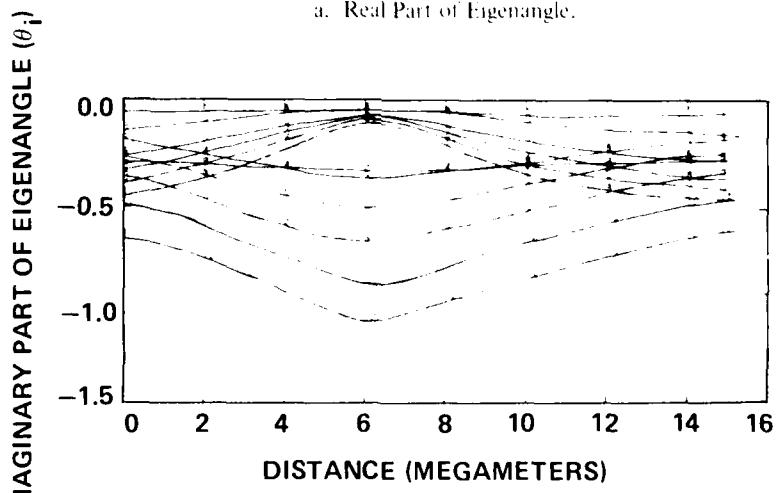


Figure 17. Geomagnetic Field Variation Along the Propagation Paths.



a. Real Part of Eigenangle.



b. Imaginary Part of Eigenangle.

Figure 18. Complex Eigenangles vs. Distance for NWC to San Diego.

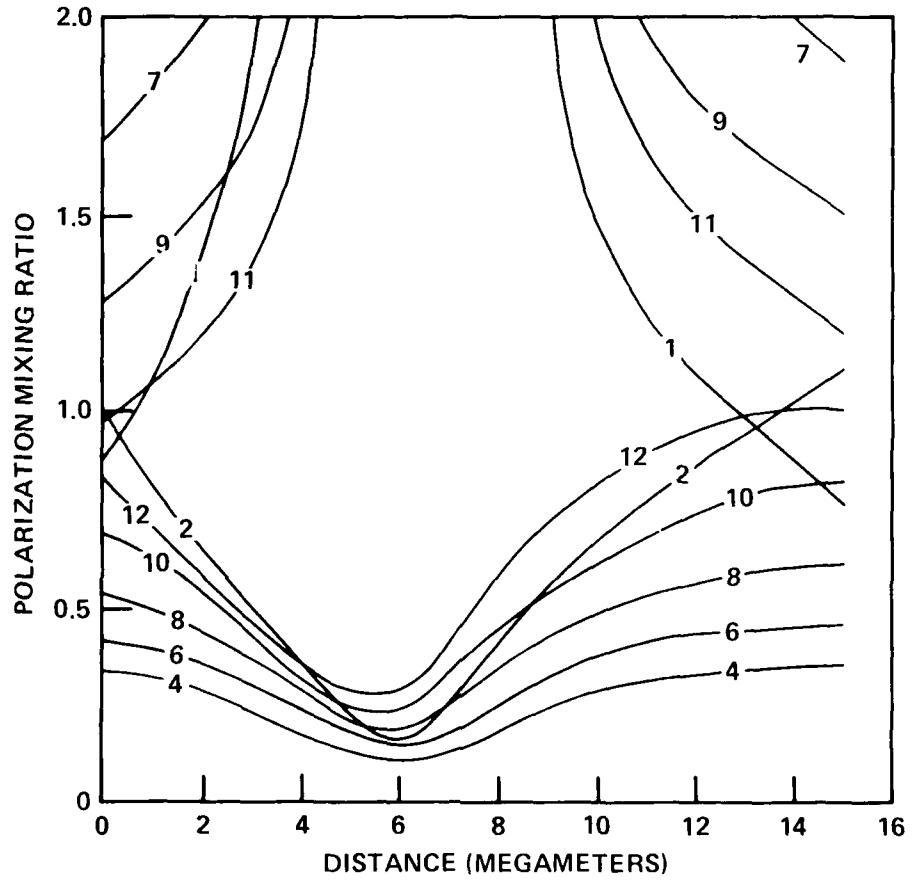


Figure 19. Polarization Mixing Ratio for NWC to San Diego.

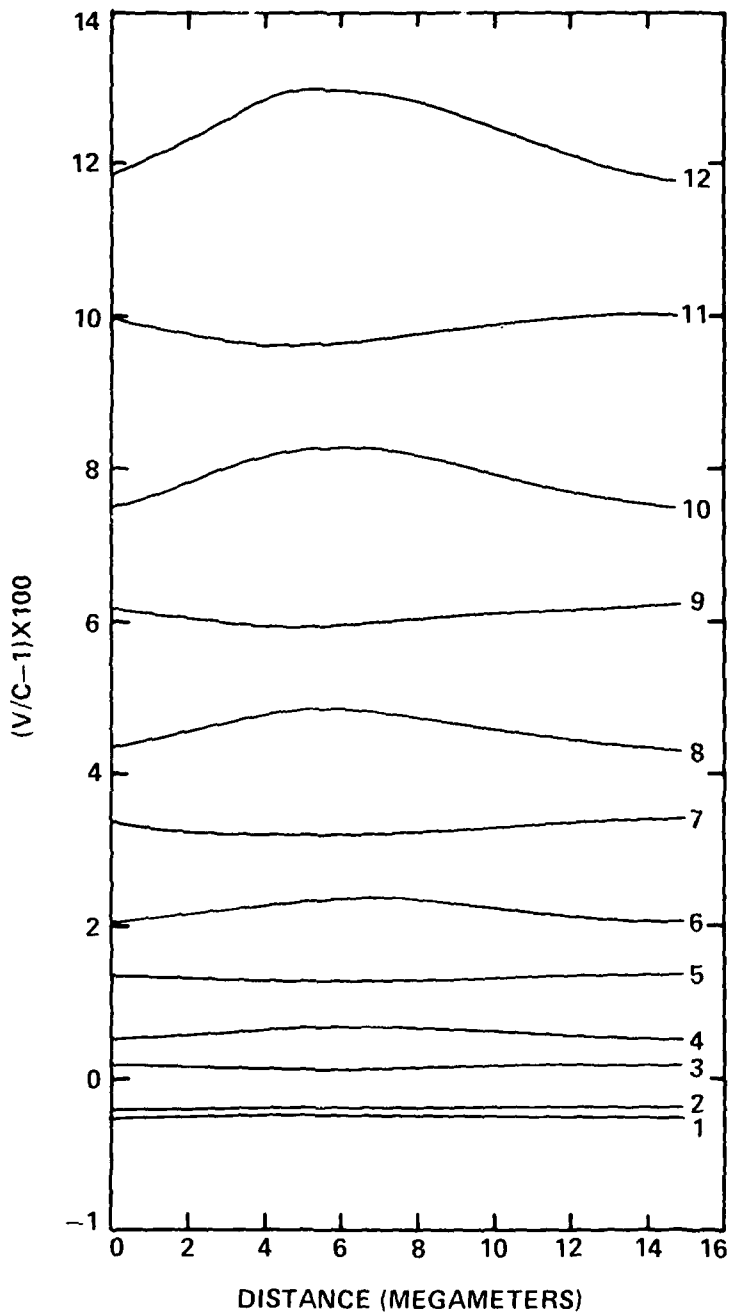


Figure 20. Normalized Phase Velocities for NWC to San Diego.

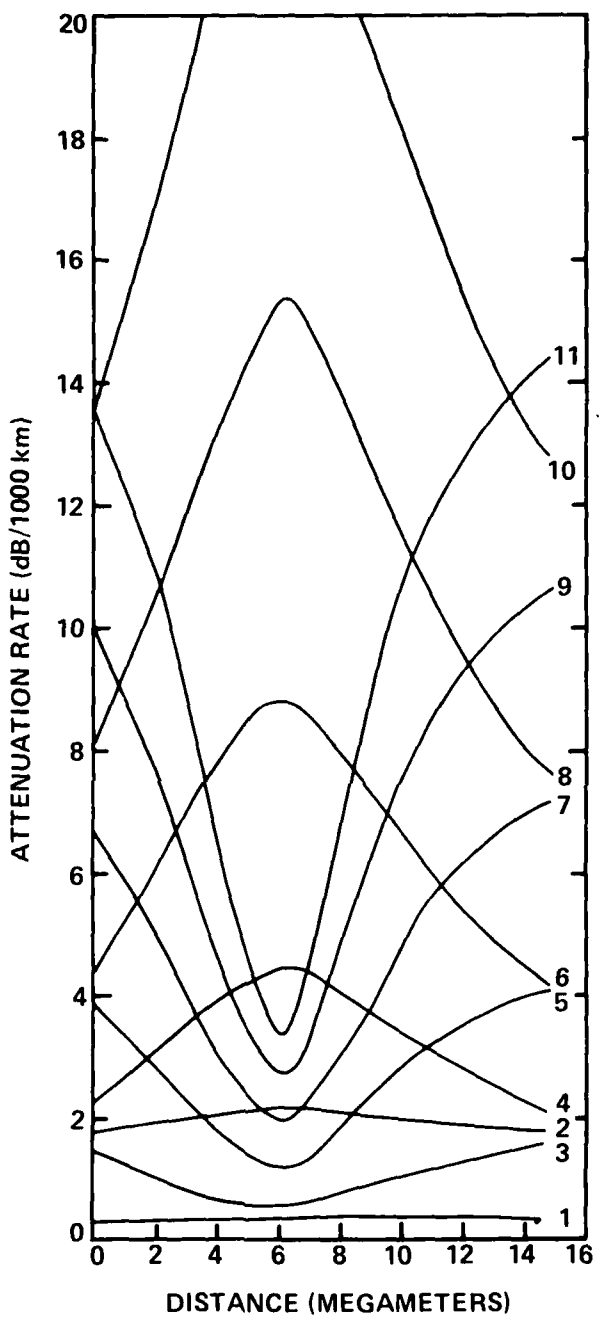


Figure 21. Attenuation Rates for NWC to San Diego.

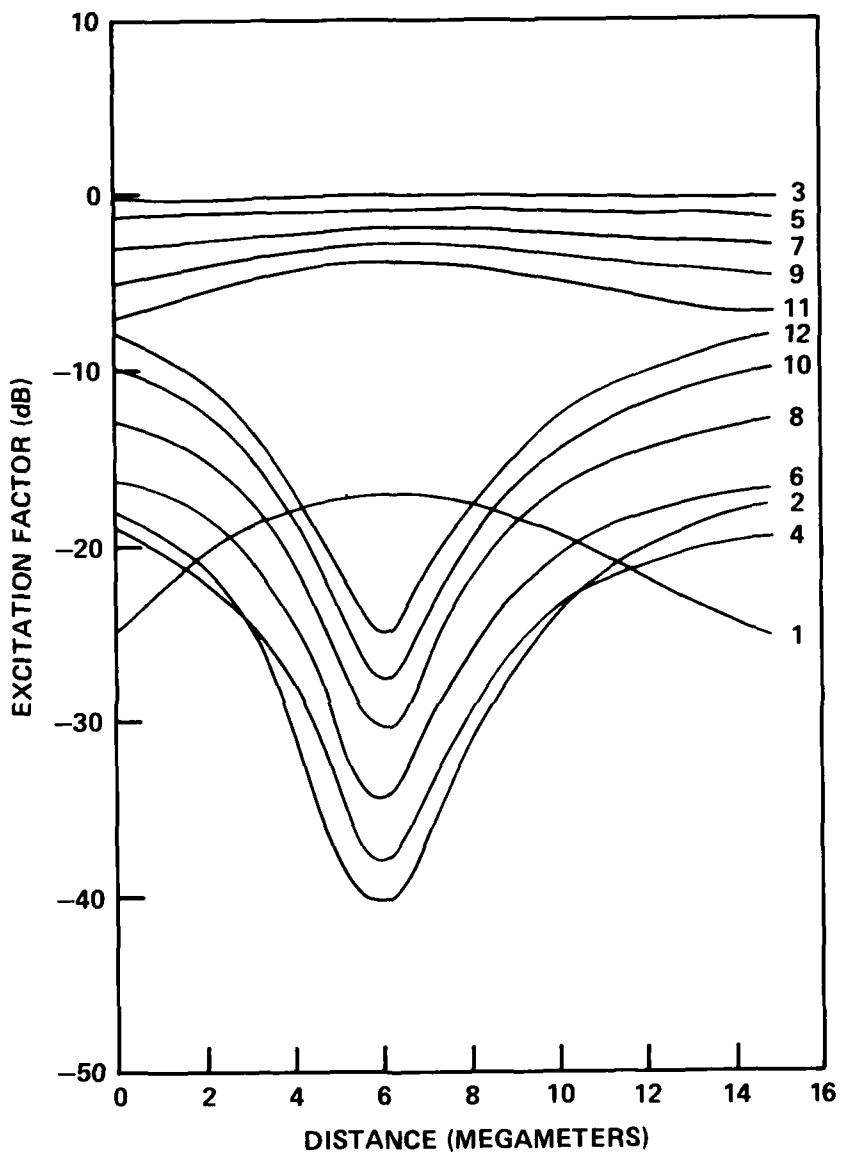


Figure 22. Excitation Factors for NWC to San Diego.

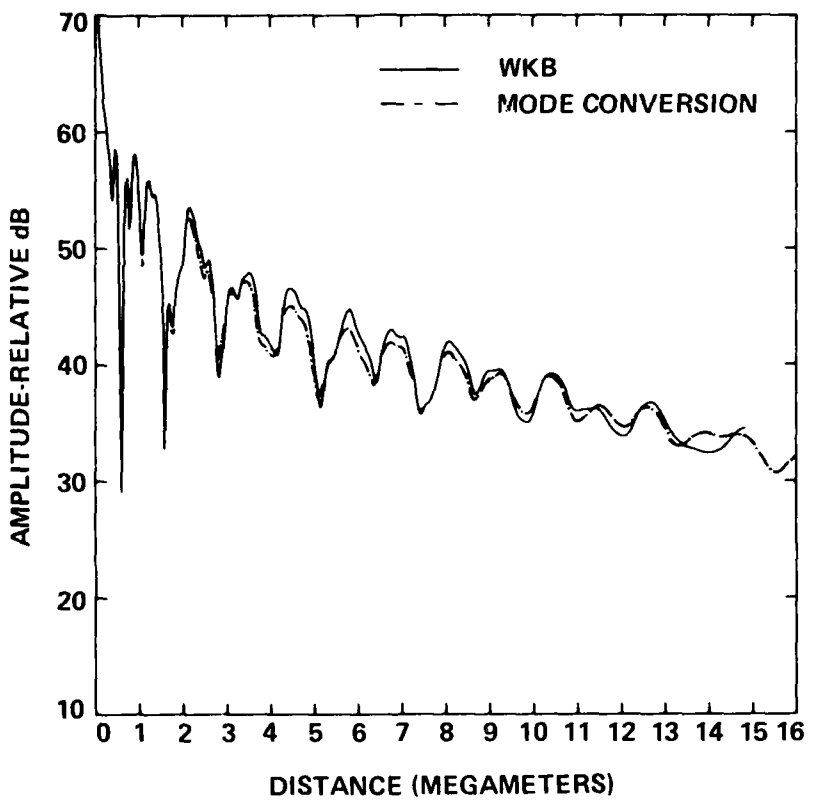


Figure 23. Mode Sums for NWC to San Diego.

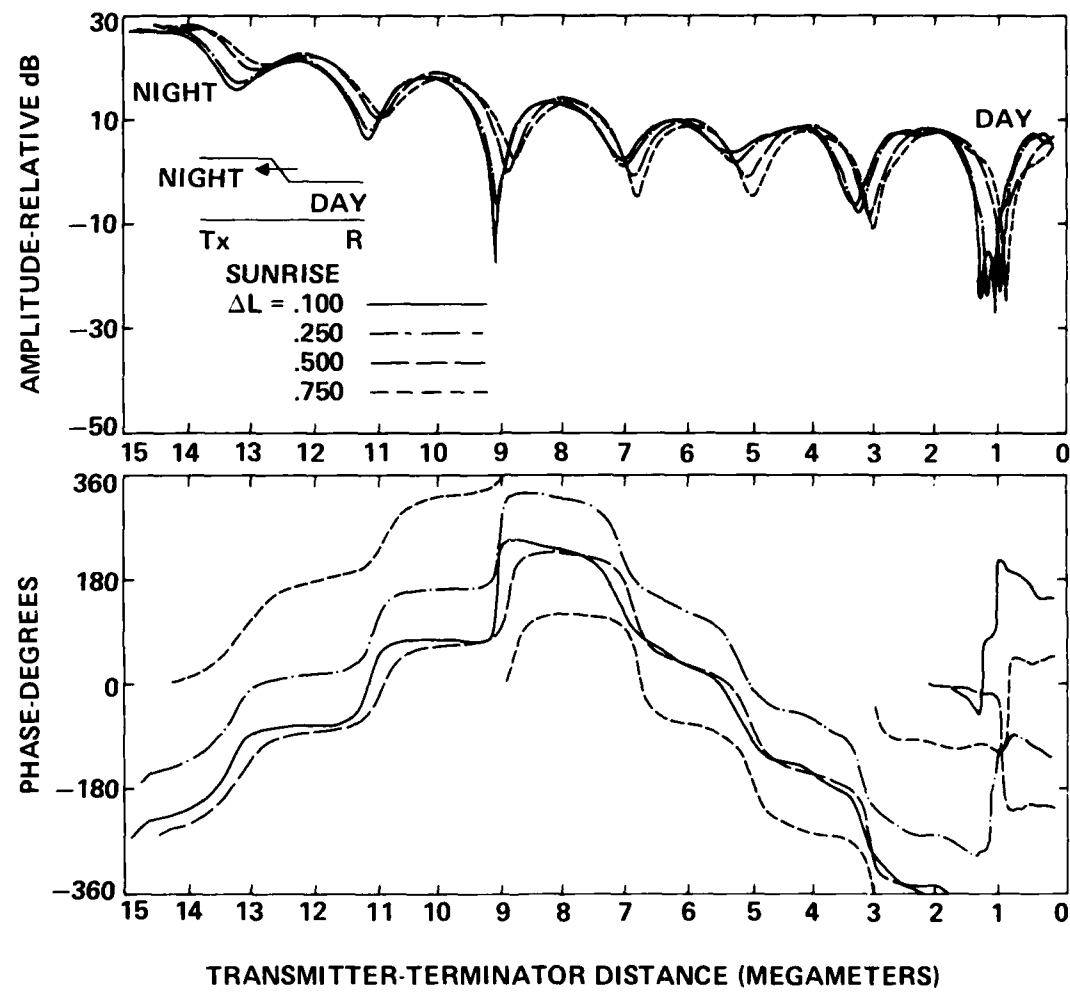


Figure 24a. Computed Transition Fading — NWC to San Diego Night to Day ($h' = 86$ km to $h' = 74$ km).

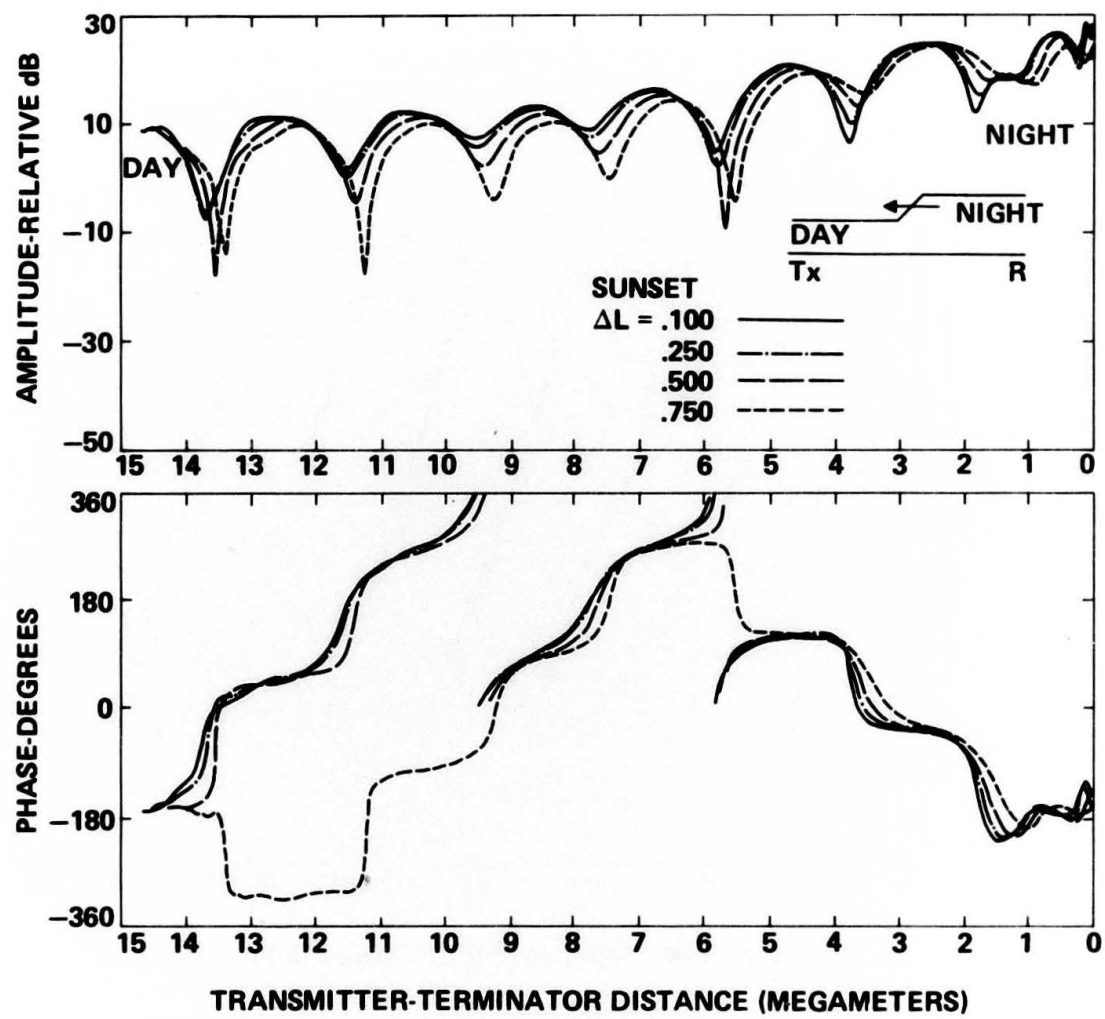


Figure 24b. Computed Transition Fading – NWC to San Diego Day to Night ($h' = 74$ km to $h' = 86$ km).

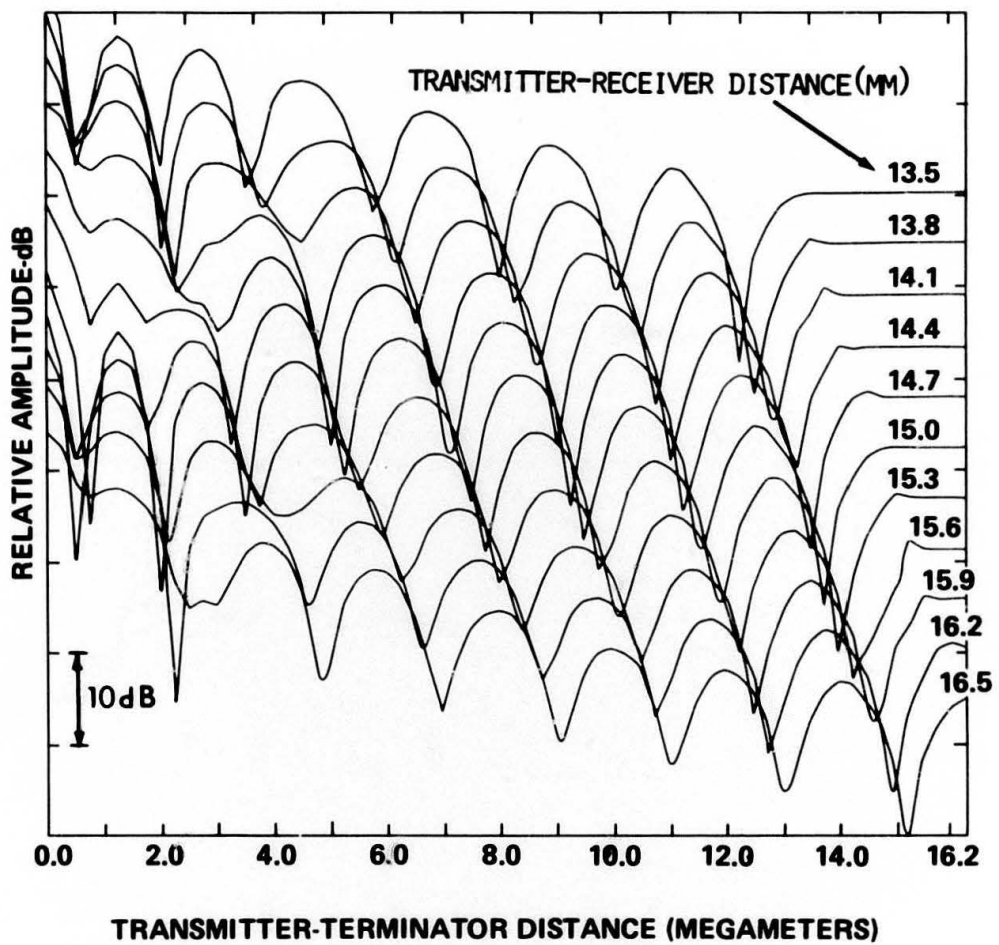


Figure 25. Computed Transition Fading – Variable Receiver Locations on NWC to San Diego Path Day to Night ($h' = 74$ km to $h' = 86$ km).

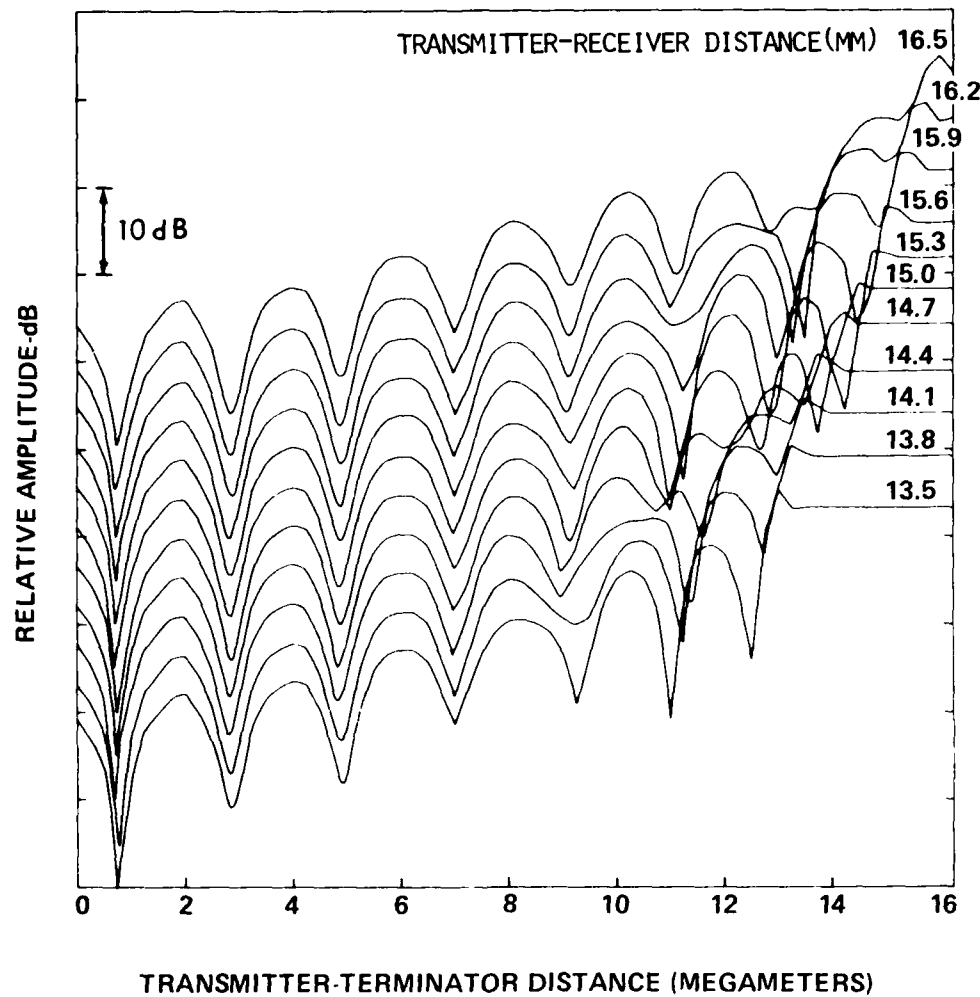


Figure 26. Computed Transition Fading—Variable Receiver Locations on NWC to San Diego Path Night to Day ($h' = 86$ km to $h' = 74$ km).

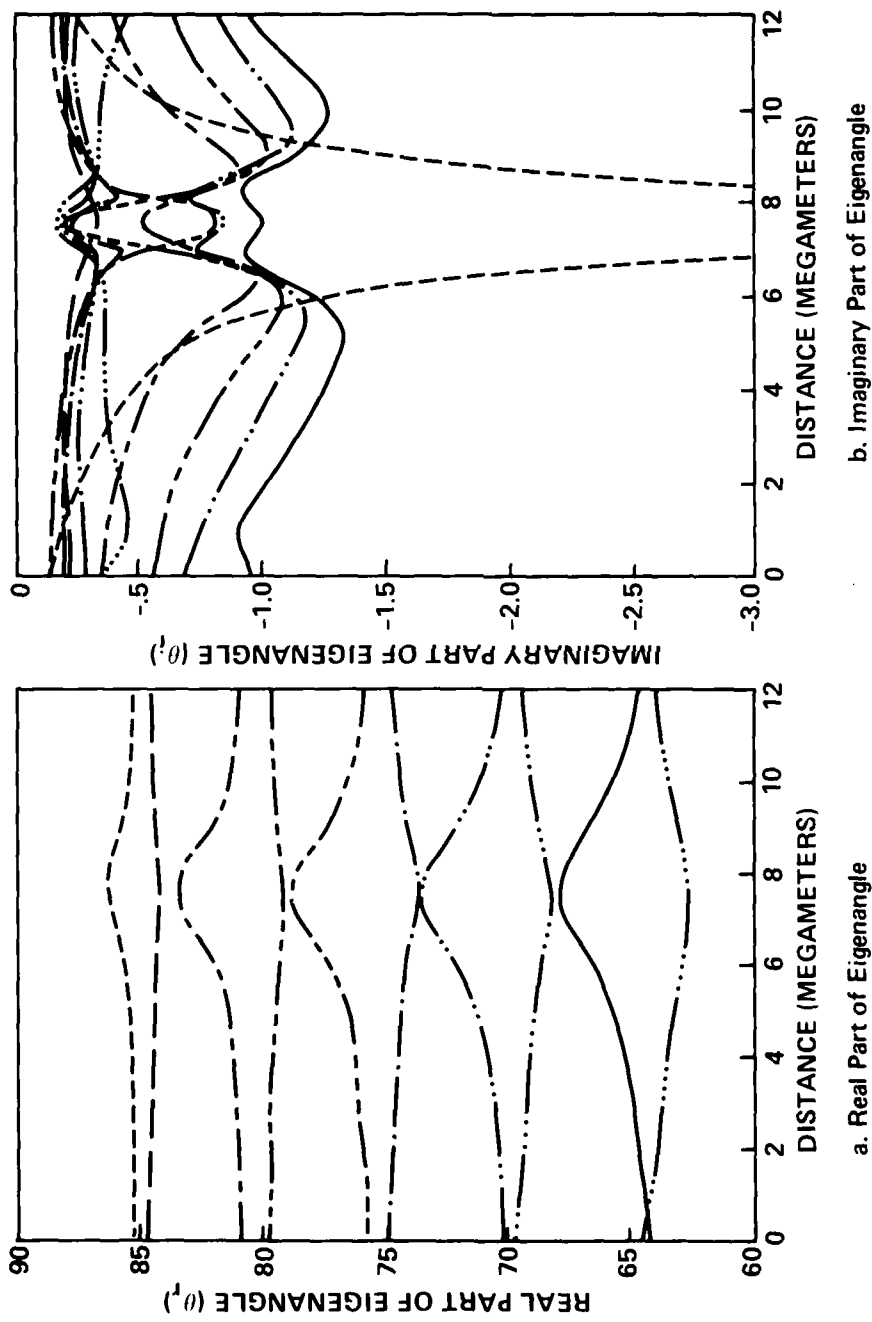


Figure 27. Complex Eigenangles vs Distance for NIK to Brisbane

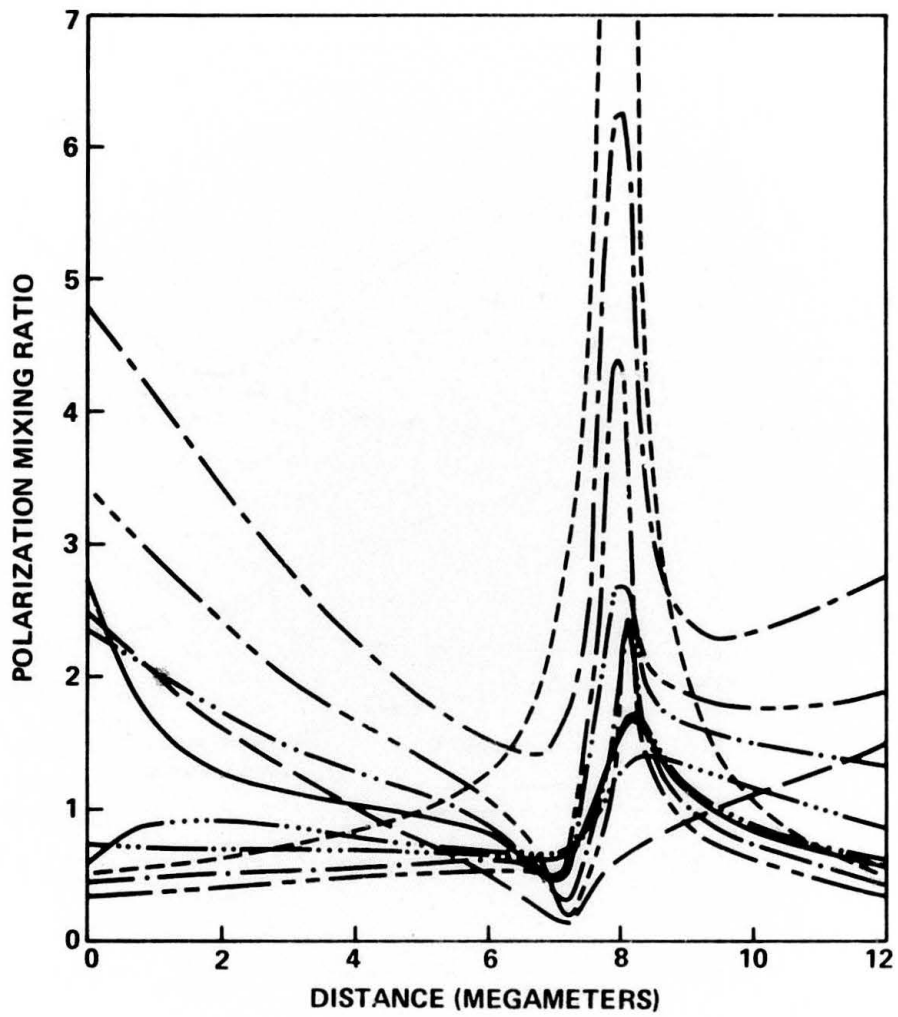


Figure 28. Polarization Mixing Ratios for NLK to Brisbane

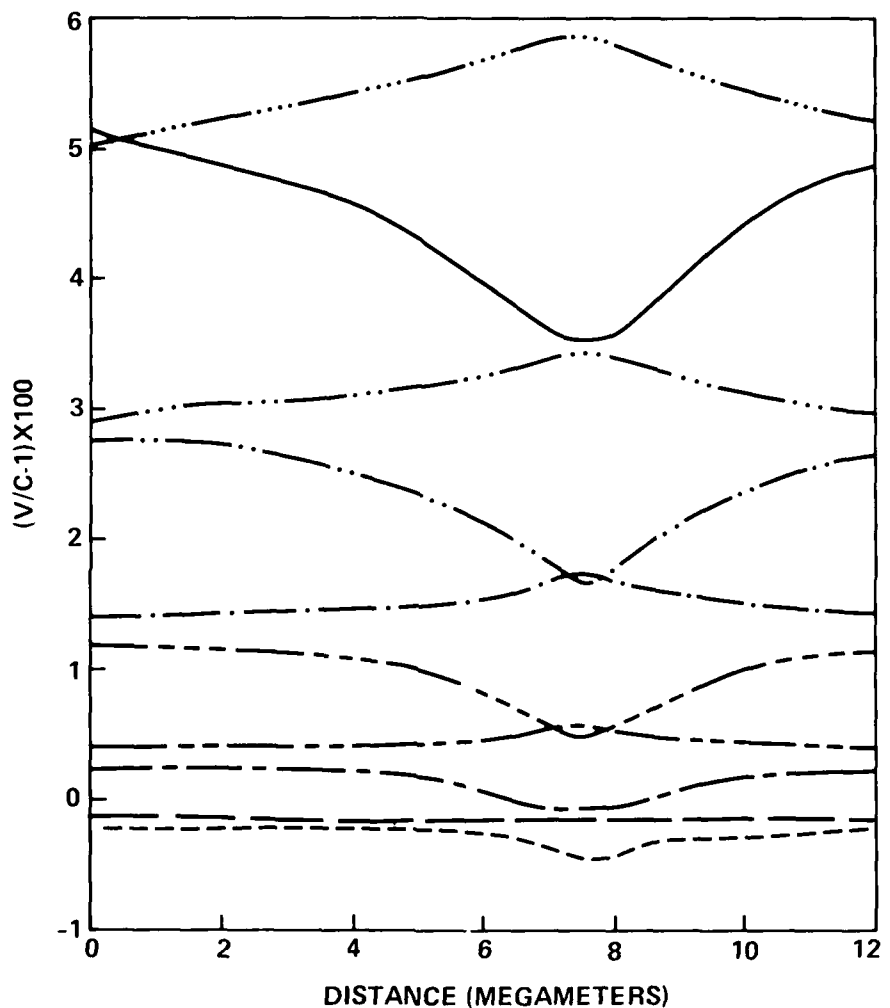


Figure 29. Normalized Phase Velocities for NIK to Brisbane

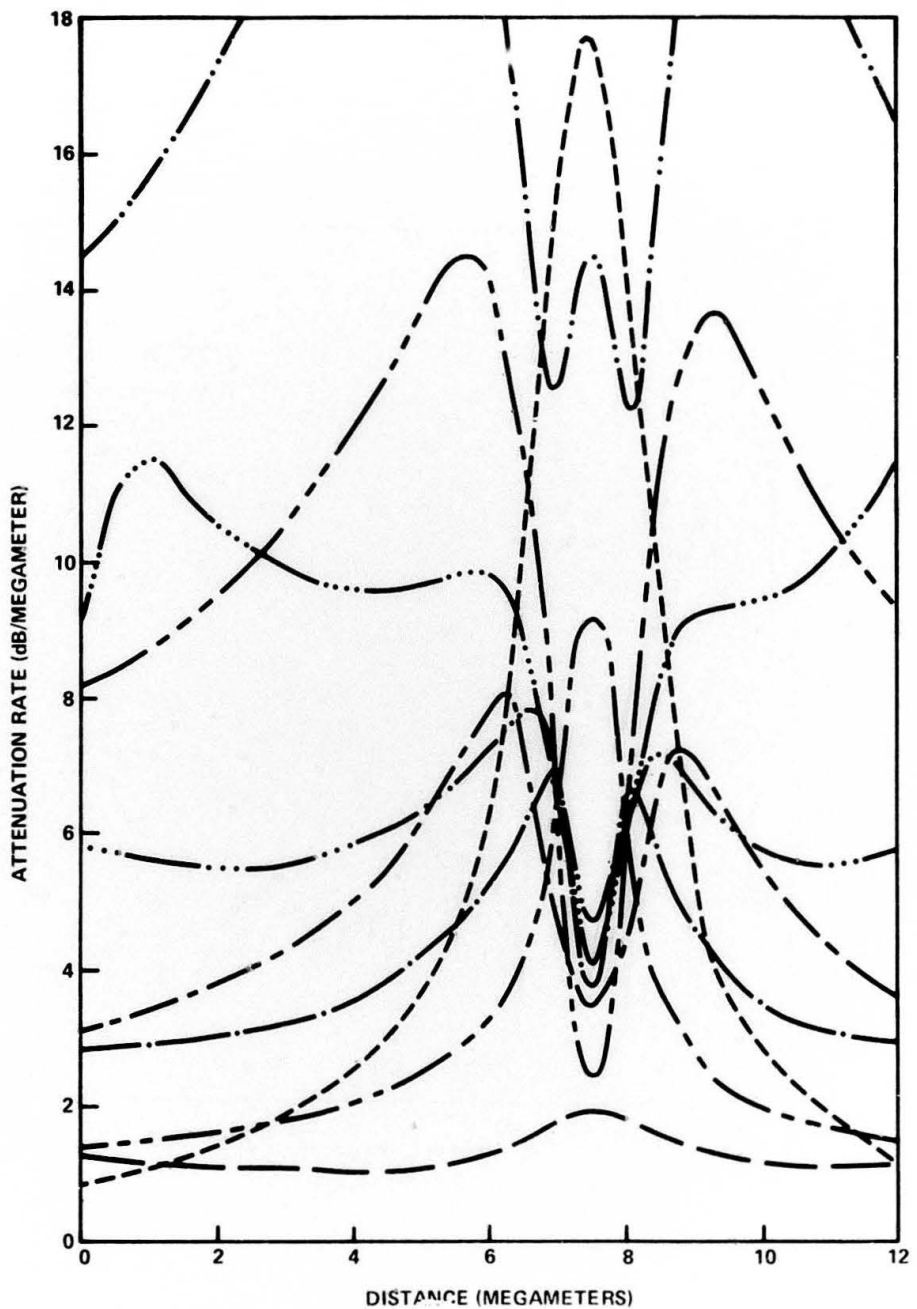


Figure 30. Attenuation Rates for NLK to Brisbane

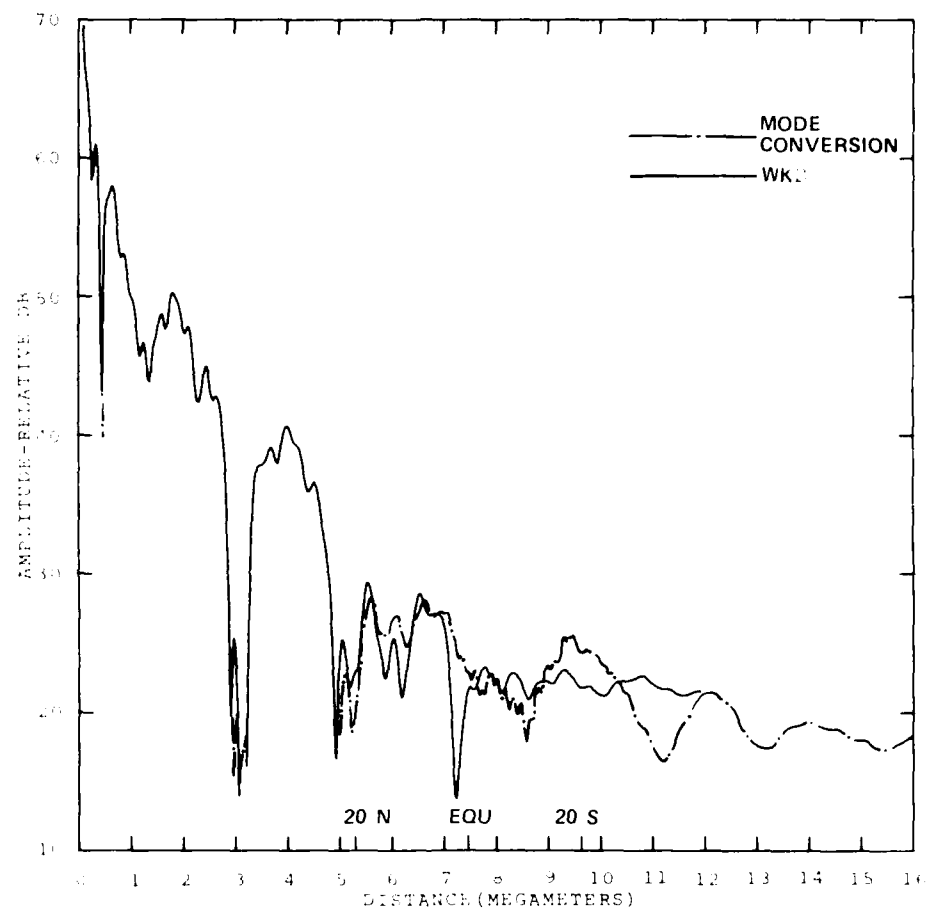


Figure 31. Mode Sums for NUK to Brisbane

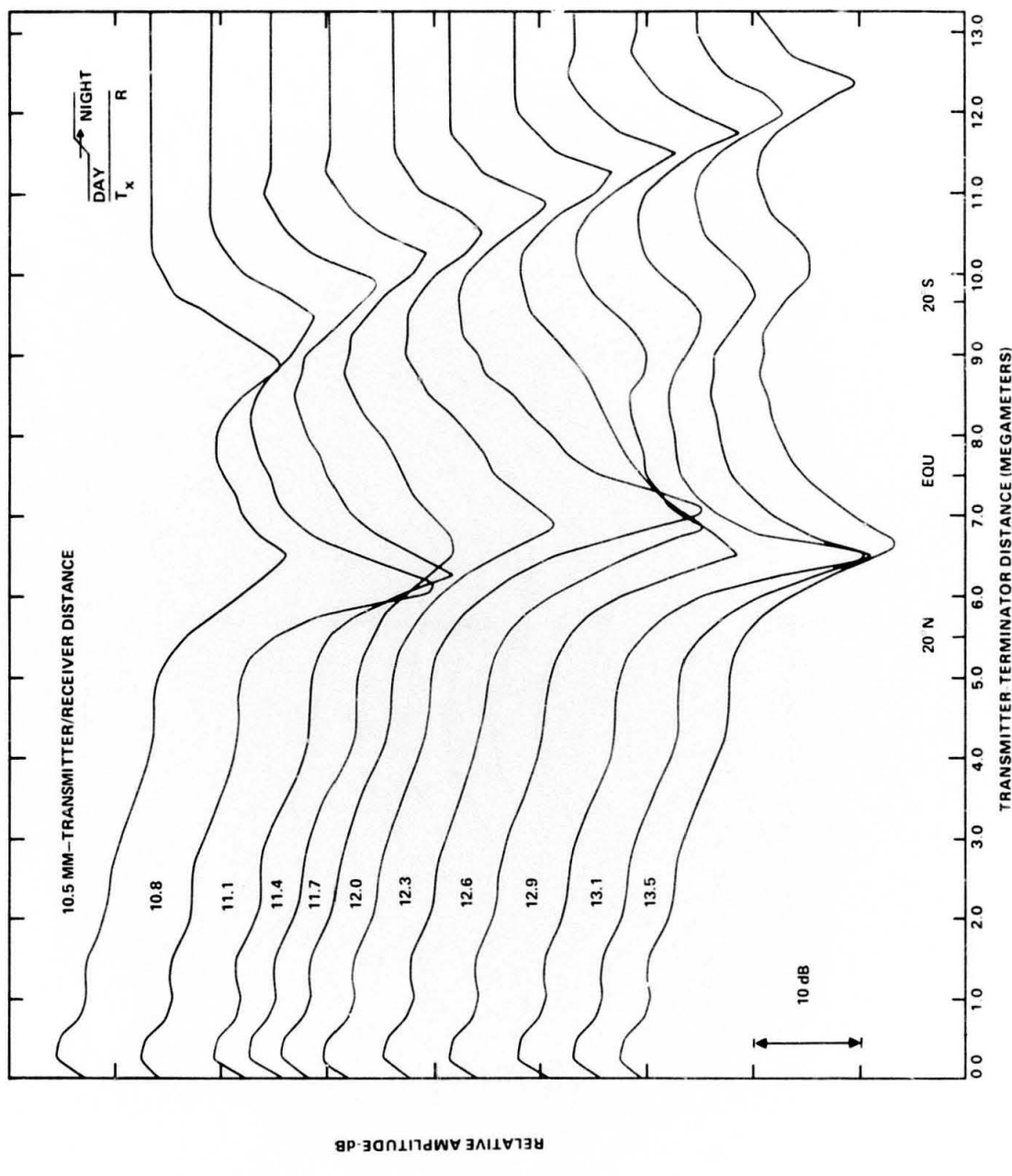


Figure 32. Computed Transition Fading-Variability Receiver Locations on NLK to Brisbane Path Day to Night ($h' = 74$ km to $h' = 86$ km)

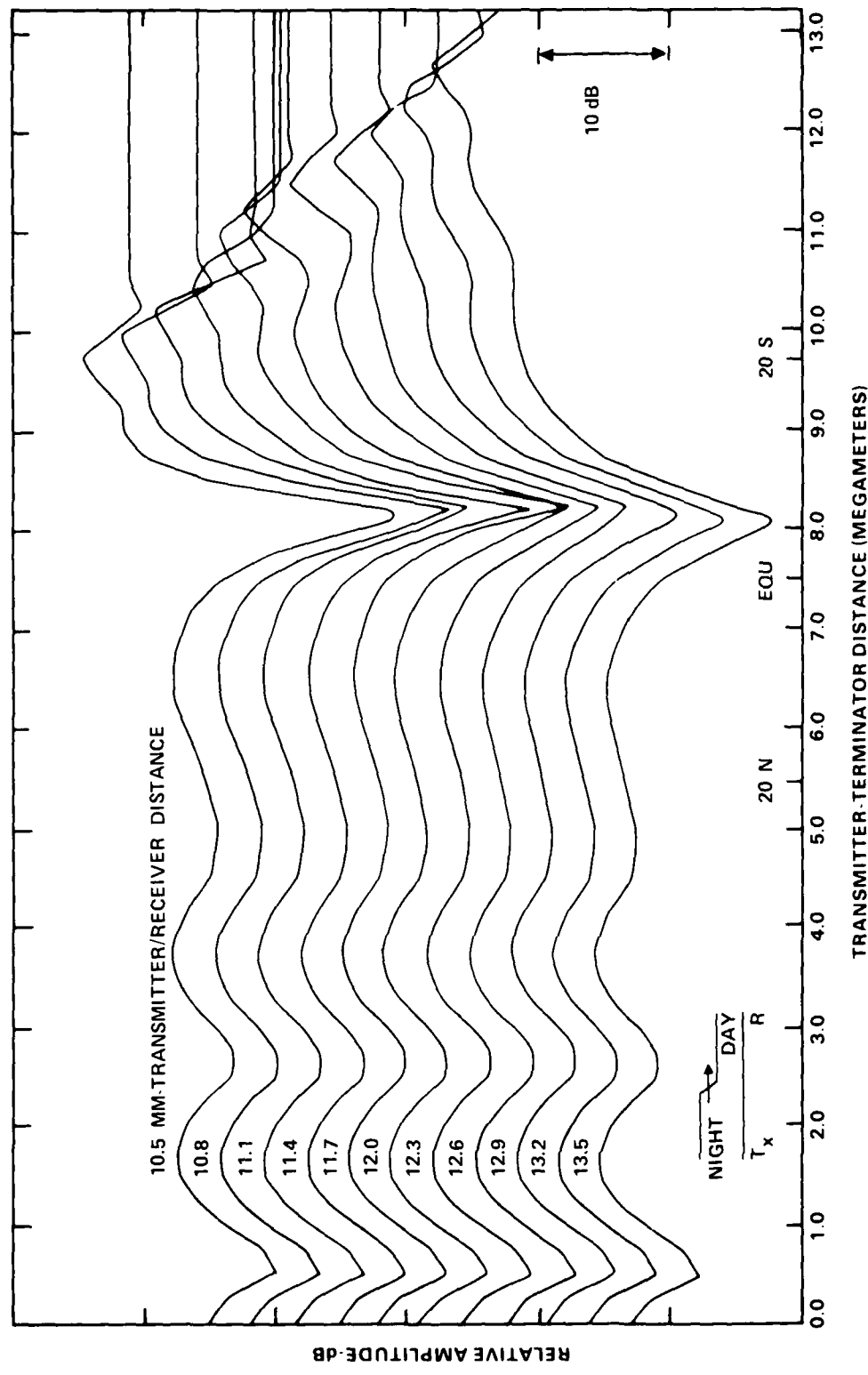


Figure 33. Computed Transition Fading-Variable Receiver Locations on NIK to Brisbane Path Night to Day ($h' \approx 86$ km to $h' \approx 74$ km)